LABORATORY STUDIES OF FLOW PROPERTIES AND ASSOCIATED CRYSTAL STRUCTURE IN HOLOCENE AND WISCONSIN ICE

by

WANG, Wei Li

Thesis submitted for the degree of Master of Science,

Cooperative Research Centre for the Antarctic and Southern Ocean Environment,

University of Tasmania.

March, 1994

DECLARATION

I hereby declare that this thesis is my own work, except where specifically stated to the contrary, and that this thesis contains no material which has been accepted for the award of any other degree or diploma in any university or institution.

AUTHORITY OF ACCESS

This thesis may be made available for loan and limited copying in accordance with the Copyright Act 1968.

WANG, Wei Li

March, 1994

CONTENTS

page

LIST OF FIGURES iv
LIST OF TABLES vi
ACKNOWLEDGMENTS vii
ABSTRACT viii

1. INTRODUCTION 1

1.1. NEED FOR INVESTIGATION 1
1.2. THE FLOW OF ICE 3
1.2.1. The flow law for ice 3
1.2.2. The flow of anisotropic ice 4
1.3. EXPERIMENTAL PROJECT FOR THE STUDIES 7

2. SELECTION OF ICE CORE TEST SAMPLES 9

2.1. SELECTION OF ICE CORE SAMPLES 9
2.1.1 Sources of ice core samples 9
2.1.2. Description of the ice core physical properties 11
2.2. PROPERTIES OF TEST SAMPLES 16
2.2.1. Crystal orientation fabrics 16
2.2.2. Crystal size and texture 23
2.2.3. Impurity content 29
2.2.4. Oxygen isotope ratio 35
2.2.5. Summary of physical properties 35
2.3. PREPARATION OF ICE TEST SPECIMENS 36
2.3.1. Ice core samples 36
2.3.2. Laboratory prepared ice samples 37

3. EXPERIMENTAL TECHNIQUE 38

3.1. CALCULATION OF APPLIED STRESS AND RESULTANT STRAIN RATE 38
3.2. DEFORMATION APPARATUS 43
3.2.1. Apparatus for uniaxial compression deformation 43
3.2.2. Apparatus for simple shear deformation 45
3.3. TEMPERATURE CONTROL 45
3.4. EXPERIMENTAL PROCEDURE 48

3.5. THIN SECTIONING 49
3.6. MEASUREMENT OF CRYSTAL ORIENTATION FABRIC 49
3.7. DETERMINATION OF CRYSTAL SIZE 50

4. ICE DEFORMATION TESTS IN UNIAXIAL COMPRESSION 51

4.1. STRAIN CURVES AND STRAIN RATES 51
4.1.1. Strain curves 51
4.1.2. Minimum strain rates 52
4.1.3. Tertiary strain rates 54
4.1.4. Enhancement factor 54
4.2. THE FACTORS AFFECTING THE FLOW OF ICE 55
4.2.1. Effect of impurities on tertiary strain rate 55
4.2.2. Effect of initial crystal orientation fabric on minimum strain rate 56
4.3. STEADY STATE FLOW OF ICE IN COMPRESSION DEFORMATION 59
4.3.1. Steady state tertiary strain rate 60
4.3.2. Steady state crystal orientation fabric 60
4.3.3. Steady state crystal size 63
4.4. SUMMARY 66

5. ICE DEFORMATION TESTS IN SIMPLE SHEAR 67

5.1. RE-MEASUREMENT TO THE ICE TEST SAMPLES 67
5.2. EXPERIMENTAL RESULTS 68
5.2.1. Strain curves and strain rates 68
5.2.2. Comparison of strain rate differences for laboratory prepared isotropic ice in shear and compression 69
5.2.3. Crystal orientation fabric 71
5.2.4. Crystal size 74
5.3. THE FACTORS AFFECTING THE FLOW OF ICE 74
5.3.1. Effect of impurities on tertiary flow 76
5.2.2. Effect of initial crystal orientation fabric on minimum strain rate 76
5.4. STEADY STATE FLOW OF ICE IN SHEAR DEFORMATION 79
5.5. SUMMARY 80

6. CONCLUSIONS AND PROPOSALS FOR FURTHER WORK 82

6.1. CONCLUSIONS 82
6.2. STEADY STATE ICE FLOW 83
6.3. PROPOSALS FOR FURTHER EXPERIMENTAL PROGRAMS 83

REFERENCES 85

APPENDIX I CREEP CURVES AND CRYSTAL STRUCTURE MEASUREMENTS FOR UNIAXIAL COMPRESSION TESTS 94

APPENDIX II CREEP CURVES AND CRYSTAL STRUCTURE MEASUREMENTS FOR SIMPLE SHEAR TESTS 118

LIST OF FIGURES

page

2.1 Profiles of AGZ 77 ice core properties 13

2.2 Profiles of BHC1 ice core properties 14

2.3 Profiles of DYE 3 ice core properties 15

2.4 Initial crystal orientation fabrics and distribution histograms of test samples 17

2.5 Initial thin section photographs of test samples 24

2.6 Dust concentrations 31

3.1 Schematic diagram of uniaxial compression 39

3.2 Schematic diagram of simple shear 41

3.3 The direct load compression apparatus 44

3.4 Simple shear apparatus 46

3.4 a Dimensions indicated are typical initial dimension for an ice sample in shear 47

4.1 Tertiary strain rates in compression as a function of dust concentration 57

4.2 Tertiary strain rates in compression as a function of soluble impurity concentration 58

4.3 Crystal size in compression as a function of total octahedral shear strain 64

5.1 Crystal size in shear as a function of total octahedral shear strain 75

5.2 Tertiary strain rates in shear as a function of dust concentration 77

5.3 Tertiary strain rates in shear as a function of soluble impurity concentration 78

APPENDIX I Creep curves and crystal structure measurements for uniaxial compression tests 94

APPENDIX II Creep curves and crystal structure measurements for simple shear tests 118

LIST OF TABLES

page

2.1 Sources of ice test samples 10

2.2 Properities of the three boreholes 12

2.3 Impurity concentrations and oxygen-isotope ratios for all test samples 34

4.1 Strain rates and strains in compression tests 53

4.2 Data for crystal orientation fabric and size resulting from compression tests 61

5.1 Data in simple shear tests 70

5.2 Data for crystal orientation fabrics resulting from simple shear tests 72

ACKNOWLEDGMENTS

I am grateful to my supervisors, Prof. W.F. Budd and Dr. T.H. Jacka for continuous encouragement and much discussion. I am much indebted to Dr. T.H. Jacka for his improvement of my written English.

Particular thanks are due to the University of Copenhagen, Geophysical Institutes, for supplying Dye3 ice core samples, Department of Environment, Canada, for supplying AGZ77 ice core samples, and to the Australian Antarctic Division for supplying BHC1 ice core samples. Colin Wookey and J.P. Steffensen measured the ice test samples for soluble and insoluble impurities, and oxygen isotope ratio.

I wish to thank the Antarctic Division Glaciology Program for supplying experimental facilities. Glaciology Program staff have also provided computing assistance, discussion of test results and instrumentation fabrication assistance. I also thank my husband and my colleague, Li Jun, for his continuous encouragement and assistance.

ABSTRACT

Ice mechanical experiments in uniaxial compression and in simple shear configurations were carried out at 0.2 MPa octahedral shear stress and - 5 °C on ice core samples deposited as snow during the Wisconsin and Holocene periods. Tested samples were selected from ice cores drilled in South Greenland (Dye 3), Ellesmere Island, Canada (Agassiz Ice Cap) and East Antarctica (Law Dome Ice Cap), with an aim to finding the reasons for different flow rates between Wisconsin ice and Holocene ice. These different flow rates, reported by some glaciologists, were inferred from field measurements of borehole closure and inclination. The ice test samples were analysed for crystal size and orientation fabric, and soluble and insoluble impurity concentrations.

The experiments, in two different stress configurations, gave coincident results. With the progression of strain, the deformation of the Wisconsin ice and of the Holocene ice tended to reach a constant tertiary (steady state) flow rate. Ice with a c-axis fabric pattern compatible with the applied stress configuration (small circle girdle pattern for compression and single maximum pattern for shear) reached steady state flow directly, without passing through a minimum creep stage. For the steady state tertiary flow, there was no evidence found of any significant difference between the flow rates of Wisconsin and Holocene ice. Crystal size and the presence of impurities (in the concentrations found in the different ice samples) seemed not to affect the ice flow rates at the temperature and stress tested. The ice flow rates were found to be determined mainly by crystal orientation fabric pattern. It is concluded therefore, that the more rapid flow measured in some field projects for the Wisconsin ice is primarily due to enhanced crystal orientation strength.

1. INTRODUCTION

1.1. NEED FOR INVESTIGATION

It has been found from field results on the Greenland, Antarctic and other ice masses, that flow rates of ice laid down on the ice sheet during the Wisconsin period (i.e. during the last Great Ice Age) are a factor of 2 to 4 greater than those for ice from the Holocene period (since the Ice Age). Hooke (1973) apparently first observed this characteristic in borehole deformation experiments on Barnes Ice Cap, Baffin Island, Canada. The borehole deformation experiments on Devon Ice Cap (Paterson, 1977) and Agassiz Ice Cap in Canada (Fisher and Koerner, 1986), and at Dye 3 in south Greenland (Dahl-Jensen and Gundestrup, 1987) documented a similar softness of Wisconsin ice. This suggests further effects on ice flow of some parameters which have not as yet been accounted for, and which are different or in different concentrations in Wisconsin ice than in Holocene ice.

Some ice core analyses, mainly in the Northern Hemisphere, have shown that the ice deposited during the glaciation has smaller crystals, a stronger fabric, and higher concentrations of soluble and insoluble impurities than has ice deposited during the Holocene period. The contrast is especially strong for ice from the last part of the glaciation (the " late Wisconsin " in North America) (Hooke and Hudleston, 1980; Hooke and others, 1988; Dahl-Jensen and Gundestrup, 1987; Herron and Langway, 1982; Thompson , 1977; Thompson and Mosley-Thompson, 1981). However, the situation in Antarctica is less clear-cut. On Law Dome for example, the Holocene ice, rather than Wisconsin ice, has relatively smaller crystals, a stronger fabric, and higher concentrations of soluble and insoluble impurities (Thwaites and others, 1984; Xie, 1985; Han and Young, 1988).

Dahl-Jensen and Gundestrup (1987) attributed the enhanced deformation rate of Wisconsin ice relative to Holocene ice at Dye 3 primarily to the high concentration of dust and other impurities (chloride and sulphate ions) and/or to the small crystal size exhibited

at the same depth. Fisher and Koerner (1986) ascribed the enhanced flow in Agassiz Ice Cap to high concentrations of dust or calcium. Paterson (1991) reviewed the data on the mechanical properties, texture, fabric, and impurity content of Holocene and Wisconsin ice from Barnes, Agassiz and Devon Ice Caps (Canada), Dye 3 and Camp Century (Greenland), Byrd Station (West Antarctica) and Vostok and Law Dome (East Antarctica). He concluded that chloride and possibly sulphate ions, in concentrations high in Wisconsin ice relative to those in Holocene ice, impeded grain-boundary migration and grain growth so that the crystals in Wisconsin ice remained small. Such ice, in shear parallel to the ice-sheet bed, developed a strong, near-vertical, single-maximum fabric. This fabric favours further deformation and this, in turn, further strengthens the fabric and keeps the crystals small. Thus the strain rate in Wisconsin ice, in simple shear, is some 2.5 times that in Holocene ice at the same stress and temperature.

Mechanical tests on the Wisconsin ice from the Dye 3 core (Shoji and Langway, 1988) and on the ice samples dated in the last interglacial period from the Vostok core (Pimienta and Duval, 1988) indicated that the high impurity concentrations in glacial ice did not seem to influence the mechanical behaviour of the Vostok core ice and Dye 3 core ice, and that the enhanced flow measured from the field appeared to be caused mainly by the vertical orientation of the c-axes.

This project examines these different flow results in the laboratory, with an aim to establishing the validity of the field measurements and to finding the reasons for the different flow rates.

Laboratory experiments involving deformation tests on ice have shown that the flow of ice is dependent on temperature and stress (Budd and Jacka, 1989). Given sufficiently high deformation (strain) a tertiary, steady state ice creep rate is established. Along with the development of this steady state creep rate, a steady state (or equilibrium) crystal size and a steady state crystal orientation fabric also develops. The actual crystal orientation fabric pattern developed is dependent on the stress configuration (i.e. whether the ice is deformed in compression, shear, extension, etc. or a combined stress configuration). The

equilibrium crystal size dependence is the subject of ongoing research, and this project will contribute in part to the crystal size knowledge.

1.2. THE FLOW OF ICE

1.2.1. The flow law for ice

The flow of ice is due to internal deformation generated by a non-hydrostatic stress field. Based on experimental data for randomly oriented polycrystalline ice in uniaxial compression, Glen (1955) found that the secondary strain rate varied as a power of the stress, suggesting an empirical power law representation of the form

$$\dot{\varepsilon}_x = A\sigma_x^n \tag{1.1}$$

where $\dot{\varepsilon}_x$ is the compressive strain rate, σ_x is the compressive stress and A and n are constants. A large range of flow rates for ice obtained from laboratory ice deformation tests as well as from field ice tunnel closure rates and borehole tilting measurements has suggested that the exponent n has the mean value of 3 and the value of A varies with temperature and other properties of the ice (e.g. Glen 1958; Budd 1968; Hooke 1981; Budd and Jacka 1989). Similar relations between shear strain rate $\dot{\varepsilon}_{xy}$ and shear stress τ_{xy} have also been found in simple shear tests (e.g. Steinemann 1958; Gao and others 1989).

Glen (1958) further discussed the theoretical possibilities of a flow law based on the relationship between the stress and strain rate tensors. He presented a general form of a three dimensional flow law of ice in which the stain rate tensor is a function of the three invariants of the stress tensor assuming isotropic polycrystalline ice for which the strain rate depends on stress alone. Glen (1958) assumed incompressibility and independence of ice flow from the first invariant of the stress tensor (Rigsby 1958; Higashi and Shoji 1979; Jones 1982). In order to compare ice flow rate data from laboratory experiments with field tunnel closure rates, Nye (1953) suggested that the components of strain rate are proportional to the components of the stress deviator, with the constant of

proportionality a function of the second invariants only. Combining these further assumptions, Glen (1958) finally proposed that the general form of the flow law can be reduced to

$$\dot{\varepsilon}_{ij} = B(I_2')\,\sigma_{ij}' \tag{1.2}$$

where $\dot{\varepsilon}_{ij}$ is the strain rate tensor, σ_{ij}' the stress deviator tensor, and B is a scalar function of I_2', the second invariant of the stress deviator tensor. Considering the effects of other factors such as temperature, crystal structure, ice density etc., Equation (1.2) may be written in terms of the polycrystalline fluidity

$$\dot{\varepsilon}_{ij} = \lambda\sigma_{ji}' \tag{1.3}$$

where $\lambda=\lambda(I2, f, \theta, \rho, \cdots)$ is a scalar function of the second deviator stress invariant, temperature θ, crystal structure f, ice density ρ and so on.

The strain rate tensor is related to the velocity gradients by the definition

$$\dot{\varepsilon}_{ij} = u_{j,i} \tag{1.4}$$

where $u_{j,i}$ are the gradients of the velocity components in each coordinate direction. In addition, the assumption of incompressibility implies

$$\dot{\varepsilon}_{ii} = 0 \tag{1.5}$$

Equation (1.3) has been widely used for most calculations in glacier and ice sheet modelling. It is clear that a successful dynamics model relies on an accurate specification of the flow law (equation 1.3) for ice.

1.2.2. The flow of anisotropic ice

The theoretical considerations of ice flow as discussed in the previous section are based on the assumption that ice consists of fine-grained randomly oriented crystals forming a statistically homogeneous and isotropic material. In natural ice sheets the compatible isotropic ice only exists at shallow depths typically less than several hundred meters. The

large amounts of deeper ice have a highly anisotropic crystal structure which is the result of continuous deformation to large strain accompanied by several processes such as crystal rotation, recrystallisation and crystal growth (Steinemann 1954, 1958; Budd 1972; Rigsby 1960; Kamb 1972; Gow and Williamson 1976; Budd and Jacka 1989). A large number of field and laboratory studies of ice deformation have indicated that the crystallographic anisotropy plays an important role in the flow of ice. The anisotropy due to flow induced crystal orientations has the most significant effect on ice flow rate. Single crystal shear deformation studies of ice have shown that single crystals oriented for easy glide (shear direction parallel to basal planes) deform faster by 2 to 3 orders of magnitude than those oriented for hard glide under similar conditions of temperature and applied stress (Shumskii 1958; Rigsby 1958, 1960; Butkovich and Landauer 1958; Vialov 1958; Wakahama 1967). Deformation tests on polycrystalline ice with a developed crystal orientation fabric have shown that creep rates are enhanced when the preferred orientation fabrics are compatible with the stress configuration and that compatible preferred orientations are induced by the flow situation (e.g. Gao and Jacka 1987; Russell-Head and Budd 1979; Shoji and Langway 1985a,b).

Following Weertman's (1963) lead, Lile(1984) made a quantitative study of the effect of preferred c-axis orientation fabrics on the flow rate of ice. He considered an ice aggregate as a collection of interconnected crystals deforming independently by basal glide but with the influence of preferred orientations on the mean intergranular rate of strain treated in terms of a redistribution of the magnitude and orientation of resolved basal shear stress and the resistance between crystals. He then established a model relating the deformation rate of an anisotropic polycrystal to that of an isotropic polycrystal developed in terms of an enhancement factor applied to the bulk isotropic fluidity in the flow law.

Laboratory ice creep tests on initially randomly oriented polycrystalline ice under constant stress indicate that the minimum strain rate is attained at about 1% octahedral shear strain. Beyond this, and associated with changes in crystal structures the strain rate increases. This can be considered as an enhancement of strain rate above the minimum as a function

a function of strain and is also related to the crystal fabric development. The enhanced strain rate asymptotically approaches a near constant final value beyond about 10% octahedral shear strain with enhancement factor of about 3 for uniaxial compression and 5 to 8 for simple shear (cf. Jacka and Maccagnan 1984; Russell-Head 1985; Gao and others, 1989; Jacka and Budd 1989).

A large number of experimental results have shown that the various crystal orientation fabric patterns found in the natural ice sheets can be produced in the laboratory by deforming ice samples through the application of a similar total strain, dominant stress configuration and temperature. Unconfined uniaxial compression produces a small circle girdle fabric with c-axes clustered in a ring centred on the compression axis (Jacka and Maccagnan 1984; Gao and Jacka 1987). This type of fabric occurs in the upper zones of the ice thickness in natural ice sheets where the ice deformation is dominated by a net vertical compression (Jacka and Gao 1989). Vertical compression confined to 2 dimensions (approximately plane strain) produces 2 maxima centred in the plane of deformation at a similar angle to the vertical (Budd and Matsuda 1974). The upper ice fabrics may be expected to vary between these two extreme cases depending on the transverse strain rate. Simple shear initially develops a fabric with two maxima but, due to rotation, this changes to a single maximum in the direction perpendicular to the plane of shear, provided the deformation continues to large strain (Bouchez and Duval 1982; Kamb 1972; Gao and others 1989). In the large polar ice sheets, single maximum fabrics, associated with fine crystals, generally exist around the third quarter of the depth where strong horizontal shear deformation dominates (e.g. Gow and Williamson 1976; Herron and Langway 1982; Hooke and Hudleston 1981). A multiple-maxima fabric pattern is sometimes exhibited in the ice near the base of ice sheets particularly where the ice temperature is warmer than -10 °C (e.g. Gow and Williamson 1976; Matsuda and Wakahama 1978; Kamb and Shreve 1963; Xie 1985). This ice invariably consists of large crystals consistent with the higher temperatures and possibly low deformation rates for the ice in which it is found. Comparable fabric patterns have also been developed in the

laboratory through crystal growth associated with stress relaxation and annealing (Gao unpublished).

1.3. EXPERIMENTAL PROJECT FOR THE STUDIES

In order to investigate why the ice deposited during the Wisconsin period is "softer" than the Holocene ice, two sets of experiments were decided upon. Ice samples, representative of both the Wisconsin and Holocene periods, were tested in uniaxial compression along the axis of the core, and in simple shear parallel to the ice basal plane.

The ice test samples were selected from Law Dome, Antarctica (supplied by the Australian Antarctic Division), from Dye 3, Greenland (supplied by the University of Copenhagen, Geophysical Institute) and from Agassiz Ice Cap (supplied by the Department of Environment, Canada). The samples, taken from dated ice cores, were from different depths in the ice masses representing both Wisconsin and Holocene ice. Each of the ice core samples was cut into two test specimens; one a cylindrical specimen for compression tests and the other, a rectangular specimen for shear tests. Each sample was measured for crystal orientation fabric, crystal size, soluble and insoluble impurity concentration, etc. in an attempt to accurately assess all differences between the test samples that might account for different flow rates. To maintain a comparison standard, laboratory prepared, "clean" samples were also measured and tested along with the core samples.

All tests were carried out at the same octahedral shear stress and temperature so that results are compatible. The ideal experimental stress and temperature would be the same as that in the ice sheet (i.e. about 0.1MPa and - 12 °C for the Dye 3 core, - 16 °C for the Agassiz core and - 1 °C for BHC1 core). With the exception of the BHC 1 core samples, tests at these temperatures would take an unacceptably long time to attain minimum and steady state creep rates (Jacka, 1984a). As a compromise, a stress of 0.2 MPa and a temperature of - 5 °C was chosen. All tests were run to tertiary steady state creep or to a total octahedral shear strain of at least 10%. In addition, some samples were tested in

compression to total strains of the order of 40%. This eliminates the effects of the original crystal orientation fabric and crystal size, so that any differences in strain rate at this stage would be due to impurities.

2. SELECTION OF ICE CORE TEST SAMPLES

2.1. SELECTION OF ICE CORE SAMPLES

2.1.1. Sources of ice core samples

Test ice samples were selected from cores drilled at Dye 3, Greenland and AGZ 77, Agassiz Ice Cap, Ellesmere Island, North-west Canada in the northern hemisphere, and in the Southern Hemisphere, from BHC 1 on Law Dome, Antarctica. The samples are from different depths (Table 2.1) in the ice masses such that they were originally deposited on the ice cap surface during different climatic epochs.

Six ice samples taken from the AGZ 77 core were supplied by the Department of Environment, Canada. Three of these samples consisted of Wisconsin ice from core depths of 331.0, 331.7 and 332.9 m and three of pre-Wisconsin ice from depths of 336.2, 337.1 and 337.9 m

Eight ice samples were from the BHC 1 core, supplied by the Australian Antarctic Division. Three of these were Holocene ice from depths of 147, 160 and 170 m, three were from the Holocene / Wisconsin transition period from depths of 217, 232 and 242 m and two were Wisconsin ice from depths of 267 and 274 m.

Four samples taken from the Dye 3 ice core were supplied by the Geophysical Institute of the University of Copenhagen. They included two Holocene samples from depths of 418.88 and 1607.37 m and two Wisconsin samples from 1812.75 and 1972.07 m.

Six laboratory prepared ice samples were also included for the study to provide a basis for comparison. These samples were prepared by the technique described by Jacka and Lile (1984). Examination of the physical properties of these samples is discussed along with the properties of the ice core samples in the following sections.

Table 2.1 Sources of ice core samples.

sample number	origin of ice	period	depth (m)
AGZ77-225A	Agassiz Ice Cap	Wisconsin	331.03
AGZ77-225B	Agassiz Ice Cap	Wisconsin	331.7
AGZ77-226	Agassiz Ice Cap	Wisconsin	332.885
AGZ77-228	Agassiz Ice Cap	pre-Wisconsin	336.18
AGZ77-229	Agassiz Ice Cap	pre-Wisconsin	337.105
AGZ77-230	Agassiz Ice Cap	pre-Wisconsin	337.9
BHC1-73B	Law Dome Ice Cap	Holocene	147
BHC1-79C	Law Dome Ice Cap	Holocene	160
BHC1-84B	Law Dome Ice Cap	Holocene	170
BHC1-108D	Law Dome Ice Cap	Transition	217
BHC1-116D	Law Dome Ice Cap	Transition	232
BHC1-121B	Law Dome Ice Cap	Transition	242
BHC1-134D	Law Dome Ice Cap	Wisconsin	267
BHC1-138C	Law Dome Ice Cap	Wisconsin	274
DYE3-T338	Greenland Ice Sheet	Holocene	418.88
DYE3-T1556	Greenland Ice Sheet	Holocene	1607.37
DYE3-T1763	Greenland Ice Sheet	Wisconsin	1812.75
DYE3-T1922	Greenland Ice Sheet	Wisconsin	1972.07

2.1.2. Description of the ice core physical properties

Table 2.2. is a summary of data from the three ice cores from which the test ice samples were taken. Profiles of shear strain rate, crystal fabric and size, dust and $d^{18}O$ for the three ice cores are presented in Figure 2.1 (AGZ 77 core), Figure 2.2 (BHC 1 core) and Figure 2.3 (Dye 3 core). Depths from which test samples were selected are indicated in the above figures. All three ice cores were drilled to near bedrock.

The AGZ 77 core, drilled in 1977, is one of three cores drilled through the Agassiz Ice Cap. The ice cap is approximately 16 000 km^2 in area. The 338 m deep AGZ 77 core is 1 km down - slope from a local ice divide, at an elevation of 1 700 m. At the site, the annual accumulation rate is 0.161 $m(H_2O)a^{-1}$ and the mean annual temperature is - 24.2 °C. As shown in Fig. 2.1a, in the lower sections of the core there are two broad zones of enhanced flow at 0.2 and 4.5 to 8 m above the bed. The Holocene / Wisconsin boundary is at the depth of 330 m. The base temperatures is - 16.7 °C (Fisher and Koerner, 1986, 1988; Fisher, 1987).

The Law Dome Ice Cap is a small (~ 200 km diameter) ice cap, isolated from the main East Antarctic Ice Sheet by two large glaciers (Vanderford Glacier and Totten Glacier). The summit elevation is 1395 m. The 300 m deep BHC 1 site is 6 km from the coastal ice cliff margin where the annual accumulation rate is 0.06 $m(H_2O)a^{-1}$ and the mean annual temperature is - 12 °C (Etheridge, 1990). Borehole inclinometer measurements (Fig. 2.2a) reveal two bands of enhanced flow indicating an upper shear zone at ~ 200 to 235 m depth and a lower shear zone at ~ 250 to 275 m. The Holocene / Wisconsin boundary occurs in the upper shear zone at ~ 225 m . The lower shear zone therefore is entirely Wisconsin ice. The basal ice is at the pressure melting point of - 1.0 °C (Etheridge, 1989; Paterson, 1991).

The 2037 m deep Dye 3 ice core is from a site 41.5 km east of a local ice divide, in southern Greenland. The annual accumulation rate is 0.5 $m(H_2O)a^{-1}$ and the mean annual temperature is - 19 °C. This core was drilled during the period 1979 to 1981 by the

Table 2.2 Properties of the three boreholes.

ice core	location	depth (m)	Holocene/ Wisconsin boundary (m)	bottom temperature (°C)	mean annual temperature (°C)	annual accumulation rate (water mm/a)
AGZ 77	80° 45' N 73° 35' W	338	330	-16.7	- 24.2	161
BHC 1	66° 07' S 110° 58' E	300.2	225	-1.0	-12	60
DYE 3	65.19° N 43.82° W	2037	1786	-12	- 19	500

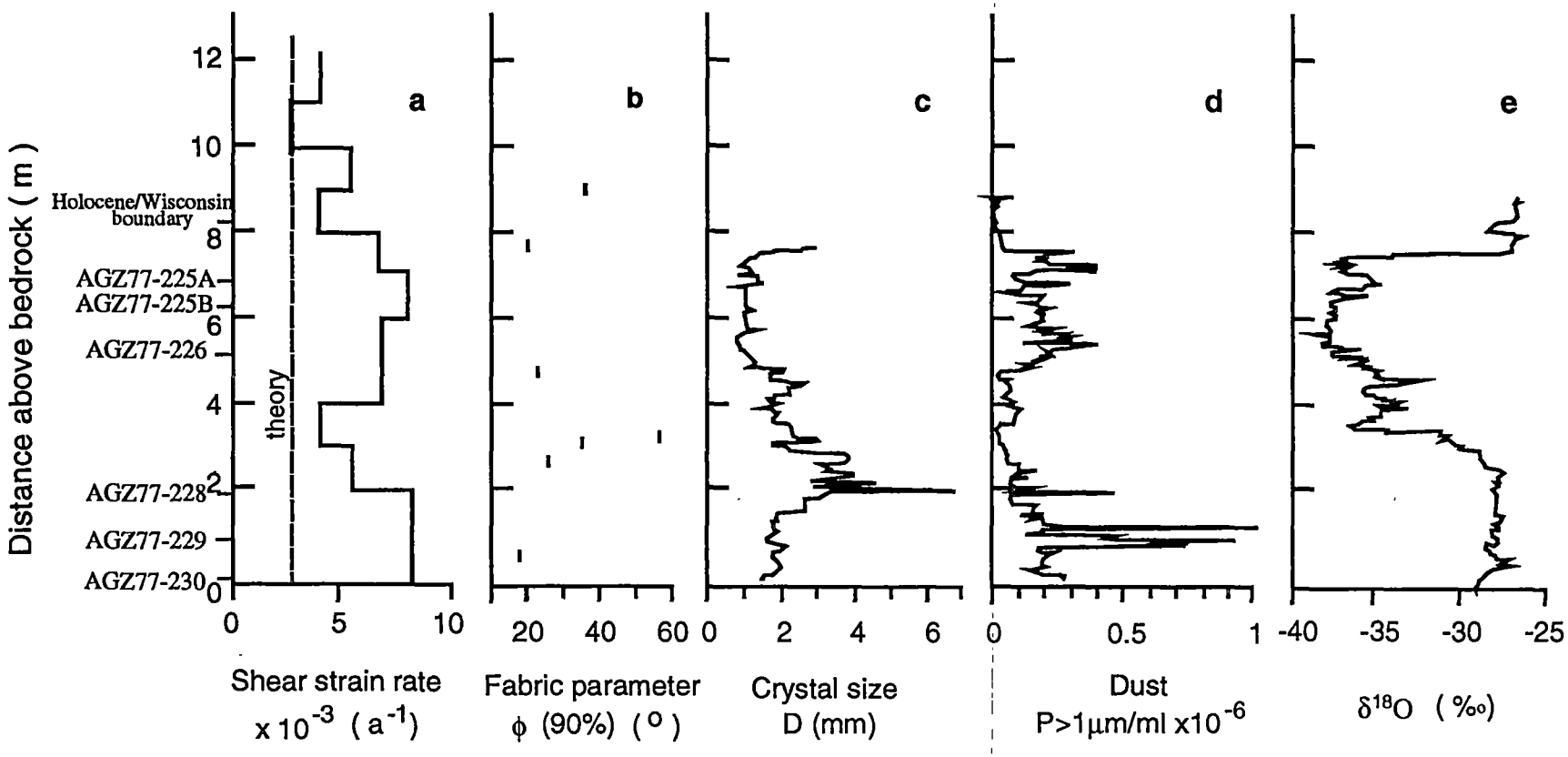

Figure 2.1 Profiles of (a) shear strain rate, (b) fabric parameter - the half-apex angles of the cones containing 90% of the c-axes, (c) crystal size, (d) dust concentration and (e) $\delta^{18}O$ for AGZ77 ice core (after Fisher and Koerner, 1986). The indicators show the positions from which the test samples were taken.

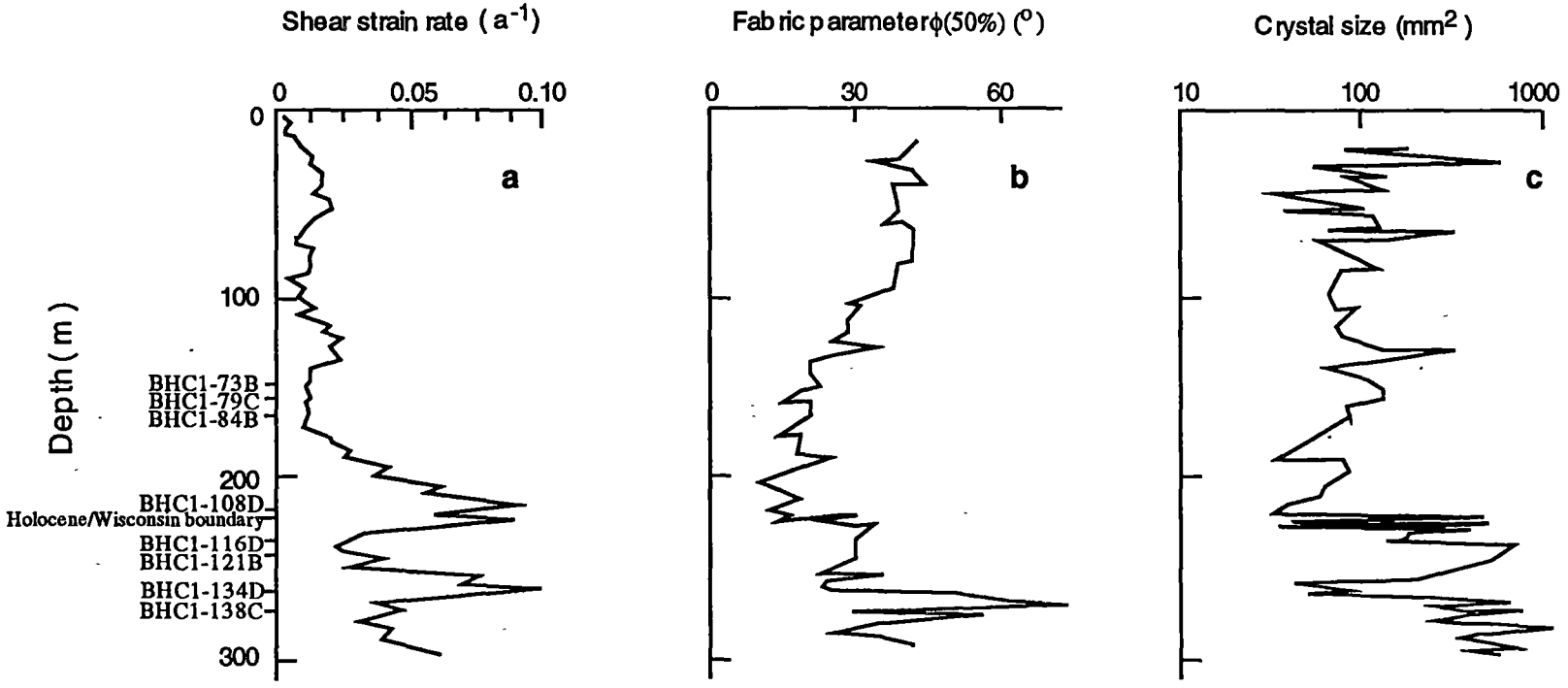

Figure 2.2 Profiles of (a) shear strain rate, (b) fabric parameter - the half-apex angles of the cones containing 50% of the c-axes and (c) crystal size for BHC1 ice core (after Han and Young, 1988). The indicators show the positions from which the test samples were taken.

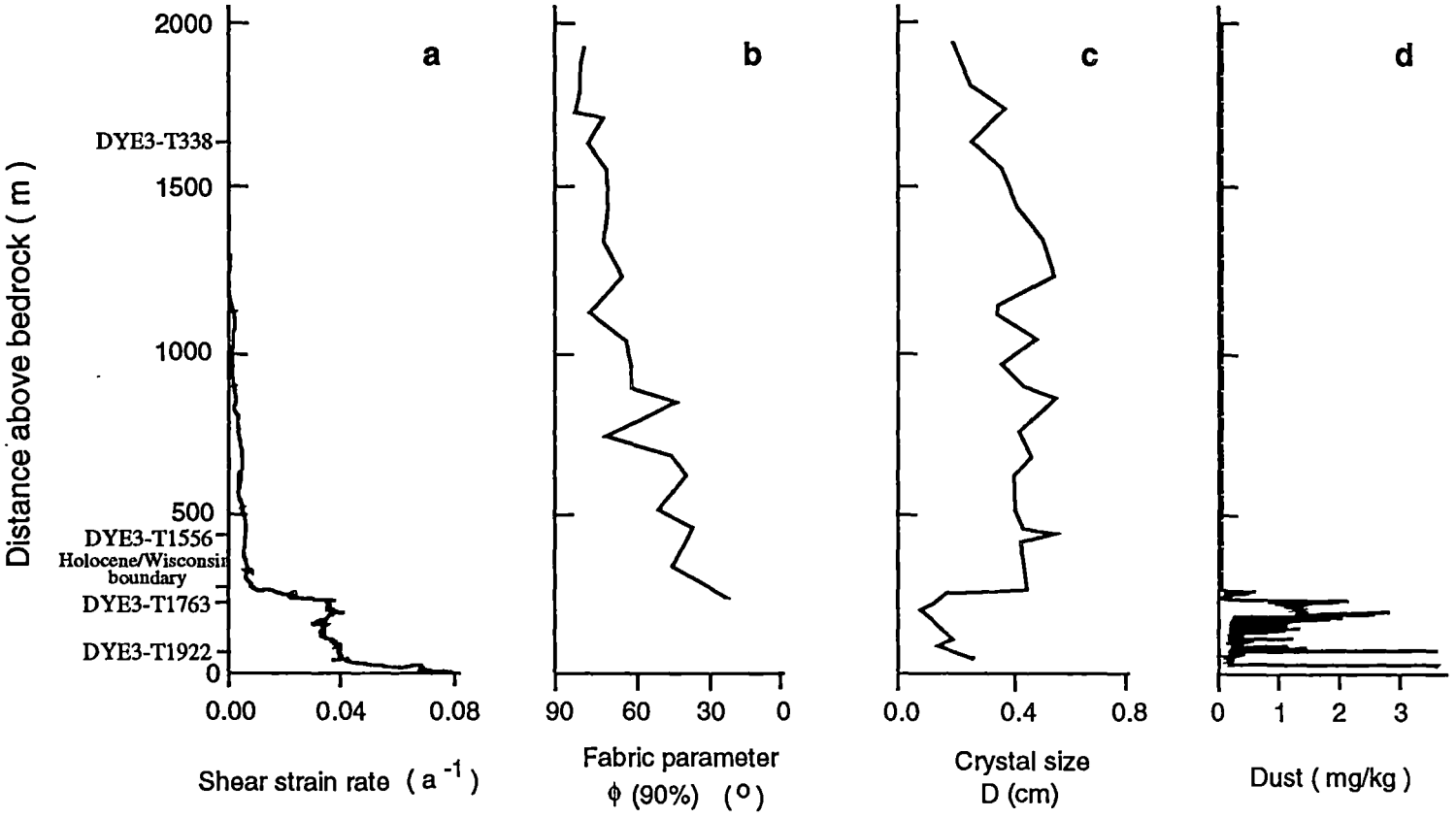

Figure 2.3 Profiles of (a) shear strain rate, (b) fabric parameter - the half-apex angles of the cones containing 90% of the c-axes, (c) crystal size and (d) dust concentration for DYE3 ice core (after Dahl-Jensen and Gundestrup, 1987). The indicators show the positions from which the test samples were taken.

Greenland Ice Sheet Program (GISP) (Langway and others, 1985). Fig. 2.3(a) shows that the shear strain rate profile can be divided into three zones - the bottom 25 m of silty ice exhibiting very high shear strain rates, the immediately overlying 230 m of Wisconsin ice, and the uppermost 1 780 m of Holocene ice, exhibiting lower shear strain rates (Dahl-Jensen and Gundestrup, 1987). The Holocene / Wisconsin boundary is at a depth of 1 786 m (Dansgaard and others, 1982, 1985). The base temperature is - 12 °C (Gundestrup and Hansen, 1984).

2.2. PROPERTIES OF TEST SAMPLES

All selected ice core samples were analysed for crystal orientation fabric, crystal size and texture, impurity content and oxygen isotope ratio.

2.2.1. Crystal orientation fabrics

Since crystal orientation fabrics in ice sheets provide a record of deformational history and strongly influence the rate of deformation, each test sample was measured for crystal orientation fabric prior to testing in both uniaxial compression and simple shear; i.e. the measured c-axis orientation fabrics were characteristic of the actual test samples, rather than the core section from which they were cut. The measurements were carried out under a modified universal stage (Morgan and others, 1984) using the technique described by Langway (1958). The fabric diagrams and associated c-axis distribution histograms for all compression test samples are shown in Figure 2.4. Those for simple shear tests are presented in Chapter 5.

For AGZ77 core samples, all six Wisconsin and pre-Wisconsin ice test samples (between depths of 331.03 and 337.9 m) show a strong single maximum with a c-axis mean angle of 26 to 15° off the vertical and a corresponding standard deviation of 14.08 to 8.15°. The c-axis mean angle and the corresponding standard deviation reduce respectively from 23 and 14.08° at 331.03 m depth to 15 and 8.15° near the base, i.e. the crystal orientation fabrics seem to strengthen and rotate towards the vertical with increasing depth and/or age. Fisher and Koerner (1986) measured the crystal c-axis orientations on seven thin sections

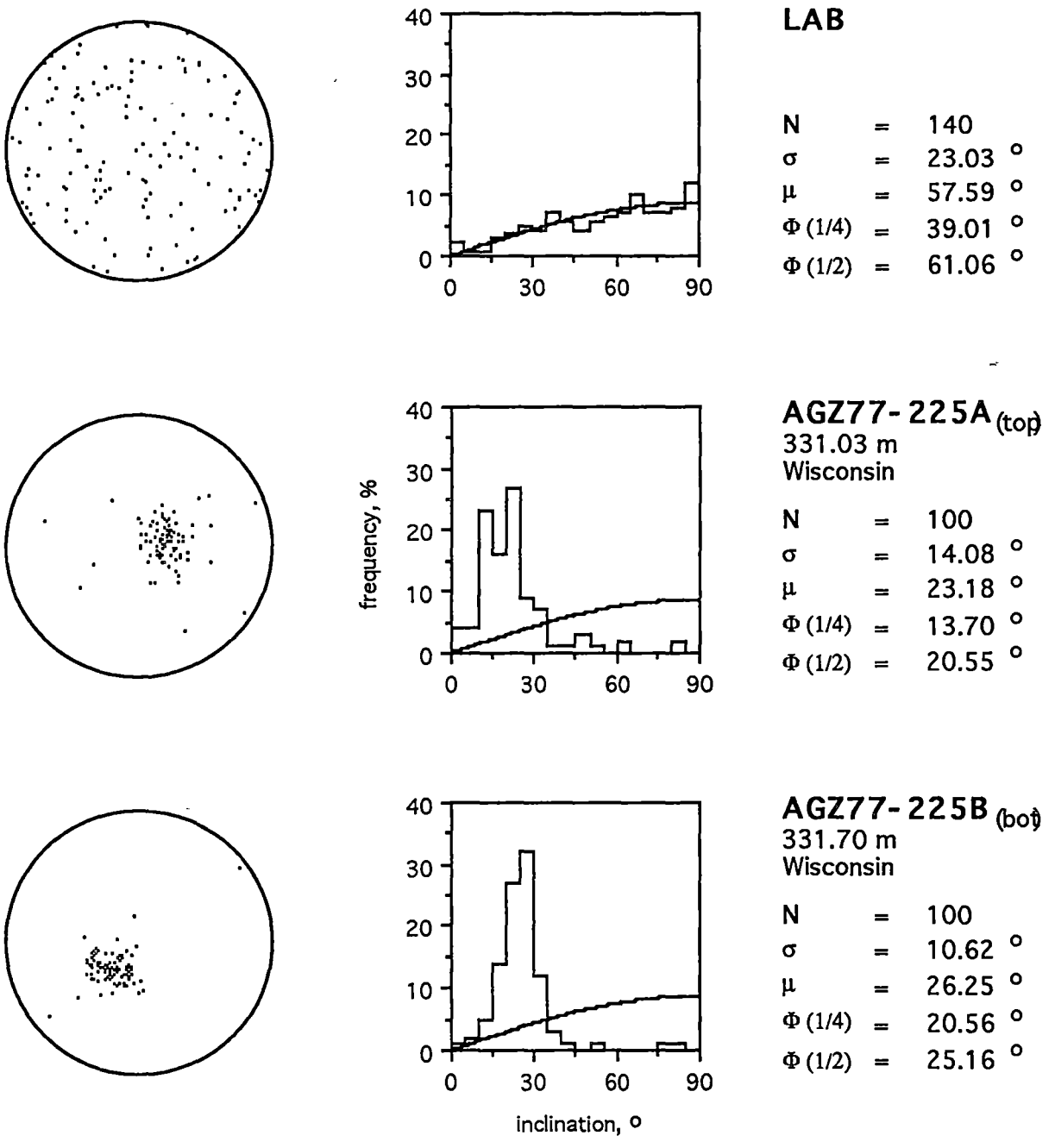

Figure 2.4 (5 pages) Initial crystal orientation fabrics and associated c-axis distribution histograms for all ice samples in compression tests. The symbol (top) or (bot) under the sample number indicates that the fabric was measured from top or bottom horizontal section. The depth and climatic period of the samples are indicated. Also indicated are the number of crystals oriented, N, the standard deviation, σ and mean, μ, of the crystal c-axis angles to the vertical. $\phi(1/4)$ and $\phi(1/2)$ indicate the half-apex angles of the cones containing 25% and 50% of the c-axes. The sine curve indicates a uniform distribution of c-axes.

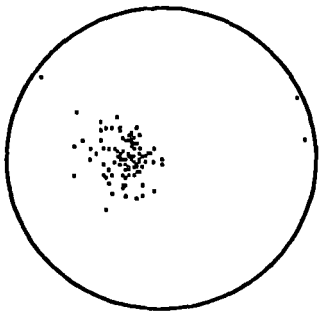

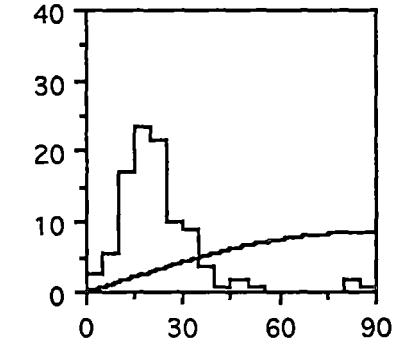

AGZ77-226 (bot)
332.885 m
Wisconsin

N	=	110
σ	=	13.96 °
μ	=	23.14 °
Φ (1/4)	=	14.86 °
Φ (1/2)	=	20.21 °

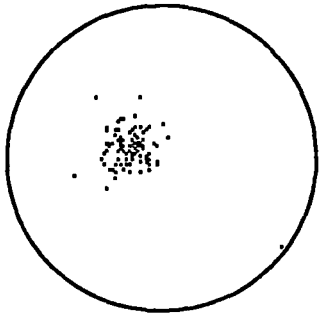

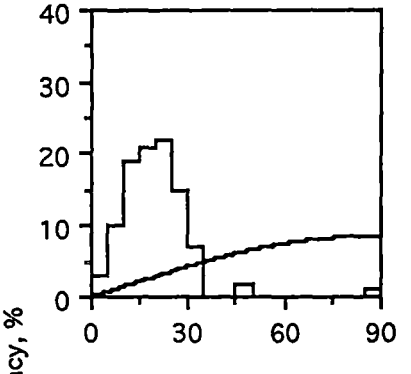

AGZ77-228 (bot)
336.18 m
Pre-Wisconsin

N	=	100
σ	=	10.71 °
μ	=	20.64 °
Φ (1/4)	=	13.16 °
Φ (1/2)	=	19.29 °

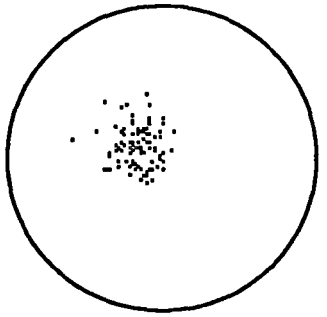

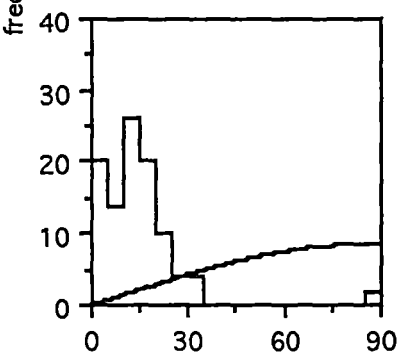

AGZ77-229 (bot)
337.105 m
Pre-Wisconsin

N	=	100
σ	=	8.78 °
μ	=	18.69 °
Φ (1/4)	=	13.00 °
Φ (1/2)	=	18.00 °

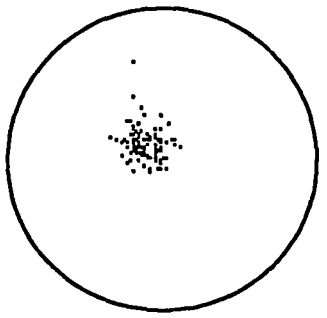

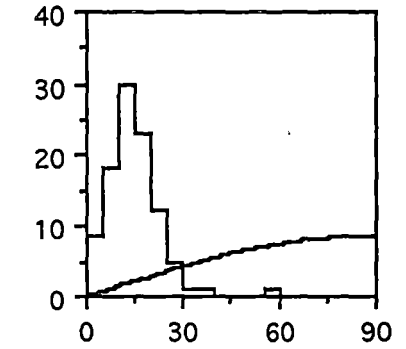

AGZ77-230 (bot)
337.90 m
Pre-Wisconsin

N	=	100
σ	=	8.15 °
μ	=	15.11 °
Φ (1/4)	=	9.45 °
Φ (1/2)	=	13.86 °

frequency, %

inclination, °

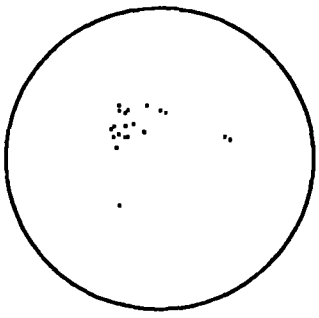

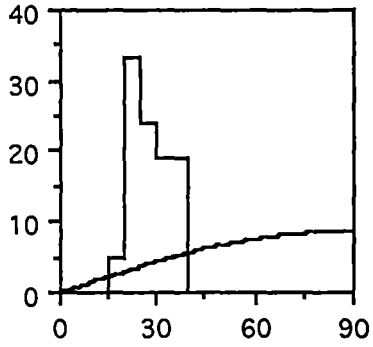

BHC1-73B (top)
147 m
Holocene

N	=	21
σ	=	6.31 °
μ	=	28.67 °
Φ (1/4)	=	25.00 °
Φ (1/2)	=	29.00 °

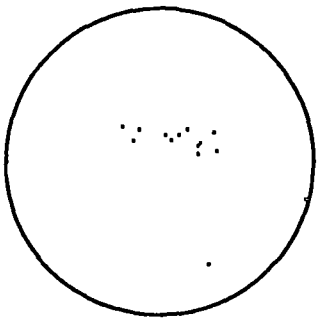

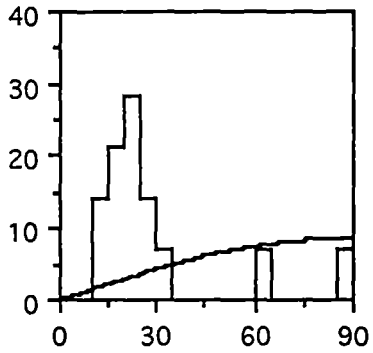

BHC1-79C (bot)
160 m
Holocene

N	=	14
σ	=	20.74 °
μ	=	29.21 °
Φ (1/4)	=	15.00 °
Φ (1/2)	=	20.00 °

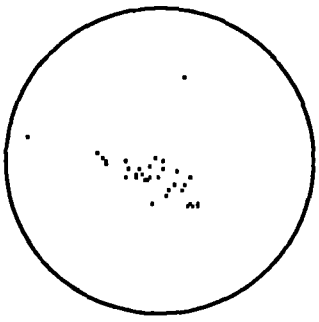

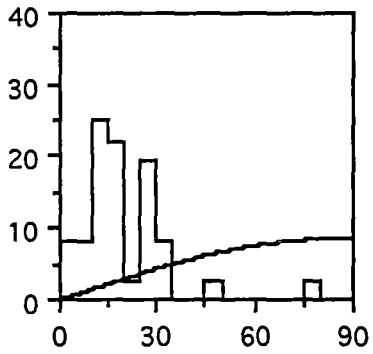

BHC1-84B (bot)
170 m
Holocene

N	=	36
σ	=	13.86 °
μ	=	20.72 °
Φ (1/4)	=	11.68 °
Φ (1/2)	=	16.89 °

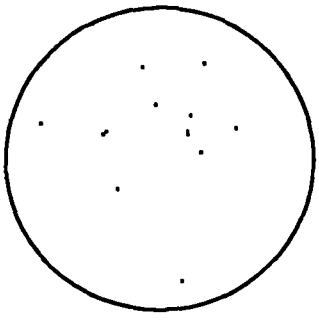

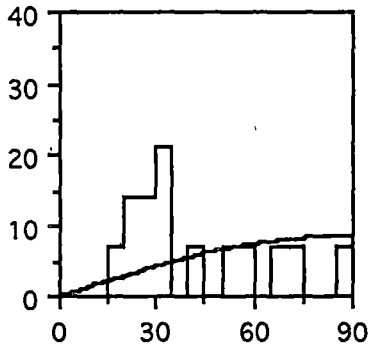

BHC1-108D (top)
217 m
Transition

N	=	14
σ	=	21.71 °
μ	=	43.00 °
Φ (1/4)	=	28.00 °
Φ (1/2)	=	33.00 °

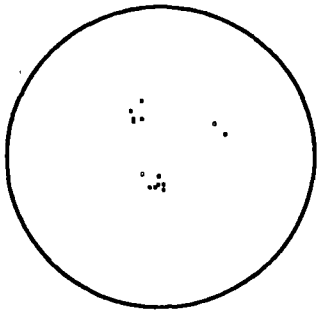

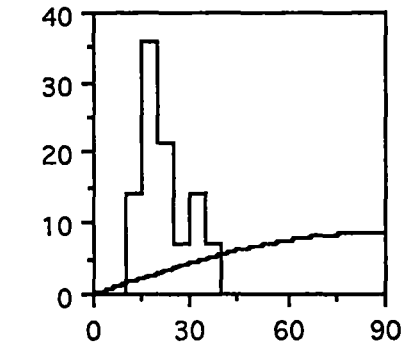

BHC1-116D(bot)
232 m
Transition

N	=	14
σ	=	8.02 °
μ	=	22.57 °
Φ (1/4)	=	16.50 °
Φ (1/2)	=	20.00 °

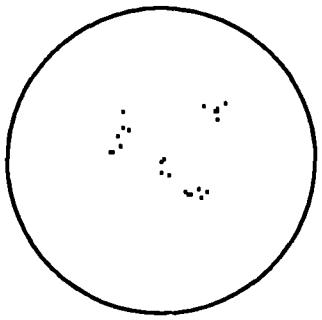

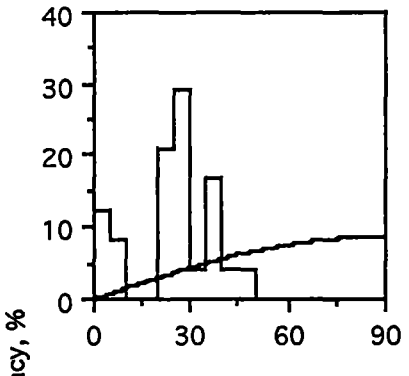

BHC1-121B(bot)
242 m
Transition

N	=	24
σ	=	12.85 °
μ	=	25.13 °
Φ (1/4)	=	21.01 °
Φ (1/2)	=	26.44 °

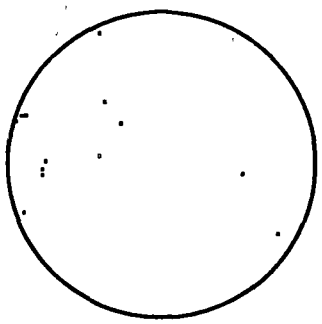

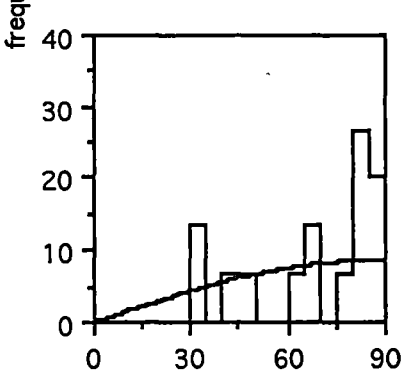

BHC1-134D(top)
267 m
Wisconsin

N	=	15
σ	=	20.45 °
μ	=	68.60 °
Φ (1/4)	=	46.00 °
Φ (1/2)	=	76.00 °

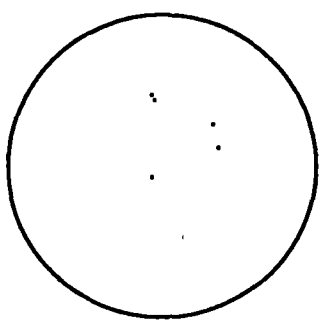

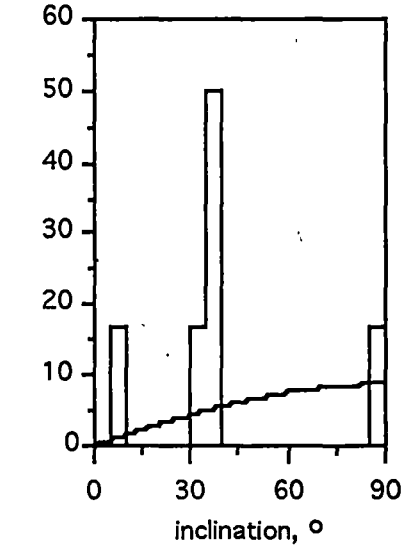

BHC1-138C(bot)
274 m
Wisconsin

N	=	6
σ	=	26.88 °
μ	=	40.50 °
Φ (1/4)	=	32.00 °
Φ (1/2)	=	36.00 °

frequency, %

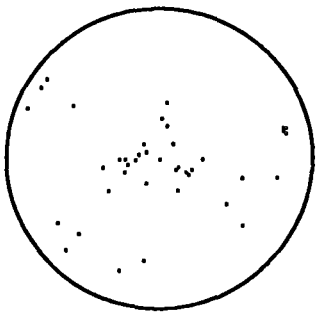

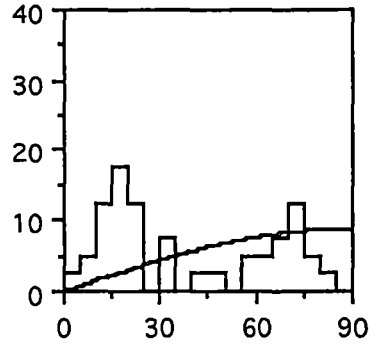

DYE3-T338 (top)
418.88 m
Holocene

N	=	40
σ	=	26.21 °
μ	=	38.45 °
Φ (1/4)	=	17.00 °
Φ (1/2)	=	23.00 °

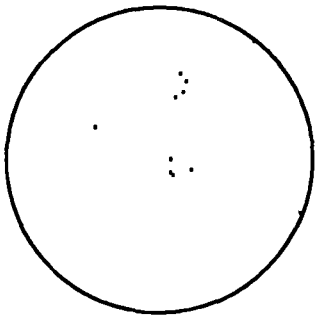

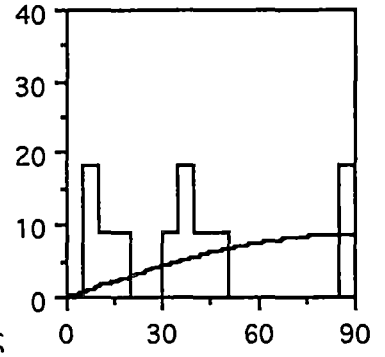

DYE3-T1556 (bot)
1607.37 m
Holocene

N	=	11
σ	=	28.56 °
μ	=	38.64 °
Φ (1/4)	=	11.00 °
Φ (1/2)	=	39.00 °

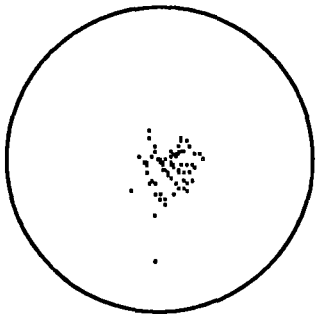

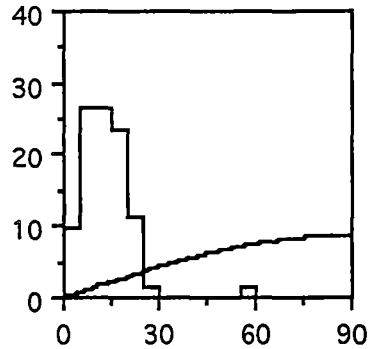

DYE3-T1763 (bot)
1812.75 m
Wisconsin

N	=	72
σ	=	8.20 °
μ	=	13.54 °
Φ (1/4)	=	7.90 °
Φ (1/2)	=	12.63 °

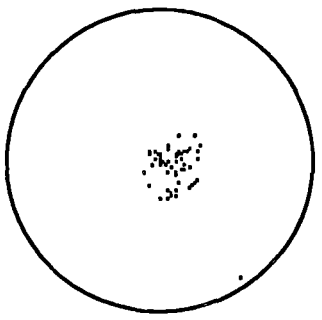

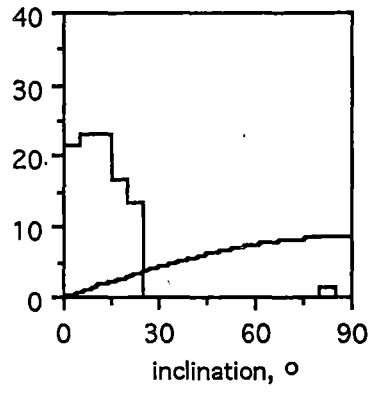

DYE3-T1922 (bot)
1972.07 m
Wisconsin

N	=	60
σ	=	11.37 °
μ	=	12.98 °
Φ (1/4)	=	7.00 °
Φ (1/2)	=	12.00 °

frequency, %

over the bottom 9 m of the core and found that the c-axis fabric was very strong and quite stable. They concluded that the c-axis average direction of 10° off vertical over the bottom 9 m was probably due to the bedrock slope of 17° averaged over several hundred metres up- and down-stream of the borehole.

For BHC 1, the measurements of fabric show that for the three Holocene samples (between 147 and 217 m), the crystal c-axis orientations for the samples BHC 1-73B at 147 m and BHC 1-79C at 160 m exhibit a weak central tendency, while sample BHC 1-84B at 217 m shows a weak pole. The three Transition and two Wisconsin ice samples (BHC 1-108D to BHC 1-138C ranging in depth from 217 m to 274 m) exhibit fabrics which are difficult to interpret due to the small number of very large crystals in the samples. These fabrics might be designated multi-maxima, although (at least for the three Transition fabrics) these may coincide with small circle girdle patterns. These observations coincide with measurements through the BHC 1 core by Thwaites and others (1984), Xie (1985) and Han and Young (1988) which describe a complete progression of fabric development from a random fabric near the surface through a small circle girdle above 90 m and a developed vertical single maximum extending to 230 m, to multi-maxima fabrics near the base.

For Dye 3 core samples, the studies of the whole core by Herron and others (1985) and of the Wisconsin ice below 1 786 m by Langway and others (1988) show the development of fabrics with a random c-axis orientation above 500 m, then a steady re-orientation of c-axis toward the vertical through a two-maxima pattern between 1 183 and 1 360 m to a well defined strong vertical maximum below 1 588 m till 1 815 m where the deepest fabric was measured. Similarly, in this study the measurements of fabric show for the Holocene ice samples (Dye 3-T338 at 418.88 m) a weak central trend and (Dye 3-T1556 at 1607.37 m) a weak girdle (although for this sample, again the large crystal size has prohibited measurement of many crystals and thus makes definition of the fabric pattern ambiguous). The Wisconsin ice samples (Dye 3-T1763 and Dye 3-T1922 at 1812.75 and 1972.07 m

respectively) exhibit a strong single maximum with c-axis mean angles of 13.54 and 12.98° off vertical and standard deviations of 8.20 and 11.37° respectively.

The ice core test samples available for the project thus exhibit a range of orientation fabric patterns including weak central tendencies, small circle girdles, single maximum and multiple maxima. It has been found that the band of multi-maxima fabrics in the lower layer of the BHC 1 core appears to correspond with a zone of large crystals and low shear rate while the bands of single maximum fabrics found at the deep levels in the Dye 3 and AGZ77 cores correspond with high shear rate and small crystals.

The laboratory prepared polycrystalline ice samples have also been measured for crystal orientation. These measurements consistently show random c-axis orientation patterns with average c-axis mean angle of 57.59° off the vertical and standard deviation of 23.03 ° (cf. theoretical values for a random sample from a uniform distribution of 57.30° and 21.56° respectively).

2.2.2. Crystal size and texture

Fig. 2.5 shows the full set of photographs taken through crossed polaroids of ice thin sections for all test samples. Included are top and bottom horizontal sections and corresponding vertical sections for all compression test samples prior to testing. Corresponding photographs for simple shear tests are presented in Chapter 5. Crystal size was measured by the count per unit area method described in Chapter 3.

The crystal size and texture within ice cores has been studied in detail for the AGZ77 core by Fisher and Koerner (1986), for BHC 1 by Han and Young (1988) and Thwaites and others (1984), and for Dye 3 by Herron and others (1985) and Langway and others (1988). For the Northern Hemisphere ice cores, a strong relationship between crystal size and microparticle concentration has been found with high microparticle concentrations coincident with small crystals (Fisher and Koerner, 1986; Langway and others, 1988). This has not been identified in the BHC 1 core. The crystals in the BHC 1 core are much

LAB

$S = 1.02\ mm^2$

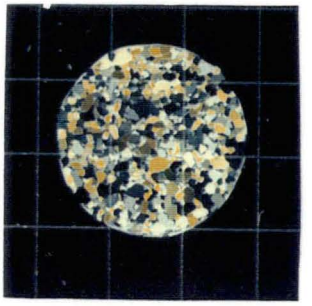

top horizontal section

vertical section

bottom horizontal section

AGZ77-225A

$S = 2.09\ mm^2$

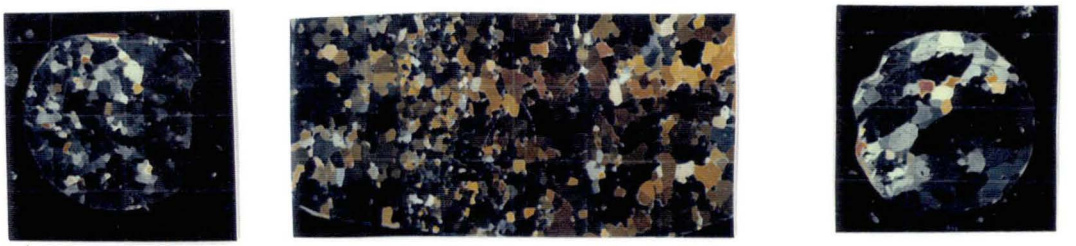

AGZ77-225B

$S = 0.84\ mm^2$

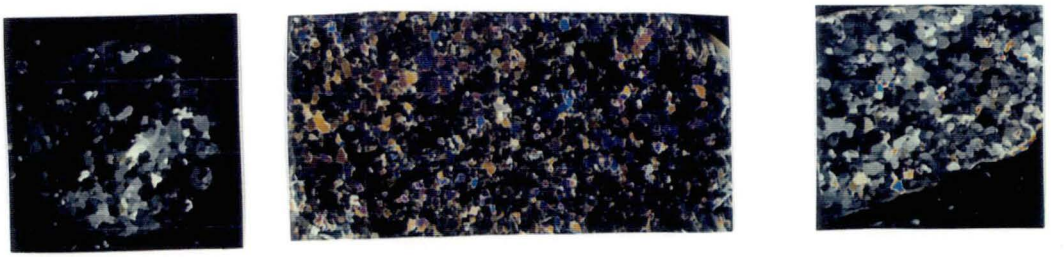

Figure 2.5 (5 pages) Initial thin section photographs for all ice samples in the compression tests. Mean crystal areas, S, averaged from top and bottom horizontal sections are indicated. The core axis is perpendicular to the horizontal thin section and parallel to the long axis of the vertical thin section.

top horizontal section

vertical section

bottom horizontal section

AGZ77-226

S = 1.49 mm ^{2}

AGZ77-228

S = 2.27 mm ^{2}

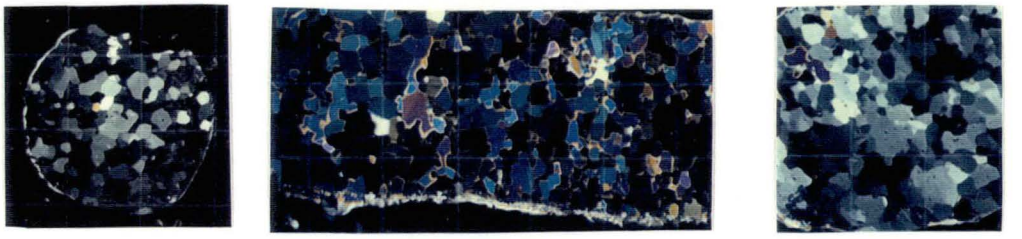

AGZ77-229

S = 2.15 mm ^{2}

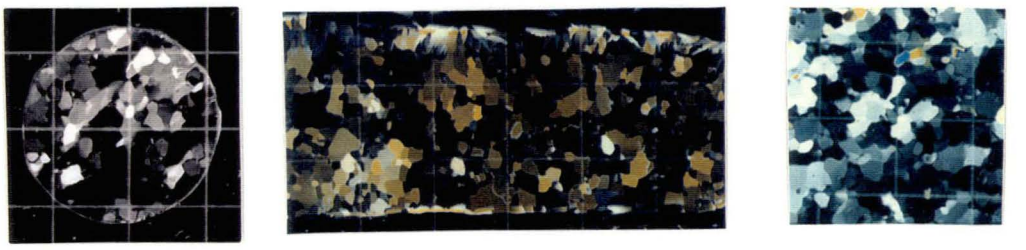

AGZ77-230

S = 2.70 mm ^{2}

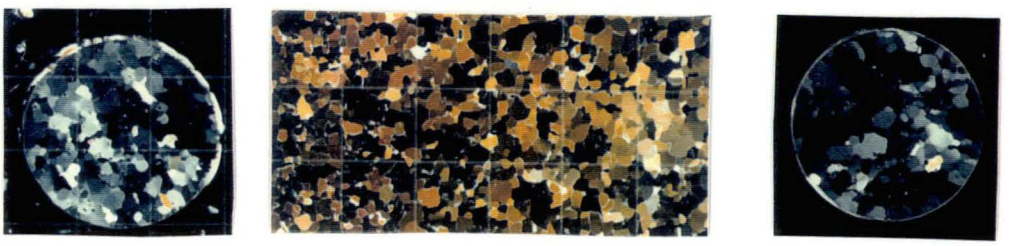

top horizontal section

vertical section

bottom horizontal section

BHC1-73B

S >41 mm ^{2}

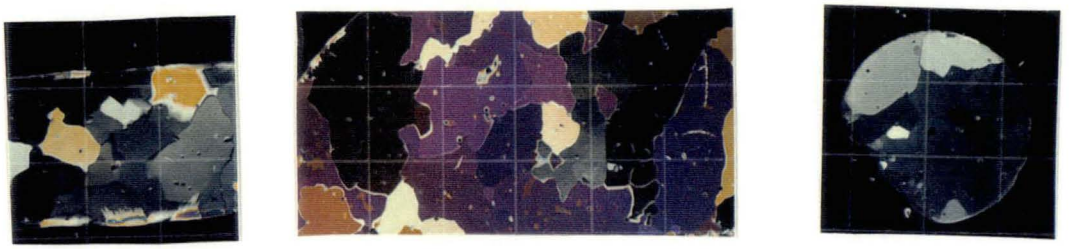

BHC1-79C

S > 45 mm ^{2}

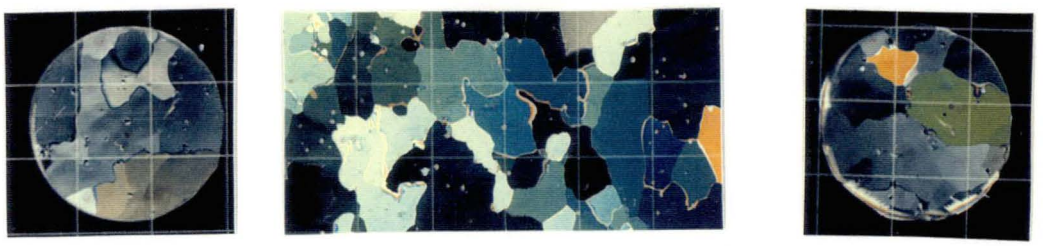

BHC1-84B

S = 18.09 mm ^{2}

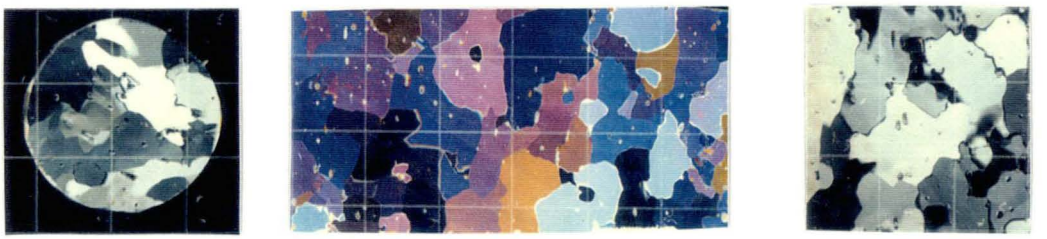

BHC1-108D

S > 100 mm ^{2}

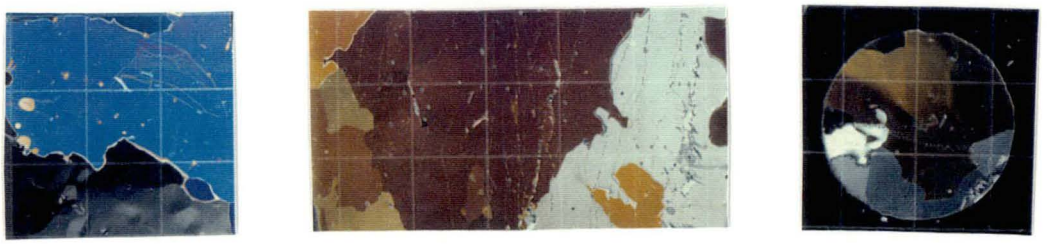

top horizontal section

vertical section

bottom horizontal section

BHC1-116D

S > 320 mm ^{2}

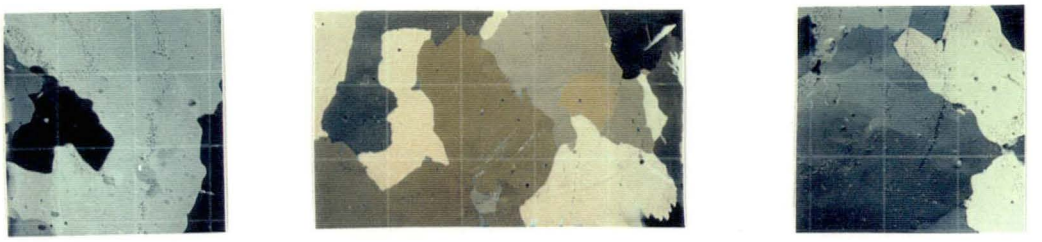

BHC1-121B

S > 91 mm ^{2}

BHC1-134D

S > 130 mm ^{2}

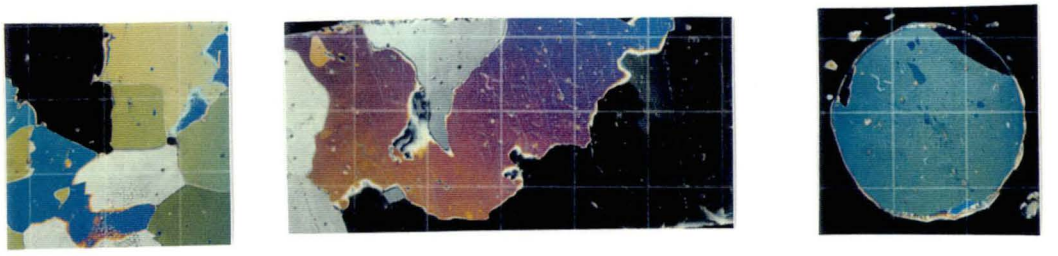

BHC1-138C

S > 310 mm ^{2}

top horizontal section

vertical section

bottom horizontal section

DYE3-T338

S = 15.14 mm ^{2}

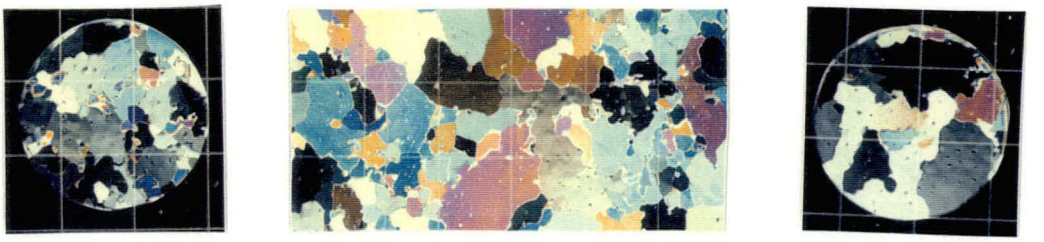

DYE3-T1556

S = 282 mm ^{2}

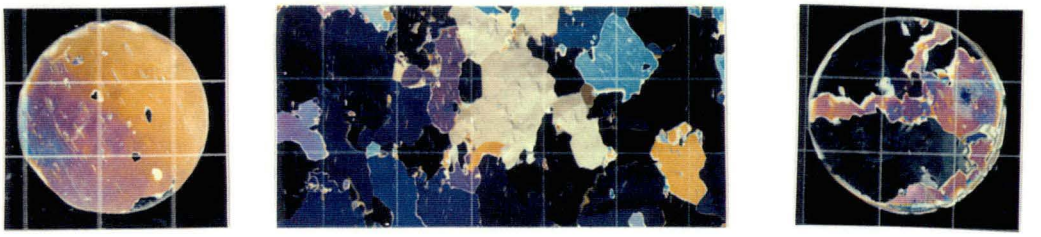

DYE3-T1763

S = 3.60 mm ^{2}

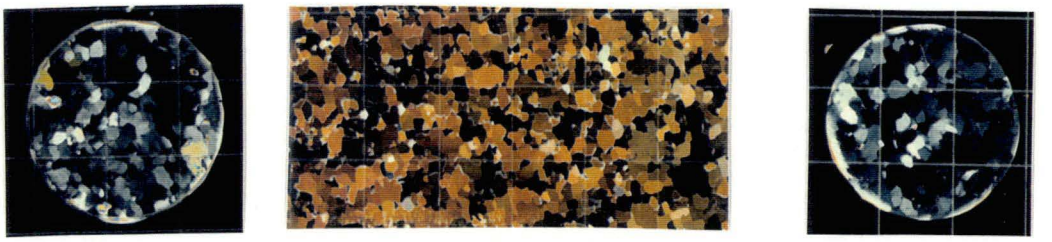

DYE3-T1922

S = 5.14 mm ^{2}

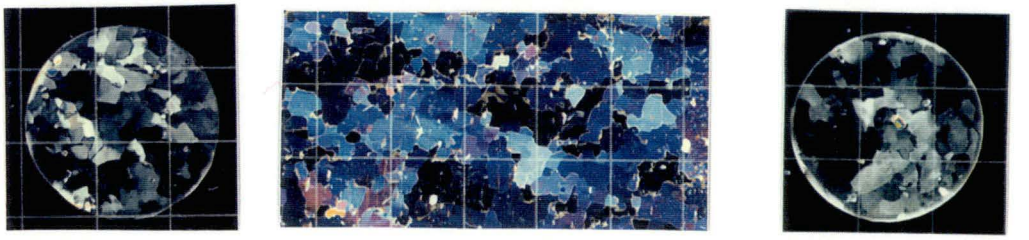

larger than those in the other two, especially near the bottom where the variations in crystal size and structure are related to the local variation in the shear strain rate. It needs to be noted that the microparticle concentrations in the BHC 1 core are an order of magnitude less that in the Northern Hemisphere cores. This is discussed further in the next section.

In the zone of high shear strain rate for BHC 1 the crystals are strongly interlocked with irregular and serrated grain boundaries while in the zone of low shear strain rate the crystals have a more regular shape, a much larger maximum grain size and gently curved boundaries (Thwaites and others, 1984).

The crystal size measurements for all test samples show that the AGZ77 core samples have the smallest crystals, ranging from 0.84 to 2.70 mm^2 with a mean value of 1.47 mm^2 for the three Wisconsin ice samples and of 2.37 mm^2 for the three pre-Wisconsin samples. The BHC 1 core exhibits the largest crystals ranging from 18.09 to larger than 310 mm^2, and with mean values of 35.95, 170 and 220 mm^2 for the Holocene, Transition and Wisconsin ice respectively. The Dye 3 core samples range in crystal size from 3.6 to 282 mm^2 with a mean value of 148.57 mm^2 for the two Holocene samples and 4.37 mm^2 for the two Wisconsin samples. The crystal size range across all test samples is 0.84 to greater than 310 mm^2 .

2.2.3. Impurity content

The impurities in polar ice sheets include insoluble and soluble matter. The insoluble impurities consist mainly of "dust ", i.e. particles in the size range 0.1 to 2 μm, which are of continental origin, and are transported to the ice sheets by wind. The soluble impurities comprise predominantly sodium, calcium and magnesium, and chloride, nitrate and sulphate ions. In both hemispheres, sodium and chloride come mainly from sea salt. Sulphate ions come mainly from sulphuric acid produced by oxidation of dimethylsulphide emitted at the ocean surface by biogenic activity in Antarctica (Langway and others, 1988) and in the Northern Hemisphere (Herron and Langway, 1985). Major

volcanic eruptions can produce significant increases in concentrations of sulphuric and hydrochloric acid, but these peaks diminish after two to three years (Hammer, 1980). The source of nitrate is neutral nitrate salt and nitric acid which is most probably formed by tropical or mid-latitude lightning in Antarctica (Legrand and Delmas, 1986, 1988). Their source is unknown in the Northern Hemisphere (Herron, 1982).

Concentrations of some or all of these impurities may influence the mechanical properties of ice (Dahl-Jensen, 1985; Paterson, 1991) or may not (Pimienta and Duval, 1988; Shoji and Langway, 1988). The effects of impurities on the deformation of the test samples are discussed in Sections 4.2.1. and 5.3.1.

Impurity concentrations were measured for each of the ice core samples. Fig. 2.6 shows dust concentrations over a range of particle sizes. Total dust concentrations over the particle size range, 0.47 to 14.6 mm are provided in Table 2.3 along with concentrations of the anions and cations Na^+, Ca^{++}, Mg^{++}, Cl^-, SO_4^- and NO_3^-. Also shown are concentrations of MSA and the oxygen isotope ratio ($\delta^{18}O$) for each ice core sample.

The AGZ77 core samples have the highest dust concentrations, ranging from 275 888 to 750 000 particles/ml. The BHC 1 core samples have the lowest dust concentrations (1 186 to 12 708 particles/ml). The Dye 3 core samples have dust concentrations ranging from 10 546 to 201 263 particles/ml. The highest dust concentration (772 515 particles/ml) is displayed by sample AGZ77-225A (the Wisconsin ice in the AGZ77 core). This value is some 650 times greater than the lowest dust concentration (1 186 particles/ml) in sample BHC 1-116D (the Transition ice in the BHC 1 core).

The mean concentrations of Ca^{++} and Mg^{++} in AGZ77 core samples are the highest. The concentration of Ca^{++} in these samples is 56 times that in the BHC 1 core samples. For Mg^{++}, AGZ77 concentrations are 20 times those in the Dye 3 samples. Na^+ and Cl^- concentrations in the BHC 1 Holocene samples are 216 and 432 µg/l respectively, i.e. 43 and 58 times respectively those in the Dye3 Holocene samples. The concentrations of SO_4^- are significantly higher in the AGZ77 Wisconsin samples than in the pre-Wisconsin

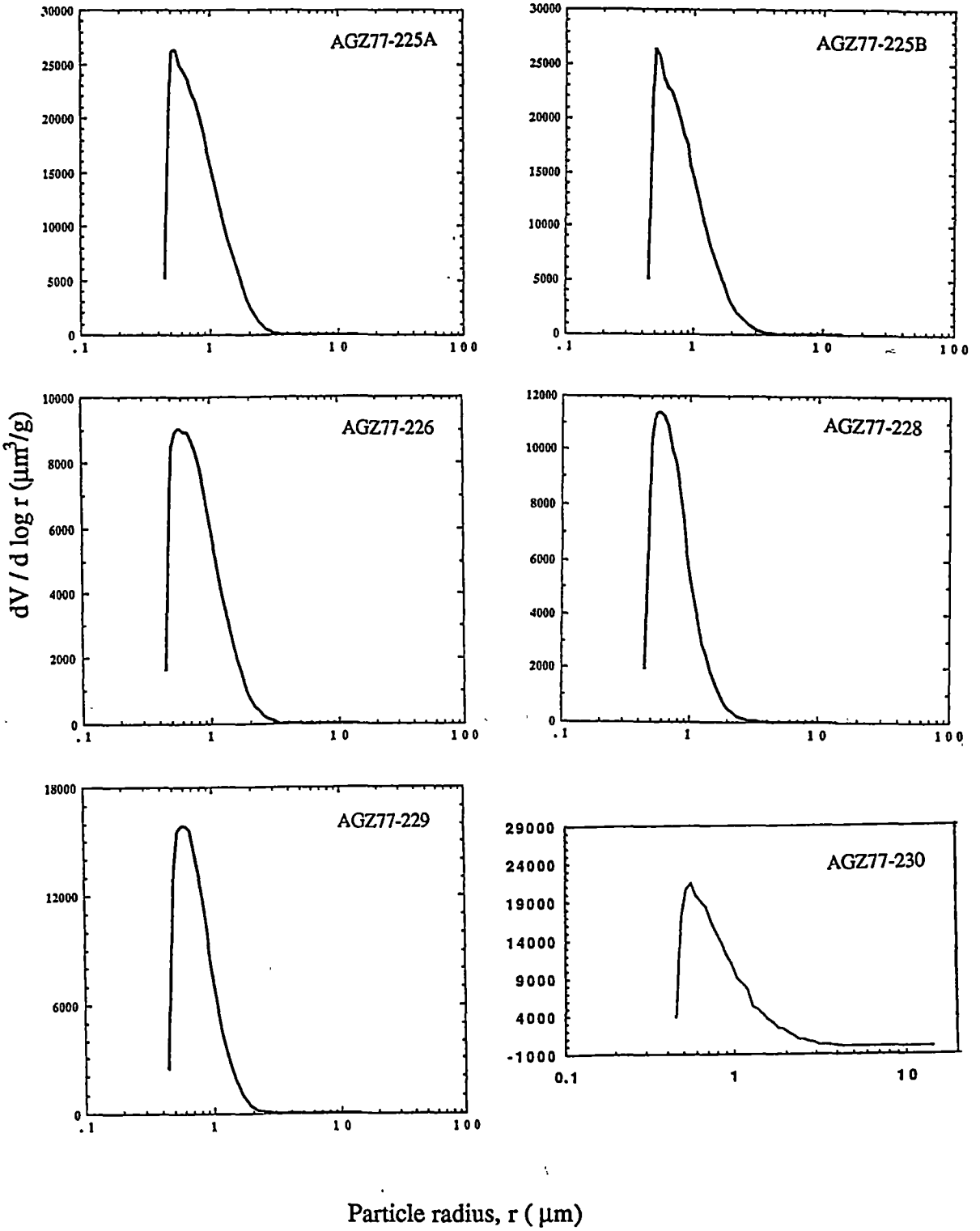

Figure 2.6 (3 pages) Mean particle size for the test samples.

$V = N \pi r^3$ where r is particle radius, N is number of particles of radius r, and V is total volume of particles of radius r.

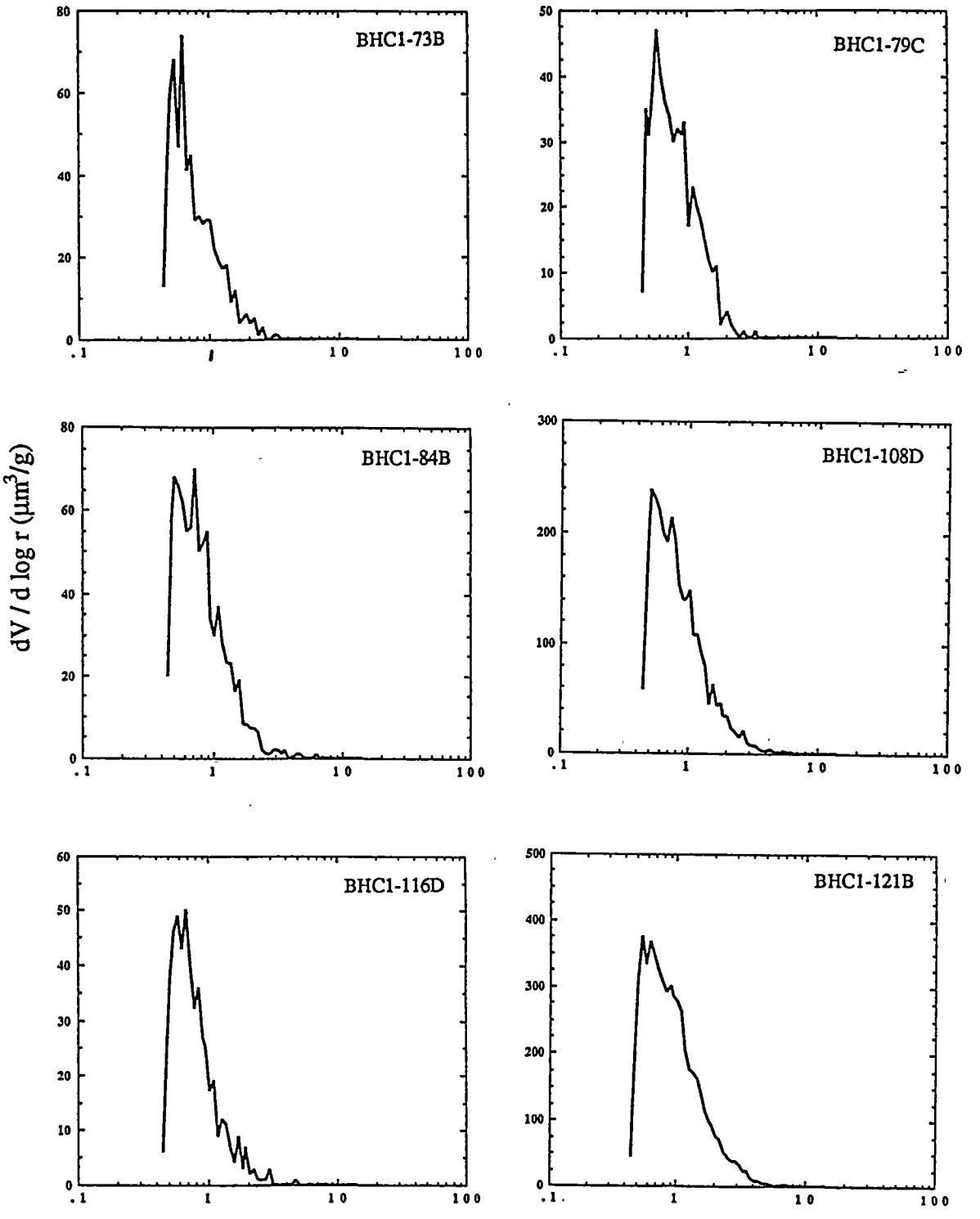
BHC1-73B
BHC1-79C
BHC1-84B
BHC1-108D
BHC1-116D
BHC1-121B
dV / d log r (μm³/g)
Particle radius, r (μm)

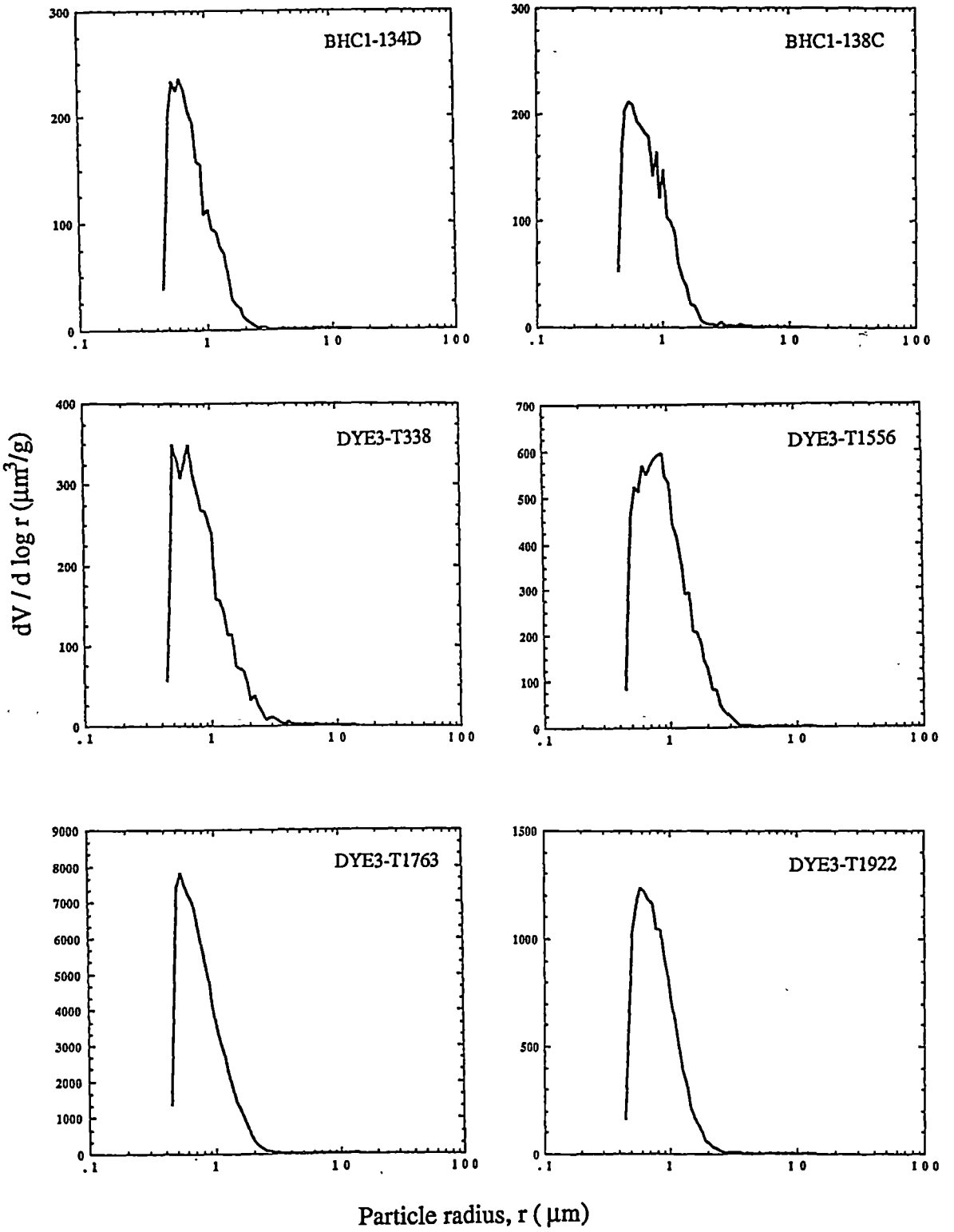
BHC1-134D
BHC1-138C
DYE3-T338
DYE3-T1556
DYE3-T1763
DYE3-T1922
dV / d log r (μm³/g)
Particle radius, r (μm)

Table 2.3 Impurity concentrations and oxygen-isotope ratios for all test samples.

sample number	dust (0.47-14.6 µm) (particles/ml)	Na^+ (µg/l)	Ca^{++} (µg/l)	Mg^{++} (µg/l)	Cl^- (µg/l)	SO_4^- (µg/l)	NO_3^- (µg/l)	MSA (µg/l)	$\delta^{18}O$ (‰)
AGZ 77 / 225A	772515.	-	-	-	438	58.0	14.8	0.38	-35.277
AGZ77 / 225B	744143.	-	276	46	110	58.5	8.6	0.32	-36.604
AGZ 77 / 226	275888.	-	-	-	43	28.8	10.0	0.15	-33.227
AGZ 77 / 228	297491.	45	850	176	18	17.5	8.5	0.52	-27.337
AGZ 77 / 229	393424.	-	-	>100	<5	12.7	3.9	0.40	-27.392
AGZ 77 / 230	750000.	167	1000	231	182	29.8	9.4	0.84	-27.891
BHC 1 / 73B	1492.	163	10	21	288	50.7	3.8	<0.1	-19.298
BHC 1 / 79C	1202.	316	-	60	627	43.0	4.0	0.75	-18.513
BHC 1 / 84B	1962.	171	36	45	380	35.6	7.7	0.62	-19.319
BHC 1 / 108D	6926.	292	12	29	596	41.8	3.4	0.25	-20.099
BHC 1 / 116D	1186.	35	1	5	68	17.9	6.0	0.12	-21.919
BHC 1 / 121B	12708.	90	14	9	160	19.1	6.0	0.65	-23.996
BHC 1 / 134D	6046.	51	8	6	81	20.4	9.8	1.35	-25.969
BHC 1 / 138C	6001.	59	8	8	110	18.3	5.8	1.15	-26.986
DYE 3 / T338	10546.	7	19	4	10	13.2	20.0	0.62	-26.376
DYE 3 / T1556	21184.	3	14	3	<5	8.0	14.4	0.24	-24.139
DYE 3 / T1763	201263.	38	118	15	65	42.5	12.2	0.75	-31.045
DYE 3 / T1922	33903.	-	-	6	15	11.5	8.0	1.05	-24.681
LAB	-	432	66	5	-	-	-	-	-5.274

samples. There is a significant decrease in concentration with increasing depth for Ca^{++}, Cl^- and SO_4^- for BHC 1 samples and the mean concentrations in Holocene ice are 2.3 to 6 times those in Wisconsin ice.

2.2.4. Oxygen isotope ratio

Oxygen isotope ratio, $\delta^{18}O$, was measured for all ice core samples available to the study (Table 2.3). Since $\delta^{18}O$ is dependent on deposition temperature, the measured values serve as a check on the climatic epoch from which the samples belong.

For the AGZ77 samples $\delta^{18}O$ values of -33.2 to -36.6 $^{o}/_{oo}$ were found for the Wisconsin samples and -27.3 to -27.9 $^{o}/_{oo}$ for the pre-Wisconsin samples. For the BHC 1 samples the Holocene, Transition and Wisconsin samples had $\delta^{18}O$ values from -18.5 to -19.3 $^{o}/_{oo}$, -20.1 to -24.0 $^{o}/_{oo}$ and -26.0 to -27.0 $^{o}/_{oo}$ respectively. The Holocene Dye 3 samples had significantly different $\delta^{18}O$ values (-24.1 and -26.4 $^{o}/_{oo}$) than the (Wisconsin) Dye 3/T1763 sample (-31.0 $^{o}/_{oo}$). However the deepest sample (Dye 3/T1922) revealed a higher value (-24.7 $^{o}/_{oo}$). This higher value corresponds with lower dust concentration, lower soluble impurity concentrations and (slightly) larger crystal size for this sample than for the Dye 3 /T1763 sample.

2.2.5. Summary of physical properties

For the AGZ77 core, the Wisconsin ice exhibited strong (off vertical) single maximum fabrics, the smallest crystals and high concentrations of dust, sulphate and nitrate ions. The pre-Wisconsin samples displayed stronger single maximum fabrics near the vertical, small crystals and the highest concentrations of dust, calcium and magnesium ions.

For the BHC 1 core, the Holocene ice showed weaker single maximum fabrics trending towards the vertical, larger crystals, the lowest concentration in dust and the highest concentrations in sodium and chloride ions. The samples from the Transition and the Wisconsin exhibited multi-maxima fabrics, the largest crystals and lower concentrations in both soluble and insoluble impurities.

The Dye 3 Holocene samples exhibited weaker central trend fabrics, larger crystals, lower concentrations of dust and the lowest concentrations in sodium, chloride and magnesium ions. The Wisconsin samples had stronger single maximum fabrics towards the vertical, smaller crystals and lower concentrations of dust, sodium, magnesium, chloride and sulphate ions.

For the Northern Hemisphere ice it was found that the Wisconsin samples have stronger fabrics, smaller crystals and higher impurity concentrations than the Holocene ice. However for the BHC 1 core these properties appeared in the Holocene ice, rather than in the Wisconsin ice.

2.3. PREPARATION OF ICE TEST SPECIMENS

2.3.1. Ice core samples

Deformation tests samples were prepared from the ice core specimens. Cylindrical samples were used for compression tests and rectangular prisms for shear tests.

It has been found for cylindrical ice specimens of isotropic polycrystalline ice in uniaxial compressive deformation that the minimum flow rate is dependent on sample diameter (Jacka, 1994). In order to limit any effect of sample size or shape on the comparison of ice flow rates in this study, the diameter of all test specimens was standardised at 25.4 mm. The initial length of the test specimens was set at 50 mm.

The cylindrical test specimens for compression tests were prepared so that the long axis of the specimen was parallel to the core axis. Thus, the specimen compression axis for each test was close to the natural compressive stress axis in situ in the ice sheet. Test samples were cut from the ice core specimens into roughly cylindrical shapes using a band saw. They were then turned on a lathe to a diameter of 25.4 mm and initial length of 50 mm.

Gao (unpublished) investigated the effect of sample size and shape of rectangular prism samples on the minimum strain rate in simple shear test. He found that the sample size (the length, height and width) and shape (ratios of each of these dimensions) did not

significantly affect the minimum strain rate. The greater the sample length, the more stable the shear geometry. Therefore sample lengths were maintained as long as possible. Lengths were limited however by the diameter of the ice core specimen available, and ranged from 33 to 59 mm. The initial height and the width of each test specimen was set at 50 and 19 mm respectively. The actual experimental height of the test samples ranged from 18 to 22 mm since the top and bottom of each specimen was frozen into a box for sample gripping during experimentation (see Figure 3.4 a).

In order to make the shear direction in the tests parallel to the basal plane of the ice core, the rectangular test specimens were cut from the ice core samples so that the height of the test specimen was parallel to the core axis and the plane of the length and width parallel to the basal plane of the ice core. They were first roughly cut into a rectangle by a band saw, then sanded with finer sandpaper into clean, square edged specimens of the designed size.

2.3.2. Laboratory prepared ice samples

Laboratory prepared polycrystalline ice samples were deformed in both uniaxial compression and simple shear.

Laboratory ice samples were prepared as outline by Jacka and Lile (1984). In a cold room at - 10 °C, a slush mixture of granulated ice and distilled water at 0 °C, was packed into a plastic mould of 25.4 mm internal diameter for compression test samples, and of 100 mm internal diameter for shear test samples. Air bubbles were removed by disturbing the slush in the mould using a stirrer. A vacuum system was used to help remove air from the 100 mm mould (Li, unpublished). Samples were left at - 20 °C after pressing the excess water from the mould.

The laboratory prepared polycrystalline test specimens were prepared to the standard size by the same method used in the preparation from ice core samples. For compression tests cylinders of diameter 25.4 mm and length 50 mm were prepared, and for shear tests, rectangular prisms 59 x 19 x 50 mm (length x width x initial height).

3. EXPERIMENTAL TECHNIQUE

3.1. CALCULATION OF APPLIED STRESS AND RESULTANT STRAIN RATE

This report describes a series of deformation tests carried out in uniaxial compression and in simple shear, on the ice samples described in Chapter 2. All deformation experiments carried out were constant load tests with an initial octahedral shear stress of 0.2 MPa.

For compression tests on a cylindrical test sample (Figure 3.1),

$$F_c = \sigma A , \qquad (3.1)$$

$$\tau_o = \frac{\sqrt{2}}{3} \sigma \qquad (3.2)$$

and

$$A = \frac{\pi D^2}{4} \qquad (3.3)$$

where F_c (kg wt.) is the load acting on the ice test sample, σ (MPa) is the axial stress, A (mm^2) is the area of the sample on which the axial stress acts, τ_o (MPa) is the octahedral shear stress, D (mm) is the diameter of the cylindrical test sample and $\frac{\sqrt{2}}{3}$ converts axial stress to octahedral shear stress (Budd, 1969).

Thus the normal load, F_c to be applied to the sample to supply an octahedral shear stress, τ_o is

$$F_c = \frac{3}{\sqrt{2}} \tau_o \cdot \frac{\pi D^2}{4} \cdot \frac{1}{9.8} \qquad (\text{kg wt.}) \qquad (3.4)$$

In this report, τ_o was 0.2 MPa and D was 25.4 mm, giving F_c = 21.94 kg wt. for all compression tests .

The octahedral shear strain rate for uniaxial compression, $\dot{\varepsilon}_{oc}$ (s^{-1}) over consecutive time intervals, t_i to t_{i+1} is calculated by

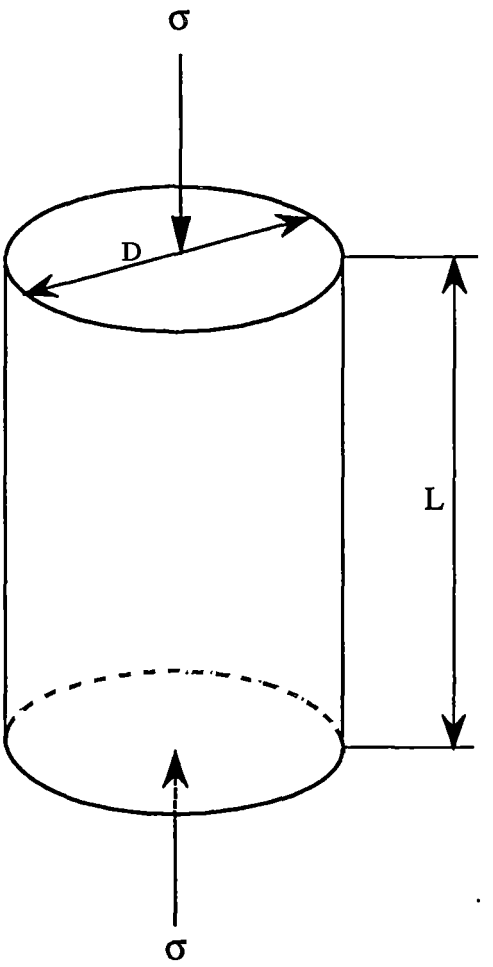

Figure 3.1 Schematic diagram illustrating uniaxial compression. σ is the stress acting on the sample of diameter, D, and length, L.

$$\dot{\varepsilon}_{oc}\,(s^{-1}) = \frac{1}{\sqrt{2}}\frac{1}{l}\frac{dl}{dt}$$

$$= \frac{1}{\sqrt{2}}\left(\frac{\delta l_{i+1}}{l_o - \delta l_{i+1}} - \frac{\delta l_i}{l_o - \delta l_i}\right)\frac{1}{3600\,(t_{i+1} - t_i)} \qquad (3.5)$$

where l_o is the initial length of the sample, δl_i and δl_{i+1} are the axial displacements of the sample since test commencement, at times t_i and t_{i+1} respectively and $\frac{1}{\sqrt{2}}$ converts axial compressive strain rate to octahedral shear strain rate (Budd,1969).

For simple shear tests with a rectangular prism test sample (Figure 3.2),

$$F_s = \tau A, \qquad (3.6)$$

$$\tau_o = \frac{\sqrt{2}}{\sqrt{3}}\tau \qquad (3.7)$$

and

$$A = L \cdot W \qquad (3.8)$$

where F_s (kg wt.) is the load acting on the ice test sample, τ (MPa) is the shear stress, A (mm^2) is the area of the sample on which the shear stress acts, τ_o (MPa) is the octahedral shear stress, L (mm) is the length of the rectangular prism test sample, W (mm) is the width of the test sample and $\frac{\sqrt{2}}{\sqrt{3}}$ converts from direct shear stress to octahedral shear stress (Budd, 1969).

Thus the constant load, F_s required to supply an octahedral shear stress, τ_o is

$$F_s = \frac{\sqrt{3}}{\sqrt{2}}\tau_o \cdot L \cdot W \cdot \frac{1}{9.8} \qquad \text{(kg wt.)} \qquad (3.9)$$

For the tests described in this report, τ_o = 0.2 MPa, W = 19 mm except for one sample in which W = 17 mm and L ranged from 31 to 60 mm. Thus F_s ranged from 14.7 to 28.5 kg wt.

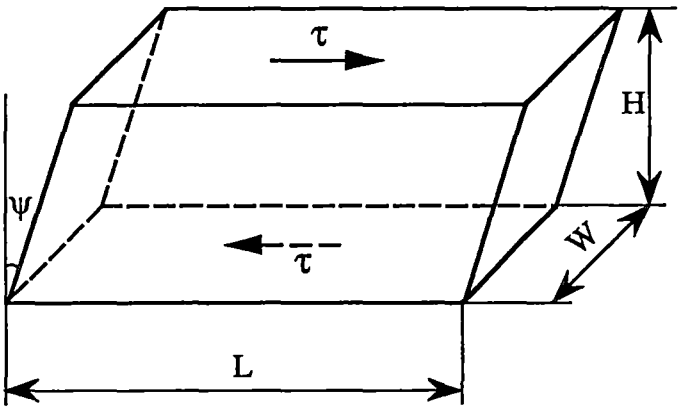

Figure 3.2 Schematic digram illustrating simple shear, showing stress, τ, strain, ψ, and sample length, L, width,W, and height, H.

For the simple shear apparatus (see Section 3.4), there is a discrepancy between the reading on the dial spring balance which creates the load applied to the sample and the actual force exerted towards shearing the ice test sample. This discrepancy is due to the system friction (Gao, unpublished) and a correction equation,

$$F_a = 1.17\,F_s + 2.06 \quad (\text{kg wt.}) \tag{3.10}$$

was utilized where F_a is the force applied on the dial spring balance to produce F_s, the force required on the sample.

The octahedral shear strain rate for simple shear tests, $\dot{\varepsilon}_{os}$, is

$$\dot{\varepsilon}_{os} = \frac{\sqrt{2}}{\sqrt{3}} \frac{\dot{\psi}}{2} \tag{3.11}$$

where

$$\dot{\psi} = \frac{dv}{dz} \,. \tag{3.12}$$

Here, z is taken equal to the constant value, H to calculate an average value for $\dot{\psi}$

$$\dot{\psi} = \frac{dv}{dz} = \frac{1}{H} \frac{dl}{dt} \,. \tag{3.13}$$

Thus

$$\dot{\varepsilon}_{os}\,(s^{-1}) = \frac{\sqrt{2}}{\sqrt{3}} \frac{\dot{\psi}}{2}$$

$$= \frac{\sqrt{2}}{\sqrt{3}} \frac{1}{2H} \frac{dl}{dt}$$

$$= \frac{\sqrt{2}}{\sqrt{3}} \frac{1}{2H} \frac{\delta l_{i+1} - \delta l_i}{3600\,(t_{i+1} - t_i)} \tag{3.14}$$

where $l = L$ is the length of the sample, $\delta\, l_i$ and $\delta\, l_{i+1}$ are the displacements of the upper edge of the sample with respect to the lower edge in the shear direction at times t_i and t_{i+1}

respectively, and $\frac{\sqrt{2}}{\sqrt{3}}$ converts from direct shear strain rate to octahedral shear strain rate (Budd, 1969).

3.2. DEFORMATION APPARATUS

3.2.1. Apparatus for uniaxial compression deformation

Uniaxial compression experiments were carried out using the direct load apparatus (Figure 3.3) described by Jacka and Lile (1984). A load is applied to the ice sample through a vertical rod to which is attached to a load beam. Thin wires attached to the ends of the load beam suspend the load to be applied. The ice sample, enclosed with a plastic cover which protects the sample from erosion, sits vertically in the centre of a bath of silicon oil which protects the sample from ablation and dampens ambient temperature fluctuations. The sample deformation is observed by means of a dial indicator which displays the vertical displacement directly over the sample. The indicator is mounted on a vertical stand fixed on the base plate.

The indicator is graduated each 0.01 mm so that a maximum error of ± 0.01 mm is expected, resulting in an estimated error in measured strain (for a 50 mm long sample) of $\pm 0.02\%$.

The compression apparatus is designed to measure creep deformation of ice, i.e. at strain rates $< \sim 10^{-6}\ s^{-1}$. Ice samples have been strained with this apparatus up to 60%. Beyond 10% strain samples show visible evidence of barrelling, but there is no evidence of distortion or cracking. Barrelling results in a stress reduction as a consequence of increased cross section area of the sample (constant load tests), especially at high strains. The experimental procedure (see Section 3.4) followed for the tests described in this report avoided this stress decrease by reshaping samples at large strains.

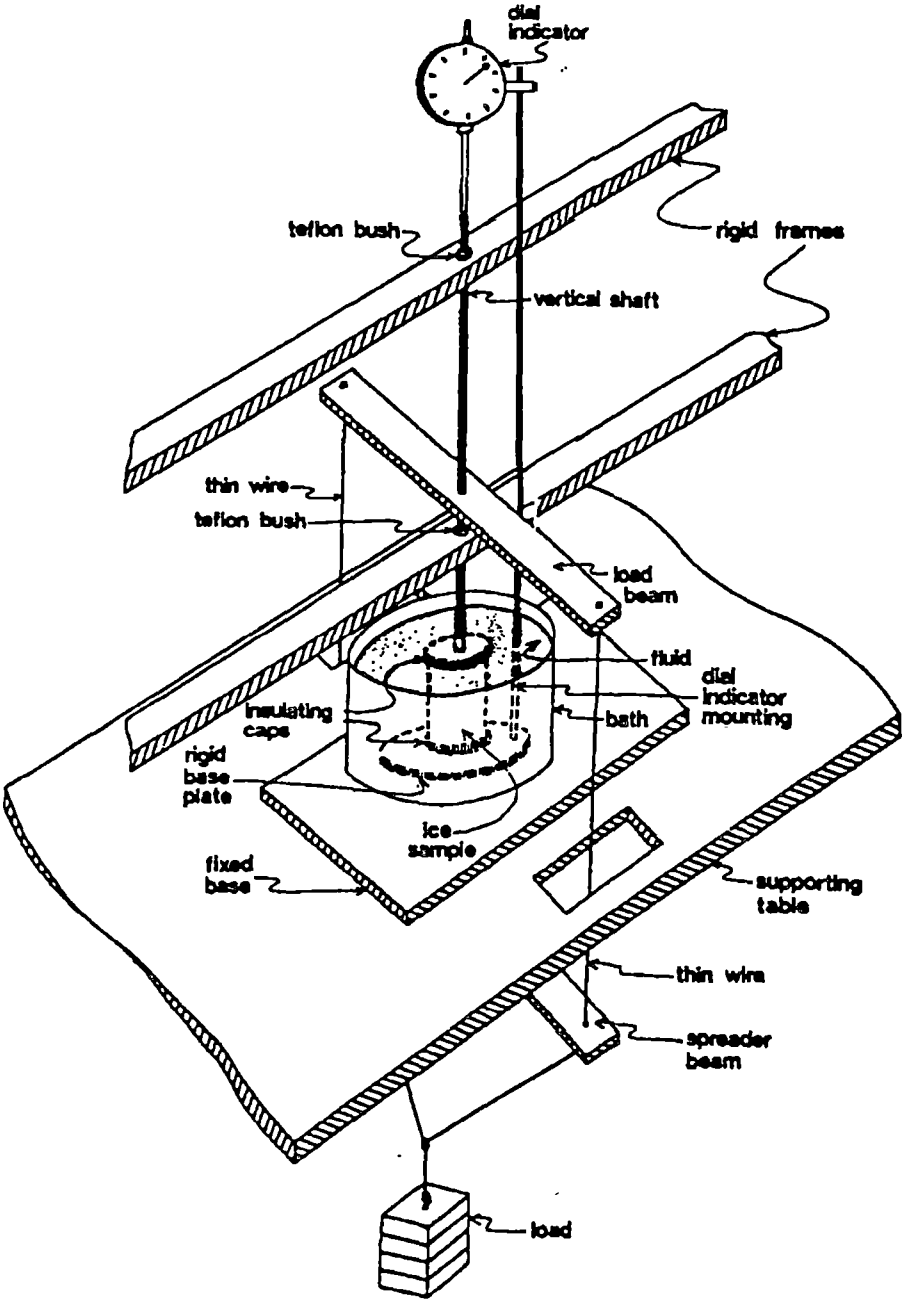

Figure 3.3 Direct load compression apparatus (after Jacka and Lile,1984).

3.2.2. Apparatus for simple shear deformation

Deformation experiments in simple shear were carried out on an apparatus (Figure 3.4) described by Gao (unpublished). A rectangular prism shaped ice sample is frozen (using an ice / water slurry) into two aluminium boxes (Figure 3.4 a). A base channel in both boxes positions the sample square and parallel to the box length. The sample is frozen into one box first, then inverted and frozen into the other box. The internal walls of the boxes are serrated to provide grip to the sample.

A shear stress is applied to the sample by supplying a load to one (moving) box with respect to the other (fixed). The load is applied through a tensioning wire (via two pulleys) to a dial spring balance. The spring balance is fixed to the same fixed frame as the stationary box.

A dial indicator measures the displacement of one box with respect to the other. The strain error expected (for the lowest sample height of 20 mm) is $\pm 0.025\%$. The application of the load to the sample boxes is adjusted such that the force is always applied co-linearly (Russell-Head, 1985).

To reduce friction during deformation tests, three or four steel rollers are placed between the sample boxes and the base plate. Friction in the system however still results in some discrepancy between the dial spring balance reading and the actual shear force exerted. Gao (unpublished) has measured this discrepancy by substituting the ice sample with another dial spring balance. This has been discussed in Section 3.1.

3.3. TEMPERATURE CONTROL

All tests were carried out within a freezer box or room with ambient temperature in the range -10 to -18 °C. The test temperature for all experiments described in this report was -5.0 °C. Samples were immersed in a fluid (silicon oil for compression tests; kerosene for shear tests; limited by size and cost) bath to prevent ablation during testing. The bath temperature was maintained at -5 °C by using small thermostatically controlled heaters

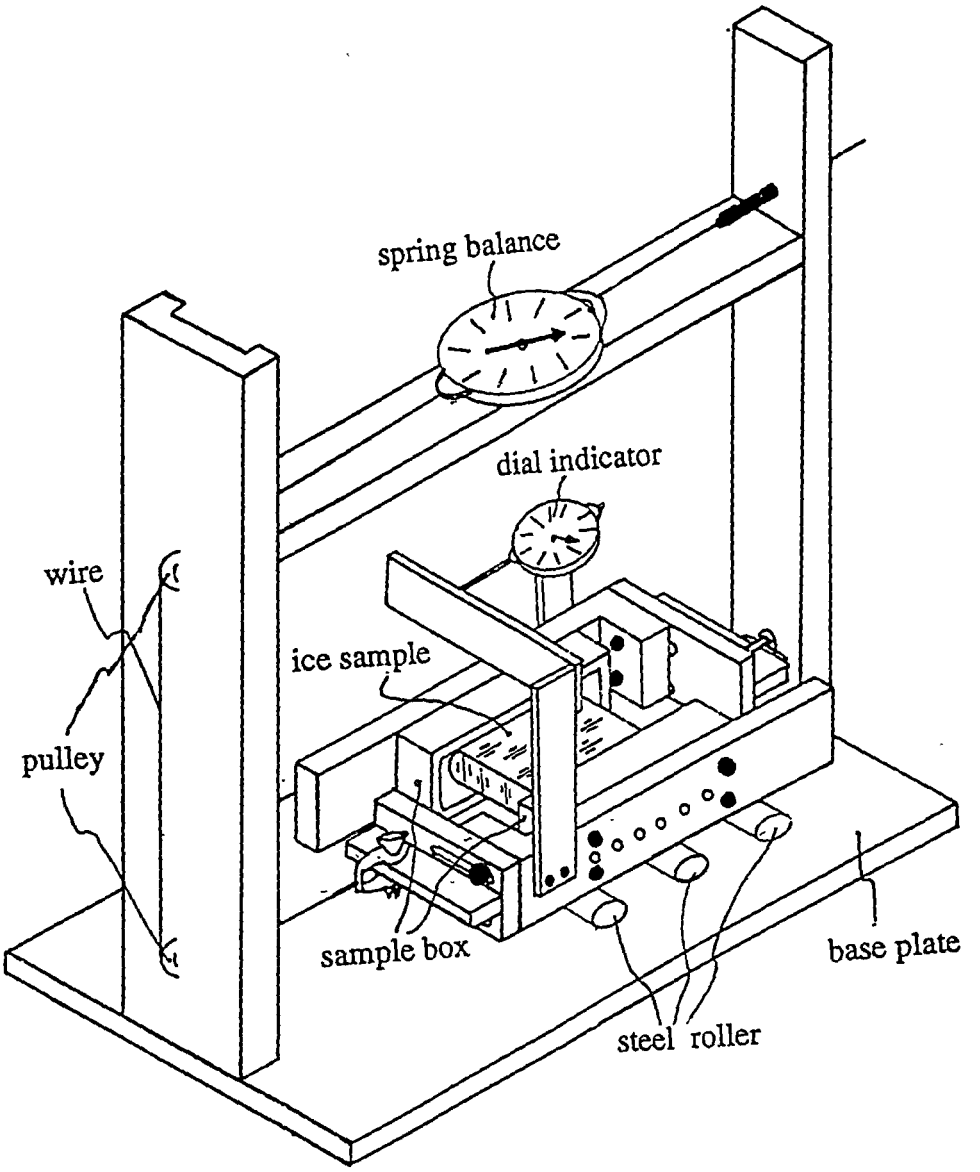

Figure 3.4 Simple shear apparatus.

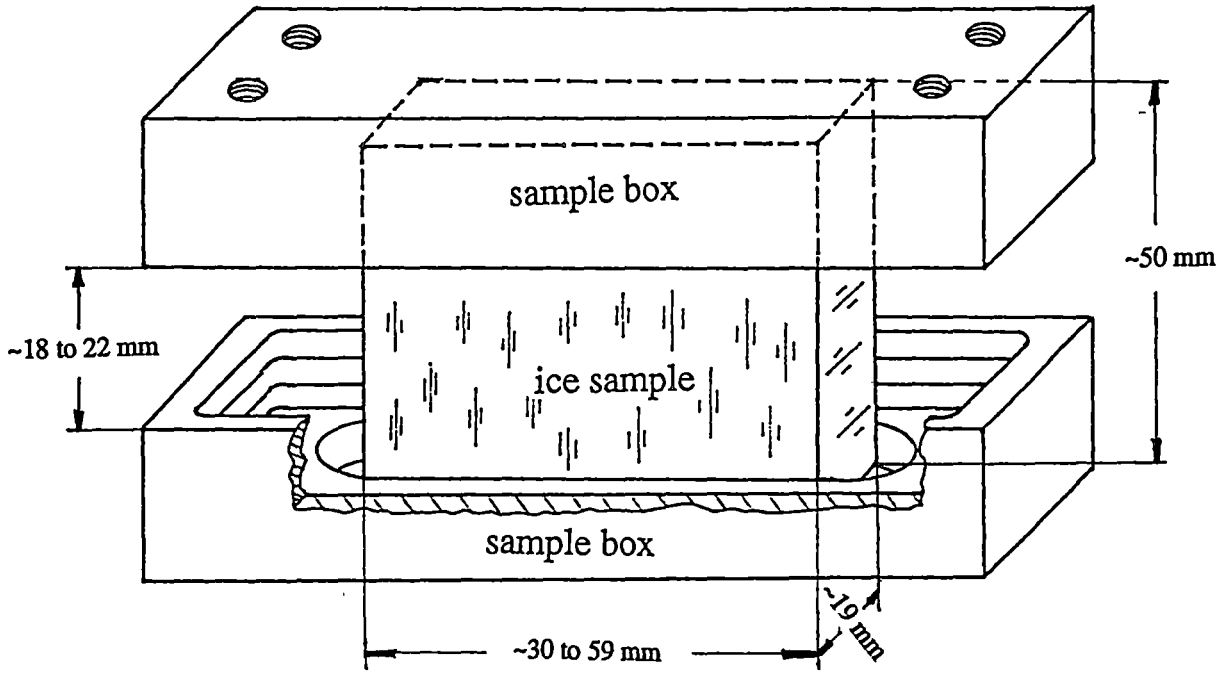

Figure 3.4 a Dimensions indicated are typical initial dimension for an ice sample in shear (see page 37).

(Morgan, 1979). In order to maintain a homogeneous temperature a small electric propeller was used to stir the fluid. Test temperature was monitored using a Platinum resistance bridge with accuracy ± 0.025 °C. The recorded maximum temperature deviation was less than ± 0.1 °C for compression tests and ± 0.2 °C for shear tests.

3.4. EXPERIMENTAL PROCEDURE

Each of the selected ice core samples described in Chapter 2, and several laboratory prepared samples were tested in uniaxial unconfined compression and in simple shear.

At strains greater than 10% test samples in compression showed visible signs of barrelling. The increased cross-section area due to the barrelling incurs a stress reduction for these constant load tests. Therefore, deformation was stopped after ~10 % strain, the samples were re-shaped and then re-tested at the same stress. In order to limit crystal structure changes between the repeat tests, the temperature was dropped to the ambient temperature (- 18 °C) by turning off the control heaters. Once the sample was cooled to the ambient temperature, it was removed from the apparatus. A thin section was cut perpendicular to the compression axis and, to reduce boundary effects, from the middle of the sample. The two halves of the sample were reshaped to the same diameter as previously (25.4 mm). The middle (cut) surfaces were squared using a lathe and were then frozen together again with a little distilled water. A mark was made on the ice test sample before it was cut so that the two halves could be frozen together again at the same relative position, i.e. without any rotation. The reshaped samples were reinstalled in the apparatus and retested for a further ~ 10% strain. Most samples were tested a total of three times.

For simple shear tests, the stress is reduced due to loss of tension as the sample deforms. This was compensated for by adjusting the dial spring balance each time a displacement reading was made, thus maintaining a constant load on the test sample. At the completion of each experiment the shear apparatus was put into a cold room at -10 °C to be cooled and unloaded. A thin section was taken from the middle of the sample and parallel to the

shear direction. Shear tests were run to as large a strain as possible. A maximum octahedral shear strain of 239% was attained without destroying the sample.

3.5. THIN SECTIONING

Thin sections were taken from each sample before and after testing. Before testing, the horizontal and vertical sections were cut perpendicular to and parallel to (respectively) the long (compression) axis of the core for all samples. After testing, horizontal sections, cut perpendicular to the compression axis for compression tests and parallel to the shear plane for shear tests, were taken. The experimental shear direction was marked on the thin sections.

Thin section preparation was carried out in a cold room at -10 °C using the technique described by Langway (1958). In order to reduce boundary effects the thin sections were taken from the middle of the samples at the completion of all tests. Each sample was cooled and unloaded, then cut into two identical parts using a band saw. A middle surface of the sample was polished smooth and flat using a fine sandpaper. This surface was then frozen to a clean pre-warmed glass slide with 124 x 124 x 1.5 mm dimensions. The sample was then cut on a band saw to ~ 1 mm thick, then sliced on a microtome until grain boundaries were clearly discernable between crossed polaroid filters. Thin section thickness was typically 0.4 to 0.8 mm.

3.6. MEASUREMENT OF CRYSTAL ORIENTATION FABRIC

Orientations of crystal c-axes were measured under crossed polaroids with a modified Rigsby Universal Stage (Morgan and others, 1984) using the technique described by Langway (1958). At least one hundred crystals were oriented for each thin section, unless (for some samples with particularly large crystals) there were not that many available. For shear samples, thin sections were mounted on the stage such that the zero azimuth value on the stage was parallel to the experimental shear direction marked on the thin section. This ensured that the experimental shear directions were correctly marked on the fabric diagrams. Inclination data have been corrected to account for air-ice refraction

(Langway,1958). The measured c-axis orientations were plotted in Schmidt equal-area nets. Associated c-axis distribution histograms and fabric statistical parameters including the mean c-axis angle off the vertical, μ, the standard deviation, σ, and the half-apex angles of the cones containing 25% and 50% of the c-axes, ϕ_{25} and ϕ_{50}, were calculated.

3.7. DETERMINATION OF CRYSTAL SIZE

Crystal size was determined from enlarged photographs of ice thin sections by the count per unit area method. Mean crystal diameter, D was estimated by counting (using a computer linked digitiser) the number of crystals, N in a measured (also using a computer linked digitiser) area, A, assuming circular cross section and using the relation

$$D^2 = \frac{4\,A}{\pi\,N} \qquad (3.15)$$

or

$$S = \frac{A}{N} \qquad (3.16)$$

where S is mean crystal area.

For the estimation of crystal size within a thin section, the mean linear intercept method (Pickering, 1976) may be better for regularly shaped, approximately equi-sized crystals. The count per unit area method seems more reliable however, for thin sections containing irregular crystals with unknown size distribution, e.g. from within an ice core from a natural ice mass (Jacka, 1984b).

4. ICE DEFORMATION TESTS IN UNIAXIAL COMPRESSION

Uniaxial compression tests were performed on each test sample described in Chapter 2 at 0.2 MPa octahedral shear stress and - 5 °C. Six laboratory prepared ice samples were also tested at the same stress and temperature. The properties of these ice test samples have been described in detail in Chapter 2. In order to reach high strains the tests were (in most cases) divided into three stages (i.e. as described in Section 3.4). Thin sections perpendicular to the compression axis were cut from the middle of the sample for crystallographic analyses between each test stage. Appendix I displays strain curves, crystal orientation fabrics and associated c-axis distribution histograms, thin section photographs, crystal size data and fabric statistical parameters for each test.

4.1. STRAIN CURVES AND STRAIN RATES

4.1.1. Strain curves

The strain curves (octahedral shear strain rate as a function of octahedral shear strain on log - log scales) for the tests on all the samples are presented across the top line of Appendix I. All strain curves were plotted as raw data points with no smoothing. The compression tests were carried out in stages as described in Section 3.4. Thus there are two or three strain curves representing the first, second or third stages respectively.

The strain curves are similar to those obtained by Gao and Jacka (1987) and Budd and Jacka (1989). The curves for most of the ice core samples are similar to those obtained for the laboratory prepared isotropic ice and exhibit the development of the octahedral shear strain rate with the octahedral shear strain. Generally the strain picture can be described thus : a primary decreasing strain rate until minimum, an accelerating strain rate and finally, a near constant tertiary strain rate at about 5 to 11 % octahedral shear strain. The compression was stopped once the steady state tertiary stage was attained. The next compression test stage on the reshaped samples was restarted with the same stress and temperature. Strain rate then decreased asymptotically to approximately the final creep

rate of the previous stage. If the compression test was stopped at some particular strain and fabric development beyond minimum strain rate, then restarted, the re-deformation strain rate for the reshaped sample went through a new minimum strain rate corresponding to the strain rate at the stage reached when the previous compression stopped. In Appendix I, the curve for sample AGZ77-230 illustrates the above description. Note that the minimum attained in the second stage of the test is equal to the final strain attained in the first stage. The strain curves for some samples (see e.g. BHC1-121B, BHC1-138CT) exhibited strain rates decreasing directly to the tertiary strain rate without passing through a minimum.

4.1.2. Minimum strain rates

Since the ice test samples taken from the natural ice masses, particularly where high deformation rates occur, have developed strong crystal anisotropy as a consequence of the deformation history, the minimum strain rate which occurred during testing is a characteristic of the anisotropy of the original sample before recrystallisation sets in to change the structure of the sample. The clear relationship between the preferred orientation of c-axes and strain rates has been demonstrated by laboratory experiments (Lile, 1978; Russell-Head and Budd, 1979; Duval, 1981; Duval and Le Gac, 1982; Azuma and Higashi, 1984) and by borehole tilting measurements (Shoji and Langway, 1984; Russell-Head and Budd, 1979; Gundestrup and Hansen 1984).

From Table 4.1, it is seen that the minimum strain rates for all the ice core samples range from 2.0×10^{-9} s^{-1} (i.e. lower than the mean of 1.2×10^{-8} for laboratory prepared isotropic ice samples) to 2.2×10^{-8} s^{-1} (higher than the isotropic minimum). There is clear evidence to show that the flow of ice with a single maximum fabric has a minimum strain rate lower than that of the laboratory prepared isotropic ice (i.e. the single maximum fabric is a hard glide fabric for uniaxial compression). The flow of ice with a multiple maximum fabric has a relative higher minimum strain rate (i.e. the multiple maximum fabric is an easy glide fabric in uniaxial compression) and this strain rate in fact is approximately equivalent to the tertiary strain rate. The results show that the stronger the single maximum fabric, the lower the minimum strain rate.

Table 4.1 Strain rates and strains in compression tests.

sample number	1st compression			2nd compression		3rd compression		mean tertiary strain rate (s^{-1})	enhancement factor
	minimum strain rate (s^{-1})	tertiary strain rate (s^{-1})	total strain (%)	tertiary strain rate (s^{-1})	total strain (%)	tertiary strain rate (s^{-1})	total strain (%)		
AGZ77-225A	8.2×10^{-9}	1.4×10^{-8}	18	2.1×10^{-8}	36	1.4×10^{-8}	44	1.6×10^{-8}	2
AGZ77-225B	3.5×10^{-9}	-	11	-	20	-	-	-	-
AGZ77-226	5.2×10^{-9}	1.8×10^{-8}	16	4.5×10^{-8}	34	1.0×10^{-8}	42	2.4×10^{-8}	4.6
AGZ77-228	5.6×10^{-9}	1.5×10^{-8}	18	1.3×10^{-8}	20	-	-	1.4×10^{-8}	2.5
AGZ77-229	2.8×10^{-9}	1.3×10^{-8}	13	1.9×10^{-8}	23	2.1×10^{-8}	29	2.3×10^{-8}	8.2
AGZ77-230	2.0×10^{-9}	-	3	-	17	3.9×10^{-8}	36	3.9×10^{-8}	19.5
BHC1-73B	6.8×10^{-9}	1.4×10^{-8}	16	1.4×10^{-8}	29	1.4×10^{-8}	29	1.4×10^{-8}	2.1
BHC1-79C	3.7×10^{-9}	1.9×10^{-8}	10	2.2×10^{-8}	22	2.5×10^{-8}	30	2.2×10^{-8}	6
BHC1-84B	3.7×10^{-9}	1.1×10^{-8}	16	2.1×10^{-8}	39	2.0×10^{-8}	55	1.7×10^{-8}	4.6
BHC1-108D	1.5×10^{-8}	1.5×10^{-8}	21	1.5×10^{-8}	40	-	-	1.5×10^{-8}	1
BHC1-116D	-	-	10	1.4×10^{-8}	19	1.1×10^{-8}	27	1.3×10^{-8}	1
BHC1-121B	2.1×10^{-8}	2.1×10^{-8}	12	1.8×10^{-8}	25	1.7×10^{-8}	33	1.9×10^{-8}	1
BHC1-134D	-	-	7	2.0×10^{-8}	26	1.4×10^{-8}	33	1.7×10^{-8}	1
BHC1-138C	1.3×10^{-8}	2.0×10^{-8}	10	2.1×10^{-8}	20	1.6×10^{-8}	36	1.9×10^{-8}	1
DYE3-338	2.2×10^{-8}	3.8×10^{-8}	17	2.3×10^{-8}	27	$1.5 \times 10-8$	33	2.5×10^{-8}	1.1
DYE3-1556	7.5×10^{-9}	3.9×10^{-8}	13	3.6×10^{-8}	20	$1.8 \times 10-8$	32	3.1×10^{-8}	4.1
DYE3-1763	3.0×10^{-9}	3.2×10^{-8}	12	$2.4 \times 10-8$	27	$3.8 \times 10-8$	43	3.1×10^{-8}	10.3
DYE3-1922	4.5×10^{-9}	4.5×10^{-8}	7	$3.2 \times 10-8$	23	-	-	3.8×10^{-8}	8.4
LAB-1	1.8×10^{-8}	3.5×10^{-8}	23	-	-	-	-	-	1.9
LAB-2	1.1×10^{-8}	5.9×10^{-8}	31	-	-	-	-	-	5.4
LAB-3	1.1×10^{-8}	3.6×10^{-8}	18	3.3×10^{-8}	34	2.3×10^{-8}	42	3.1×10^{-8}	2.8
LAB-4	1.2×10^{-8}	3.7×10^{-8}	20	3.0×10^{-8}	33	2.0×10^{-8}	43	2.9×10^{-8}	2.4
LAB-5	1.2×10^{-8}	3.7×10^{-8}	17	3.1×10^{-8}	33	2.3×10^{-8}	43	3.0×10^{-8}	2.5
LAB-6	1.1×10^{-8}	3.6×10^{-8}	16	2.9×10^{-8}	34	2.8×10^{-8}	49	3.1×10^{-8}	2.8

4.1.3. Tertiary strain rates

All creep curves (except for sample AGZ77-225B) exhibit tertiary strain rate at about 5 to 10% strain. As shown in Table 4.1, the tertiary strain rate averaged over the three compression test stages ranged from 1.3×10^{-8} to 3.9×10^{-8} s^{-1} with a mean of 2.2×10^{-8} s^{-1}, a factor of 1.4 lower than the mean of 3.0×10^{-8} s^{-1} attained for laboratory prepared isotropic ice samples. Gao (unpublished) also found a discrepancy for the tertiary strain rates of laboratory prepared isotropic ice samples compared with those for ice core anisotropic samples. He attributed the discrepancy to differences in the mean angle of the initial (small circle girdle) fabrics. For the present tests, this discrepancy seems to decrease with the sample re-deformation stages (i.e. with the attainment of high strains). The important point to note in any case, is that the tertiary strain rates for all test samples were very close to each other and tended to a constant strain rate, even though their minimum strain rates differed by an order of magnitude.

4.1.4. Enhancement factor

Enhancement factor, the ratio of the tertiary strain rate to the minimum strain rate, is calculated and listed in Table 4.1. Here, the tertiary rate is an average of the measured tertiary strain rate over the three compression tests stages for each sample.

As shown in the data, the enhancement factor has a wider range (1 to 19.5) for the ice core samples than for laboratory prepared samples (mean of 3). There is a strong relationship between the enhancement factor and the crystal orientation fabric.

Generally, for initially isotropic ice the enhancement factor is about 3 in compression (Jacka and Maccagnan, 1984; Steinemann, 1958) and about 8 to 10 in shear (Russell-Head, 1985; Duval, 1981). For this study, the strain rates of all ice samples tended eventually to a constant steady state tertiary strain rate, and the enhancement factor may reach as high as 19.5 or more for the ice initially with stronger single maximum fabrics. Enhancement factor is as low as 1 for ice initially exhibiting a multiple maximum fabric.

4.2. THE FACTORS AFFECTING THE FLOW OF ICE

Shoji and Langway (1988) carried out a set of constant strain rate uniaxial compression tests on samples of Wisconsin ice from the DYE3 core. Pimienta and Duval (1988) carried out uniaxial and biaxial tests on ice samples from the last interglacial period from the Vostok, Antarctica core. They obtained similar results. The insoluble (dust) and soluble (mainly Cl^-, NO_3^- or SO_4^- ions) impurity concentrations did not seem to influence the mechanical behaviour, and the enhancement factor, measured in various stress fields, appeared to be dependent mainly on the orientation of the c-axes.

It has been expected (Paterson, 1991) for uniaxial compression of the Wisconsin and Holocene ice along the axis of the core, that if "softness" results from impurities alone, the Wisconsin ice (containing higher impurity concentration and with stronger fabric and smaller crystals) should deform more rapidly than the Holocene ice (containing lower impurity concentration and with weaker fabric and larger crystals) at all stages of the deformation. If crystal orientation fabric and different rates of its development are the flow rate determining factors, the minimum strain rate of the Holocene ice should be greater than for the Wisconsin samples and, although both samples should eventually reach the same tertiary strain rate, the Wisconsin ice sample should reach it first. Therefore, there is a requirement to inspect, separately, the effects of impurities on tertiary strain rate and of initial crystal orientation fabric on minimum strain rate in order to separate the effects of crystal orientation fabric pattern and of impurity concentrations on the flow.

4.2.1. Effect of impurities on tertiary strain rates

From Table 2.3 and Table 4.1, the sample AGZ77-225A (the Wisconsin ice from the AGZ77 core) exhibits higher dust concentration (by a factor of 651) than sample BHC1-116D (the Transition ice from the BHC1 core). As stated above, if dust has a softness effect, sample AGZ77-225A should deform more rapidly than sample BHC1-116D at all stages of the deformation, i.e. sample AGZ77-225A should show relatively higher tertiary and minimum strain rates than sample BHC1-116D. However, the tertiary strain rates for

these two samples are similar, even though the minimum strain rate for sample AGZ77-225A was 2 times lower than the tertiary strain rate. The minimum strain rate for sample BHC1-116D was nearly the same as the tertiary strain rate.

Another example is provided by DYE3 core samples. The dust concentration for sample DYE3-T1763 (Wisconsin ice) was 9.5 times higher than for sample DYE3-T1556 (Holocene ice). The concentrations of Na, Ca, Mg, Cl and SO_4 ions in sample DYE3-T1763 were respectively 12.7, 8.4, 5.0, 13.0 and 5.3 times higher than for sample DYE 3-T1556. However, the tertiary strain rates are similar even though the minimum strain rate for sample DYE3-T1763 was 2.5 times lower than for sample DYE3-T1556.

This phenomenon above will be explained in Section 4.2.2 by the crystal orientation fabric pattern in the samples. Figures 4.1 and 4.2 are respectively, plots of the dust concentration and soluble impurity concentrations (Na, Ca, Mg, Cl, SO_4 and NO_3 ions), as functions of the tertiary strain rate. These figures show no correlation between dust concentration or soluble impurity concentration and tertiary strain rate despite significant variations in the impurity concentrations. These results coincide with those of Shoji and Langway (1988) and of Pimienta and Duval (1988).

4.2.2. Effect of initial crystal orientation fabric on minimum strain rate

As described in Section 4.1.2, compared with laboratory prepared isotropic ice, the ice samples with an initial single maximum fabric show a relatively lower minimum strain rate and the ice samples with an initial multiple maximum fabric show a relative higher minimum strain rate (equivalent to the tertiary strain rate). This is in agreement with the expectation of Paterson (1991); i.e. if fabric is the determining factor of "softness" the minimum strain rate for the Holocene ice should be greater than for the Wisconsin ice. In addition, this may explain , as mentioned in Section 4.2.1, why samples AGZ77-225A and DYE3-T1763 exhibited lower minimum strain rates than samples BHC1-116D and DYE3-T1556. That is, sample AGZ77-225A initially showed a single maximum fabric pattern (a hard glide fabric pattern in compression) which resulted in a lower minimum strain rate. In

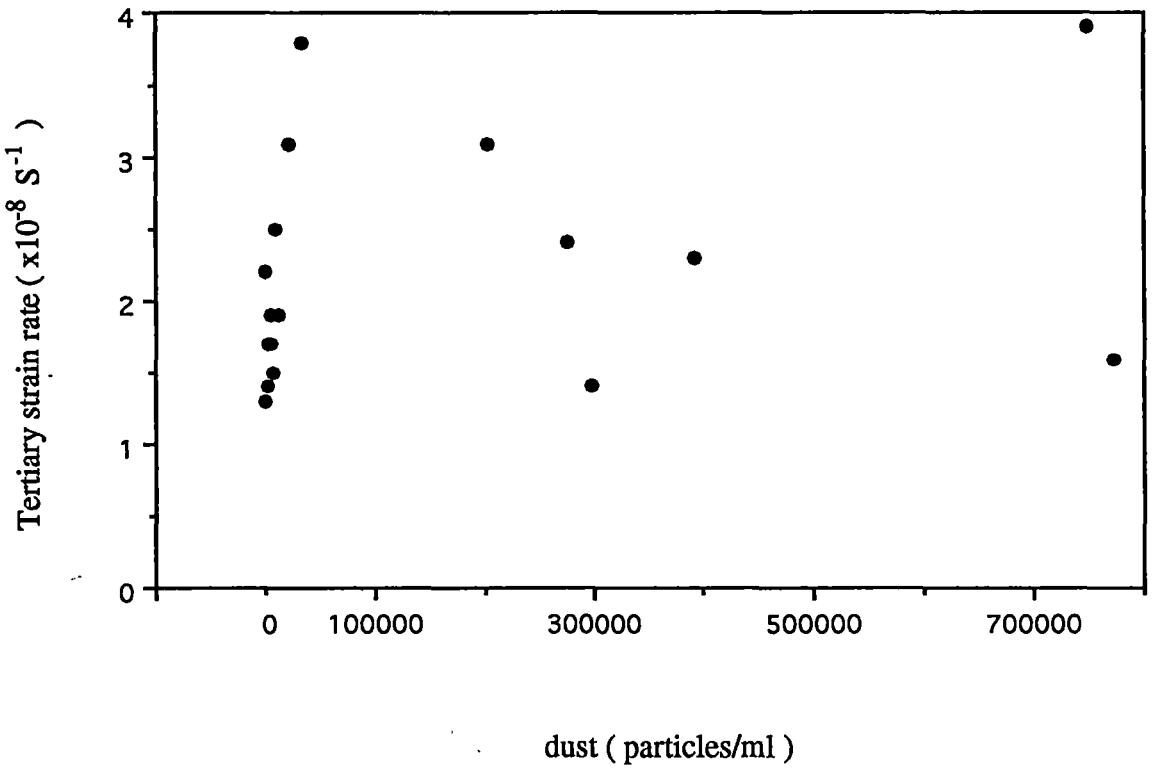

Figure 4.1 Tertiary strain rates in compression as a function of dust concentrations

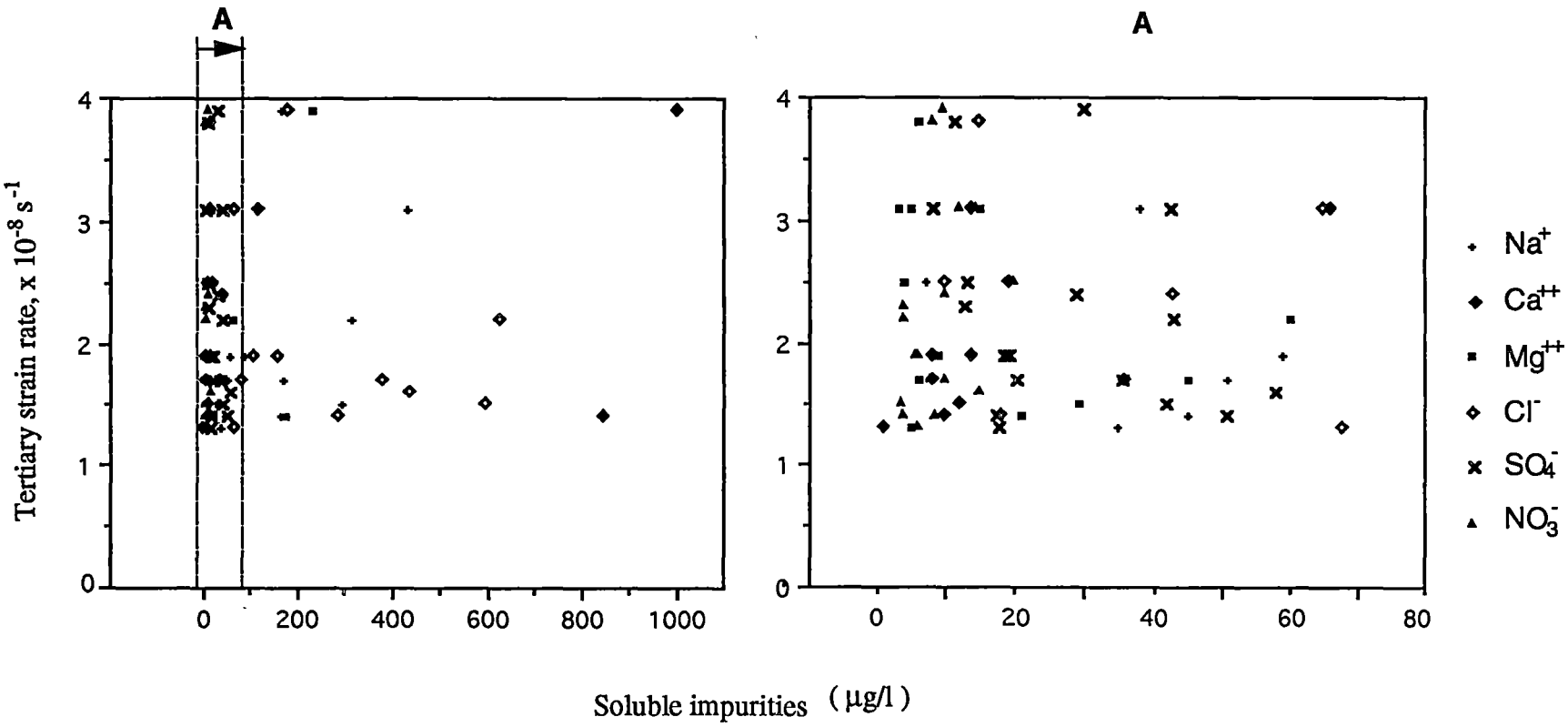

Figure 4.2 Tertiary strain rates in compression as a function of soluble impurities. The right figure is an enlargement of the section between the two dashed lines shown in the left figure.

addition, sample BHC1-116D initially showed a multiple maximum pattern (similar to a girdle fabric pattern and an easy glide fabric pattern in compression), which resulted in a constant creep rate close to tertiary strain rate. Similarly sample DYE3-T1763 (strong single maximum fabric) resulted in a lower minimum strain rate than sample DYE3-T1556 (multiple maximum fabric).

The results show that the minimum strain rate is primarily determined by initial crystal orientation fabric. This result however has been known for some time (e.g. Gao and Jacka, 1987; Budd and Jacka, 1989) and supports the conclusion made by Shoji and Langway (1988) and by Pimienta and Duval (1988).

4.3. STEADY STATE FLOW OF ICE IN COMPRESSION DEFORMATION

Steady state ice flow in compression has been observed in previous laboratory experiments (e.g. Budd and Matsuda, 1974; Wilson and Russell-Head, 1982; Jacka, 1984b; Jacka and Maccagnan, 1984; Gao and Jacka, 1987) and further confirmed by the results in this Chapter. Given sufficiently high deformation (strain) a tertiary steady state creep rate is established dependent on test temperature and stress. Along with the development of this steady state creep rate, a steady state crystal orientation fabric and a steady state (or equilibrium) crystal size is also developed. The results obtained here show that this steady state ice flow is independent of the initial sample parameters; i.e. no matter whether the sample initially exhibits a single maximum, random or small circle girdle fabric pattern, no matter what the initial crystal size and no matter what the initial impurity concentrations, the same steady state tertiary flow rate will be attained once sufficient strain is attained. The results also show the independence of the steady state flow from the sample origin or history; i.e. no matter whether the test sample is laboratory-prepared or from an ice core drilled from a natural ice mass, no matter whether it is Holocene or Wisconsin in origin and no matter whether from the Northern or Southern hemisphere - still the steady state flow rate will be the same.

4.3.1. Steady state tertiary strain rate

As show in Appendix I, the compression tests on all samples (except for sample AGZ77-225B) reached the tertiary stage. The steady state tertiary strain rate for all the samples was close to 3.0×10^{-8} s^{-1}. This constant tertiary strain rate was maintained for up to 55% strain.

4.3.2. Steady state crystal orientation fabric

The crystal orientation fabrics and associated c-axis orientation histograms resulting from the three compression test stages on each of the samples are presented in the second and third rows of Appendix I. The initial fabric data are presented in Figure 2.4. Table 4.2 summarises the fabric data.

Theoretically in compression the maximum shear occurs in a right circular conical surface whose normals are at 45° to the unique axis, i.e. forming a girdle around that axis (Budd, 1972). This small circle girdle fabric pattern has been obtained by previous compression tests on laboratory prepared isotropic ice (Watanabe and Oura, 1968; Wilson and Russell-Head, 1982; Huang and others, 1982, Jacka and Maccagnan, 1984) and on anisotropic ice from natural ice masses (Steinemann, 1958; Tanaka, 1972; Huang and others, 1988; Azuma and Higashi, 1985; Gao and Jacka, 1987).

The results described here further confirm that, along with attainment of tertiary strain rate at 5 to 11% strain, a preferred crystal orientation fabric (small circle girdle centred about the compression axis) develops, and this fabric continues to strengthen with increasing strain until ~55 % strain. The c-axis mean vertical angles of these final small circle girdle fabrics ranged from 28.54 to 34.92° with a mean of 31.5° for initially isotropic laboratory prepared ice and from 23.73 to 36.74° for initially anisotropic ice core samples. Gao and Jacka (1987) and Gao (unpublished) have found that the c-axis mean angle of the small circle girdle fabric asymptotically decreases to a limiting value of about 26° to the vertical.

Table 4.2 (2 pages) Data for crystal orientation fabric and size resulting from compression tests. σ and μ indicate standard deviation and mean angle of the c-axes of crystals to the vertical, and $\phi(1/4)$ and $\phi(1/2)$ the half-apex angles of the cones containing 25% and 50% of the c-axes.

sample number	fabric (before compression)					crystal size	fabric (after 1st compression)					total strain	crystal size
	description	μ_0 (°)	σ_0 (°)	ϕ_0 (1/4) (°)	ϕ_0 (1/2) (°)	S_0 (mm^2)	description	μ_1 (°)	σ_1 (°)	ϕ_1 (1/4) (°)	ϕ_1 (1/2) (°)	ε (%)	S_1 (mm^2)
AGZ 77 / 225A	single maximum	23.18	14.08	13.70	20.55	2.1	weak girdle	29.52	11.08	21.13	30.56	18	2.53
AGZ77 / 225B	single maximum	26.25	10.62	20.56	25.16	0.8	single maximum	19.15	18.27	9.00	13.00	11	0.91
AGZ 77 / 226	single maximum	23.14	13.96	14.86	20.21	1.5	weak single max.	17.68	13.66	7.87	12.85	16	0.92
AGZ 77 / 228	single maximum	20.64	10.71	13.16	19.29	2.3	girdle	33.55	9.21	27.10	33.04	18	6.73
AGZ 77 / 229	single maximum	18.69	8.78	13.00	18.00	2.2	?	30.71	17.88	21.36	29.67	13	5.85
AGZ 77 / 230	single maximum	15.11	8.15	9.45	13.86	2.7	single maximum	10.61	4.03	7.15	10.53	3	
BHC 1 / 73B	central trend	28.67	6.31	25.00	29.00	>41	weak girdle	27.81	15.79	18.00	25.00	16	4.08
BHC 1 / 79C	central trend	29.21	20.74	15.00	20.00	>45	weak central trend	26.97	14.07	18.03	25.12	10	2.27
BHC 1 / 84B	central trend	20.72	13.86	11.68	16.89	18	girdle	25.89	6.47	21.22	24.59	16	2.60
BHC 1 / 108D	?	40.00	21.70	28.00	33.00	>100	weak girdle	33.62	15.78	23.00	31.21	21	3.12
BHC 1 / 116D	multiple maximum	22.57	8.02	16.50	20.00	>320	weak girdle	30.15	14.13	20.87	31.45	10	4.75
BHC 1 / 121B	multiple maximum	25.13	12.85	21.01	26.44	>91	girdle	36.76	12.09	30.91	36.10	12	6.24
BHC 1 / 134D	multiple maximum	68.60	20.45	46.00	76.00	>130	-	-	-	-	-	7	-
BHC 1 / 138C	multiple maximum	40.50	26.88	32.00	36.00	>310	girdle	29.88	13.56	21.11	24.44	10	11.60
DYE 3 / T338	weak central trend	38.45	26.21	17.00	23.00	15.1	girdle	26.46	9.86	20.85	24.47	17	13.20
DYE 3 / T1556	?	38.64	28.56	11.00	39.00	282	?	36.17	17.39	27.83	34.59	13	13.10
DYE 3 / T1763	single maximum	13.54	8.20	7.90	12.63	3.6	weak single max.	36.46	16.38	29.48	35.49	12	2.93
DYE 3 / T1922	single maximum	12.98	11.37	7.00	12.00	5.1	?	38.31	20.75	30.82	40.96	7	1.53
LAB-1	random	57.59	23.03	39.01	61.06	1.0	girdle	34.92	11.06	26.38	33.74	23	1.66
LAB-2	random						girdle	28.54	8.37	22.69	27.52	31	2.09
LAB-3	random	theoretical	theoretical				week girdle	31.26	12.60	26.82	33.06	18	2.11
LAB-4	random	57.30	21.56				girdle	34.67	7.12	30.45	34.47	20	2.11
LAB-5	random						weak girdle	38.85	17.00	25.42	37.53	17	1.59
LAB-6	random						girdle	33.56	9.03	26.31	32.80	16	1.40

sample number	fabric (after 2nd compression)					total strain	crystal size	fabric (after 3rd compression)					total strain	crystal size
	description	μ_2 (°)	σ_2 (°)	ϕ_2 (1/4) (°)	ϕ_2 (1/2) (°)	ε (%)	S_2 (mm^2)	description	μ_3 (°)	σ_3 (°)	ϕ_3 (1/4) (°)	ϕ_3 (1/2) (°)	ε (%)	S_3 (mm^2)
AGZ 77 / 225A	girdle	27.59	9.97	21.00	27.00	36	2.02	girdle	29.00	11.82	23.00	28.00	44	2.15
AGZ77 / 225B	single maximum	17.58	14.28	8.00	14.00	20	0.78	-	-	-	-	-	-	-
AGZ 77 / 226	girdle	33.97	12.70	27.06	33.65	34	1.95	girdle	25.63	10.48	19.17	25.21	42	0.66
AGZ 77 / 228	-	-	-	-	-	20	-	-	-	-	-	-	-	-
AGZ 77 / 229	girdle	33.29	14.13	22.10	32.02	23	9.04	girdle	24.80	8.37	17.64	24.26	29	5.96
AGZ 77 / 230	weak single max.	18.00	13.09	7.82	14.05	17	1.91	girdle	29.82	7.22	25.30	30.26	36	1.65
BHC 1 / 73B	girdle	30.94	12.50	24.00	30.00	29	2.06	girdle	30.11	12.56	22.00	28.00	29	2.15
BHC 1 / 79C	central trend	23.11	10.54	16.18	23.49	22	1.70	weak girdle	29.80	16.75	18.95	25.75	30	1.22
BHC 1 / 84B	girdle	24.54	8.53	18.71	23.52	39	2.22	girdle	27.11	9.82	19.00	28.00	55	2.19
BHC 1 / 108D	girdle	31.40	9.41	25.00	31.00	40	3.06	-	-	-	-	-	-	-
BHC 1 / 116D	girdle	27.80	8.50	20.00	28.33	19	9.88	girdle	23.73	6.37	20.26	23.01	27	21.30
BHC 1 / 121B	weak girdle	36.14	21.75	17.10	32.52	25	3.18	weak girdle	28.03	11.13	17.39	30.18	33	2.87
BHC 1 / 134D	?	48.31	24.24	27.63	45.09	26	10.80	weak girdle	34.77	16.10	24.69	33.25	33	5.04
BHC 1 / 138C	girdle	29.90	16.18	17.50	23.76	20	6.21	girdle	34.38	15.22	18.74	36.23	36	8.68
DYE 3 / T338	girdle	26.71	5.42	21.72	26.25	27	10.40	girdle	28.58	13.34	19.56	28.10	33	19.20
DYE3 / T1556	girdle	29.05	7.27	22.82	29.29	20	11.50	weak girdle	35.60	14.32	24.82	30.91	32	11.50
DYE 3 / T1763	girdle	30.79	8.94	25.26	30.78	27	3.55	girdle	30.16	9.74	23.03	27.89	43	1.61
DYE3 / T1922	girdle	36.74	10.44	30.41	34.16	23	3.01	-	-	-	-	-	-	-
LAB-1	-	-	-	-	-	-	-	-	-	-	-	-	-	-
LAB-2	-	-	-	-	-	-	-	-	-	-	-	-	-	-
LAB-3	girdle	30.53	7.96	24.17	29.23	34	2.51	girdle	31.89	10.31	23.97	30.38	42	2.79
LAB-4	girdle	31.61	7.65	25.34	29.80	33	2.75	girdle	30.65	9.10	23.34	28.58	43	2.71
LAB-5	girdle	30.90	8.74	23.30	29.38	33	2.73	girdle	32.74	12.02	24.08	31.73	43	2.61
LAB-6	weak girdle	40.43	18.50	23.16	32.46	34	1.78	girdle	30.10	8.97	24.40	27.64	49	2.51

It may be that higher strains are required in the tests described in this report, especially for the initially anisotropic ice with hard glide single maximum fabrics, to attain these stronger small circle girdle fabrics. In addition, examining the evolution of the girdle fabric with increasing strain for samples AGZ77-225B, AGZ77-226 and AGZ77-230 (all of which initially displayed single maximum fabrics of varying strengths) it appears that the amount of strain required for the development of the girdle fabric was greater than that for initially isotropic samples. For example, minimum strain rate (and thus, the beginning of the development of the girdle fabric) was not attained until 19.6% strain for sample AGZ77-225B. More work is required to clarify this explanation.

4.3.3. Steady state crystal size

It has been found that the initial crystal size of the ice sample has little or no effect on the ice flow rate in compression for stress ranges typically found in the natural ice sheets. Further, it has been found that crystal size itself is affected by the deformation (Duval and Le Gac, 1980; Jones and Chew, 1981, 1983; Jacka, 1984b; Gao, unpublished). Along with the attainment of tertiary strain rate a steady state (or equilibrium) crystal size is established. The actual value of the equilibrium crystal size seems to be dependent on the stress and temperature (Jacka, 1984b; Jacka and Maccagnan, 1984; Gao and Jacka, 1987) or stress alone (Jacka and Li, 1994), but independent of the initial crystal size or orientation.

Figure 4.3 is a plot of the crystal size as a function of the octahedral shear strain for the compression tests of this study. It is clear that an equilibrium crystal size is established with the attainment of tertiary flow beyond 5 to 11% octahedral shear strain. The line on Figure 4.3 indicates the mean final (equilibrium) crystal size of 2.24 mm^2. It is seen that the change in mean crystal size, from an initially wide range of 0.84 to 310 mm^2 (the largest crystal size is 369 times greater than the smallest one) to a final range of 0.7 to 21 mm^2, involves a mean increase for initially smaller crystals and a mean decrease for initial larger crystals. For instance, the mean crystal size for all laboratory prepared ice samples increased from 1.02 to 2.24 mm^2, while for all BHC1 core samples the mean crystal size

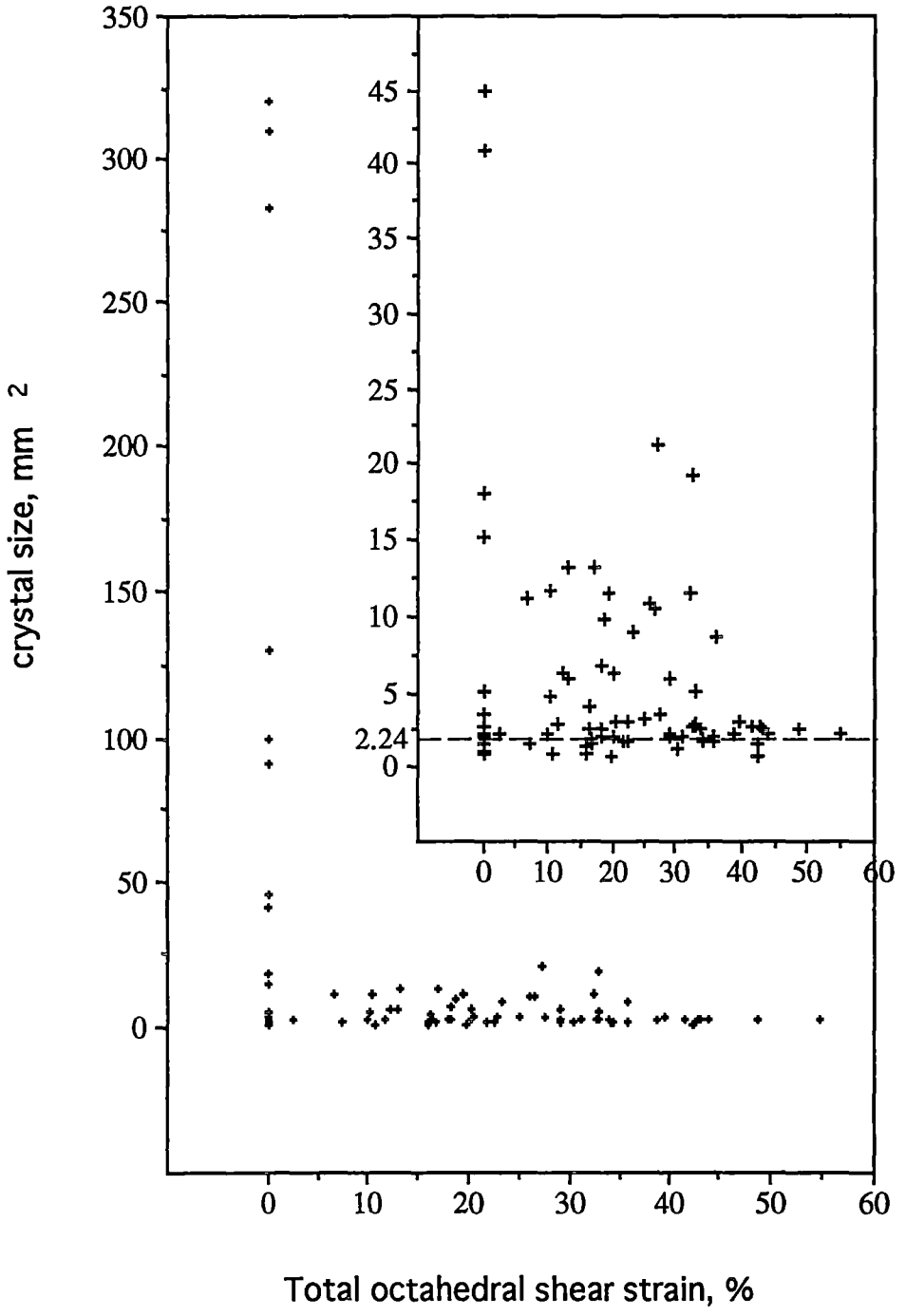

Figure 4.3 Crystal size in compression as a function of total octahedral shear strain. The dashed line indicates the mean crystal size of laboratory prepared ice samples beyond 16% octahedral shear strain.

decreased from a range of 18.09 to 320 mm^2 to a final range (with the exception of one point) of 1.22 to 8.68 mm^2. The one exception is for a sample with final mean crystal size, 21.25 mm^2. This larger final crystal size has developed as a consequence of decreasing stress due to increasing sample cross-sectional area.

The strain required for the establishment of the equilibrium crystal size seems dependent on the initial crystal size and crystal orientation fabric. The results show that the crystal size tends from 0.66 to 21.25 mm^2 by 35 % strain, from 0.66 to 3.06 mm^2 after 35 % strain and from 2.15 to 2.61 mm^2 after 43 % strain.

Because a high negative correlation between crystal size and impurity concentration was found for the AGZ77 core (Fisher and Koerner, 1986), for the DYE3 core (Hammer and others, 1985; Langway and others, 1988), and in several other cores (Koerner and Fisher, 1979), they attributed the smaller crystal size to reduced crystal growth rate caused by the concentrations of microparticles (dust) (Koerner and Fisher, 1979) and soluble impurities (mainly Cl and Na or SO_4 ions) (Alley and others, 1986a, 1986b; Langway and others, 1988). But Duval and Lorius' (1980) calculation shows that at Dome C, Antarctica, even an ice age dust concentration 100 times higher than the Holocene levels would not reduce the crystal growth rate significantly. This is supported by the results obtained in this set of compression tests on the Wisconsin and Holocene ice drilled from natural ice masses in the Northern Hemisphere and Antarctica. From Tables 2.3 and 4.2, the dust concentrations in the AGZ77 core samples were two orders of magnitude higher than those in the BHC1 core ice samples. The crystal sizes were two orders of magnitude lower. Along with the attainment of tertiary flow, the mean crystal size for the AGZ77 core samples increased while the mean crystal size for the BHC1 core samples decreased. Thus, Both mean crystal sizes approached a similar equilibrium crystal size. Also, the equilibrium crystal size was unaffected by dust concentration or by chloride, sodium, sulphate or other soluble impurities.

4.4. SUMMARY

Uniaxial compression tests on the Wisconsin and Holocene ice from the AGZ77, BHC1 and DYE3 cores show that the deformation of both the Wisconsin and the Holocene ice tends to reach a constant steady state tertiary stage. No evidence has been found to indicate that the deformation of the Wisconsin ice is more rapid than that of the Holocene ice.

The enhanced flow for ice with an easy glide fabric (small circle girdle pattern for compression) may reach as much as 19.6 times faster than the flow for ice with a hard glide fabric (e.g. single maximum pattern for compression) and 3 times faster than the flow of isotropic ice. This indicates that the crystal orientation fabric pattern is the main factor affecting the ice flow rates. The measured enhanced flow in the Wisconsin ice for the AGZ77 core and in the DYE3 core seems to be mostly dominated by the crystal orientation fabric at the temperature and stress considered here.

The results also indicate that the soluble (dust) and insoluble impurity concentrations do not affect the flow rates, again, at the temperature and stress considered here.

This set of experiments has further extended studies of the steady state ice flow in compression to the anisotropic ice of the Wisconsin and Holocene climatic periods as evidenced in ice cores from Agassiz, Greenland and Antarctica.

5. ICE DEFORMATION TESTS IN SIMPLE SHEAR

A set of simple shear tests at an octahedral shear stress of 0.2 MPa and a temperature of -5.0 °C was carried out on the sixteen ice test samples described in Chapter 2. These test parameters were deliberately chosen for direct comparison with the results in uniaxial compression described in Chapter 4. The six laboratory prepared ice samples described earlier were also included in this set of tests. The experimental technique used in the simple shear tests has been described in Chapter 3. Appendix II displays the strain curves resulting from the simple shear tests. Crystal orientation fabrics, associated c-axis distribution histograms, thin section photographs and total strain and crystal size data are also included in Appendix II for each ice sample both prior to testing and after test conclusion.

5.1 RE-MEASUREMENT TO THE ICE TEST SAMPLES

The uniaxial compression tests in Chapter 4 show that the flow of ice is highly related to the initial crystal orientation fabric. Therefore, each of the samples was remeasured for crystal orientation fabric and crystal size from the prepared shear test specimens before experiments were commenced. This ensured that the crystallography of each sample was well documented prior to each new test.

As shown in Appendix II, the measurements of crystal orientation fabric and crystal size for the shear test specimens (prior to testing) exhibit quite similar characteristics to the measurements for the compression test specimens (see Chapter 2) for most of the samples.

It is noted that the sample AGZ77-225B (the Wisconsin sample from the AGZ77 core) exhibits different characteristics from the compression test specimen (Chapter 2) in both the crystal orientation fabric (a very strong single maximum fabric pattern compared to a weak single maximum fabric pattern) and the crystal size (from 0.84 to 4.7 mm^2). This sample, in the compression test described in Chapter 4, showed a lower minimum strain rate than others with a multi-maxima fabric, until the test concluded at 19.6% strain. This

result might be expected of a sample exhibiting a strong single maximum fabric off the vertical, i.e. the results of Chapter 4 may be more compatible with the crystallographic structure now seen for the shear test sample. The difference in fabric structure measured for the two initial samples from one core piece may be attributable to variations in the structure within short depths in the sample. Alternatively, changes may have occurred in the structure during sample storage between the two studies.

For all the shear test samples, the initial crystal orientation fabric ranged in type from small circle girdles, weak central tendencies, and multiple-maxima to single maximum patterns. The initial crystal size ranged from 1.2 to >306 mm^2 (cf. an initial crystal size range from 0.8 to >310 mm^2 for the compression test specimens). The largest crystal size was greater than the smallest one by a factor of >255.

For laboratory-prepared ice samples, the crystal orientation fabric and crystal size were measured from a prepared shear test specimen. This specimen exhibited a random c-axis orientation pattern with a c-axis mean vertical angle of 52.39° and a standard deviation of 20.67° (cf. theoretical values of 57.30° and 21.56° respectively), and a crystal size of 0.9 mm^2.

5.2 EXPERIMENTAL RESULTS

5.2.1 Strain curves and strain rates

Unsmoothed raw data points of octahedral shear strain rate were plotted as a function of experiment duration time and of octahedral shear strain on log - log scales. These plots are shown across the top row of Appendix II.

The strain curves are similar to those resulting from the compression tests in Chapter 4. Generally, they exhibit the development of a steady state tertiary flow with increasing strain through a primary decreasing strain rate followed by an accelerating strain rate. They also show that the strain rates for some of the samples with a single maximum fabric, which resulted in a lower minimum strain rate in the compression tests (Chapter 4),

decreased directly to the tertiary strain rate without passing through a minimum. This confirms that the single maximum fabric is compatible for shear yet incompatible for compression (Gao, unpublished; Budd and Jacka, 1989).

Each of the simple shear tests was run until a steady tertiary strain rate was established at an octahedral shear strain of 29 to 239% without sample destruction.

Table 5.1 provides a summary of the experimental data for all the ice core samples. The minimum strain rates ranged from 1.8×10^{-8} s^{-1} (lower than the mean of 5.0×10^{-8} s^{-1} for laboratory prepared isotropic ice samples) to 8.0×10^{-8} s^{-1} (equivalent to the tertiary strain rate) at octahedral shear strains of ~ 1 to 4%. The tertiary strain rates for the ice core samples ranged from 1.3×10^{-7} to 8.0×10^{-7} s^{-1} with a mean of 3.5×10^{-7} s^{-1} at octahedral shear strains of ~1 to 30%. The mean value for the tertiary strain rates for all the ice core samples is higher than a mean of 2.8×10^{-8} s^{-1} for the laboratory prepared ice samples by a factor of 1.2.

There is clear evidence that the deformation in shear of ice with a circle girdle fabric results in a minimum strain rate lower than that for the laboratory prepared isotropic ice. The flow of ice with a single maximum fabric (especially if the maximum is near vertical) results in a relative high minimum strain rate, about equal to the tertiary strain rate.

5.2.2 Comparison of strain rate differences for laboratory prepared isotropic ice in shear and compression

It has been reported for the experiments on laboratory prepared isotropic ice at 0.2 MPa octahedral and -5.0 °C, that the mean minimum strain rate is 1.3×10^{-8} s^{-1} with an enhancement factor of 3 in compression (Chapter 4), and 5.0×10^{-8} $s^{-1}$with an enhancement factor of ~ 6 in shear (this Chapter), respectively. All strain rates presented here are in terms of octahedral values to compare the flow properties of ice under different stress configurations (Nye,1953; Budd,1968).

Table 5.1 Data in simple shear tests.

sample number	sample dimension	crystal size(mm^2)		strain rate (s^{-1})		total strain (%)	enhancement factor
	LxWxH (mm)	before test	after test	minimum	tertiary		
AGZ77-225A	41x19x21	2.4	1.3	6.4×10^{-8}	3.0×10^{-7}	53	4.7
AGZ77-225B	53x19x21	4.7	2.4	4.8×10^{-8}	2.5×10^{-7}	57	5.2
AGZ77-229	33x19x21	2.5	2.9	2.0×10^{-7}	2.0×10^{-7}	38	1
AGZ77-230	34x19x21	3.1	1.9	3.0×10^{-7}	3.0×10^{-7}	91	1
BHC1-73B	46x19x21	>31	1.6	2.0×10^{-7}	5.0×10^{-7}	70	2.5
BHC1-79C	47x17x21	>24	1	5.0×10^{-7}	5.0×10^{-7}	92	1
BHC1-84B	59x19x21	>62	1.1	7.0×10^{-7}	7.0×10^{-7}	98	1
BHC1-108D	54x19x18	>217	5.2	1.3×10^{-7}	1.3×10^{-7}	50	1
BHC1-116D	53x19x20	>138	5.4	5.5×10^{-8}	2.3×10^{-7}	79	4.2
BHC1-121B	52x19x21	>83	3.6	1.8×10^{-7}	1.8×10^{-7}	78	1
BHC1-134D	51x19x22	>152	1.1	5.0×10^{-8}	5.0×10^{-7}	239	10
BHC1-138C	58x19x21	>306	7	2.0×10^{-8}	1.7×10^{-7}	29	8.5
DYE3-T338	35x19x21	>56	3.2	1.8×10^{-8}	2.6×10^{-7}	35	14.4
DYE3-T1556	39x19x21	12.9	3.5	1.8×10^{-8}	1.8×10^{-7}	70	10
DYE3-T1763	38x19x22	1.2	0.9	8.0×10^{-7}	8.0×10^{-7}	89	1
DYE3-T1922	31x19x21	6.8	1.7	6.0×10^{-7}	6.0×10^{-7}	42	1
LAB-1	59x19x22	0.9	1.5	6.1×10^{-8}	2.6×10^{-7}	59	4.3
LAB-2	59x19x21	0.9	1.3	4.0×10^{-8}	2.6×10^{-7}	62	6.5
LAB-3	59x19x21	0.9	1.3	5.0×10^{-8}	3.1×10^{-7}	65	6.2
LAB-4	59x19x21	0.9	1.9	6.0×10^{-8}	3.0×10^{-7}	80	5
LAB-5	60x19x21	0.9	1.1	4.0×10^{-8}	-	8	-
LAB-6	60x19x21	0.9	1	5.0×10^{-8}	-	9	-

Budd and Jacka (1989, figure 5) compared the difference between the minimum strain rates for shear and compression at 0.1 MPa octahedral with that between shear tests at 0.2 MPa shear stress and compression tests at 0.2 MPa compressive stress. They found that the minimum strain rates were much closer with the octahedral conversion applied than without it. The strain rates were, however, higher in shear than in compression by a factor of ~2. Gao and others (1989, figure 4) found at -2.0 °C that the minimum octahedral shear strain rates for the shear tests were higher by a factor of 2.3, than those for the compression tests in the range 0.01 to 0.41 MPa octahedral shear stress. The shear results, converted to octahedral, found in this report seem to be a factor of ~ 4 higher than those for compression.

Many experiments on initially isotropic ice have revealed that the enhancement factor is about 3 in compression and about 5 to 8 in shear (Budd and Jacka, 1989). The mean enhancement factors obtained in this study are 3 for compression and 6 for shear. This result compares well with earlier findings (Budd and Jacka, 1989).

5.2.3 Crystal orientation fabric

The crystal orientation fabrics and associated c-axis orientation histograms pertaining to the test ice samples before and after testing in simple shear are displayed in the second and third lines of Appendix II. Table 5.2 summarises the fabric data.

The laboratory studies have revealed that a single maximum or two-maximum fabric was developed in the simple shear experiments . The single maximum was developed after very high strain (Shumskii, 1958; Rigsby, 1960; Kamb, 1972; Duval, 1981; Bouchez and Duval, 1982; Russell-Head, 1985; Gao and others, 1989).

The final c-axis orientation fabrics obtained here, for laboratory prepared ice with an initially random c-axis orientation fabric, were similar to those established by previous experiments (Steinemann, 1958; Kamb, 1972; Duval, 1981; Gao and others, 1989). Two-maximum fabrics were well developed at 59 to 80% strain. A strong maximum developed within an angle of 20° to the normal of the shear plane and another weaker one about 25°

Table 5.2 Data for crystal orientation fabrics resulting from simple shear tests. σ and μ indicate standard deviation and mean angle of the c-axes of crystals to the vertical, and $\phi(1/4)$ and $\phi(1/2)$ the half-apex angles of the cones containing 25% and 50% of the c-axes. Angle 1 and angle 2 are respectively the angles between the two maxima and between the weaker maximum and the shear plane.

sample number	fabric (before testing)					total strain (%)	fabric (after testing)						
	description	μ (°)	σ (°)	$\phi(1/4)$ (°)	$\phi(1/2)$ (°)		description	μ (°)	σ (°)	$\phi(1/4)$ (°)	$\phi(1/2)$ (°)	angle 1 (°)	angle 2 (°)
AGZ 77 / 225A	weak maximum	27	16	15	22	53	weak maximum	31	21	15	23		
AGZ77 / 225B	weak maximum	33	20	20	26	57	central trend	27	22	12	19		
AGZ 77 / 229	single maximum	25	17	15	21	38	weak maximum	27	25	18	27		
AGZ 77 / 230	single maximum	19	11	12	18	91	central trend	32	23	14	23		
BHC 1 / 73B	central trend	21	9	14	21	70	central trend	27	19	14	21		
BHC 1 / 79C	central trend	19	15	10	15	92	central trend	24	14	15	19		
BHC 1 / 84B	central trend	21	10	12	20	98	central trend	24	16	12	21		
BHC 1 / 108D	?	48	26	30	35	50	weak central trend	44	27	21	44		
BHC 1 / 116D	multi maximum	26	7	21	25	79	weak central trend	29	15	19	24		
BHC 1 / 121B	multi maximum	36	26	11	28	78	weak central trend	33	26	10	25		
BHC 1 / 134D	?	58	29	28	71	239	central trend	22	11	14	23		
BHC 1 / 138C	multi maximum	46	46	30	40	29	weak central trend	39	22	30	34		
Dye 3 / T338	girdle	52	17	38	57	35	weak central trend	34	23	14	26		
Dye 3 / T1556	central trend	23	20	12	13	70	weak central trend	32	24	9	28		
Dye 3 / T1763	single maximum	17	9	10	16	89	single maximum	20	15	12	18		
Dye 3 / T1922	single maximum	16	11	9	14	42	weak maximum	25	19	11	18		
LAB 1	random	52	21	37	52	59	two maximum	36	25	15	26	47	24
LAB 2	random	theoretical:				62	two maximum	33	27	12	21	54	20
LAB 3	random	57.30	21.56			65	two maximum	34	24	12	27	45	27
LAB 4	random					80	two maximum	28	24	9	18	49	26

away from the shear plane in the experimental shear direction. The angle between the two maxima was about 50°. Both maxima appear elongated perpendicular to the plane containing the length and height of the ice sample. From Table 5.2 and Appendix II, it seems that the angle between the strong maximum and the vertical of the shear plane decreases and the angle between the weak maximum and the shear plane increases with increasing strain, which implies that all crystal c-axes rotated towards the vertical of the shear plane with increasing strain.

All ice core samples (exhibiting various initial degrees of anisotropy) showed a tendency for c-axis orientation towards the vertical of the shear plane and formed a c-axis orientation concentration within 44° of the shear plane with increasing strain. This c-axis orientation concentration shows an elongation perpendicular to the plane containing the length and height of the ice samples. The tests on the ice initially with a single maximum or central trend fabric pattern basically resulted in no change. This implies that the single maximum fabric (especially if near the vertical of the shear plane) is a compatible fabric for shear. More strain is required for an initially incompatible fabric like a circle girdle fabric to develop a compatible fabric.

In shear, it is clear that the single maximum fabric is an " easy glide " fabric and the circle girdle fabric is a " hard glide " fabric. For the multiple maxima fabric the compatibility, in shear, seems dependent on the crystal c-axes distribution . If some of the crystal c-axes within a multiple maxima fabric are located at the vertical of the shear plane, this multiple maxima fabric would exhibit the characteristics of an easy glide fabric. Sample BHC1-121B is an example of this. The fluctuation of tertiary strain rates evident in some creep curves could be explained by the fabric change during deformation. By contrast, if none of the crystal c-axes within a multiple maxima fabric is located at the vertical of the shear plane, this multiple maxima fabric will exhibit the characteristics of a hard glide fabric. The further the crystal c-axes distribute from the vertical , the harder the ice with this fabric deforms, i.e. the minimum strain rate is even lower than that for a circle girdle fabric. Samples BHC1-116D and BHC1-138C are examples of this phenomenon.

5.2.4 Crystal size

Changes in crystal size in shear tests are similar to those occurring in compression tests. In Chapter 4 it was seen that with attainment of the tertiary flow an equilibrium crystal size is established. Figure 5.1, a plot of the crystal size as a function of the octahedral shear strain, shows that with increasing strain to beyond 80% at the tertiary stage, the crystal size changed from an initial range of 0.9 to 306 mm^2 (the largest one is greater than the smallest one by a factor of >255) to a final range of 0.9 to 1.9 mm^2. The mean final crystal size of 1.5 mm^2 for four laboratory prepared ice samples beyond 59% strain is indicated by a dashed line on the figure. The strain required to establish the equilibrium crystal size seems dependent on the initial crystal size and crystal orientation fabric.

The mean crystal size for the laboratory prepared ice samples in the shear tests was 1.5 mm^2. For compression, the mean crystal size at test completion was 2.24 mm^2. This would seem to support the hypothesis that equilibrium steady state crystal size is independent of stress configuration (Jacka and Maccagnan, 1984; Gao, unpublished, Jacka and Li, 1994).

In addition, the development of the crystal size seems unrelated to impurity concentrations in the shear tests. This coincides with a similar conclusion for the compression tests of Chapter 4.

5.3 THE FACTORS AFFECTING THE FLOW OF ICE

For the uniaxial compression tests on the Wisconsin and Holocene ice from the drilled ice cores, in order to separate the effects of crystal orientation fabric and impurity concentrations on the flow, the impurity concentration effects on the tertiary flow were studied while the initial crystal orientation fabric effect on minimum strain rate was examined. It was found that the flow seemed primarily determined by the crystal orientation fabric, rather than impurity concentrations. Similarly, for the simple shear tests, the same inspection is required to clarify the factors affecting the flow in simple shear.

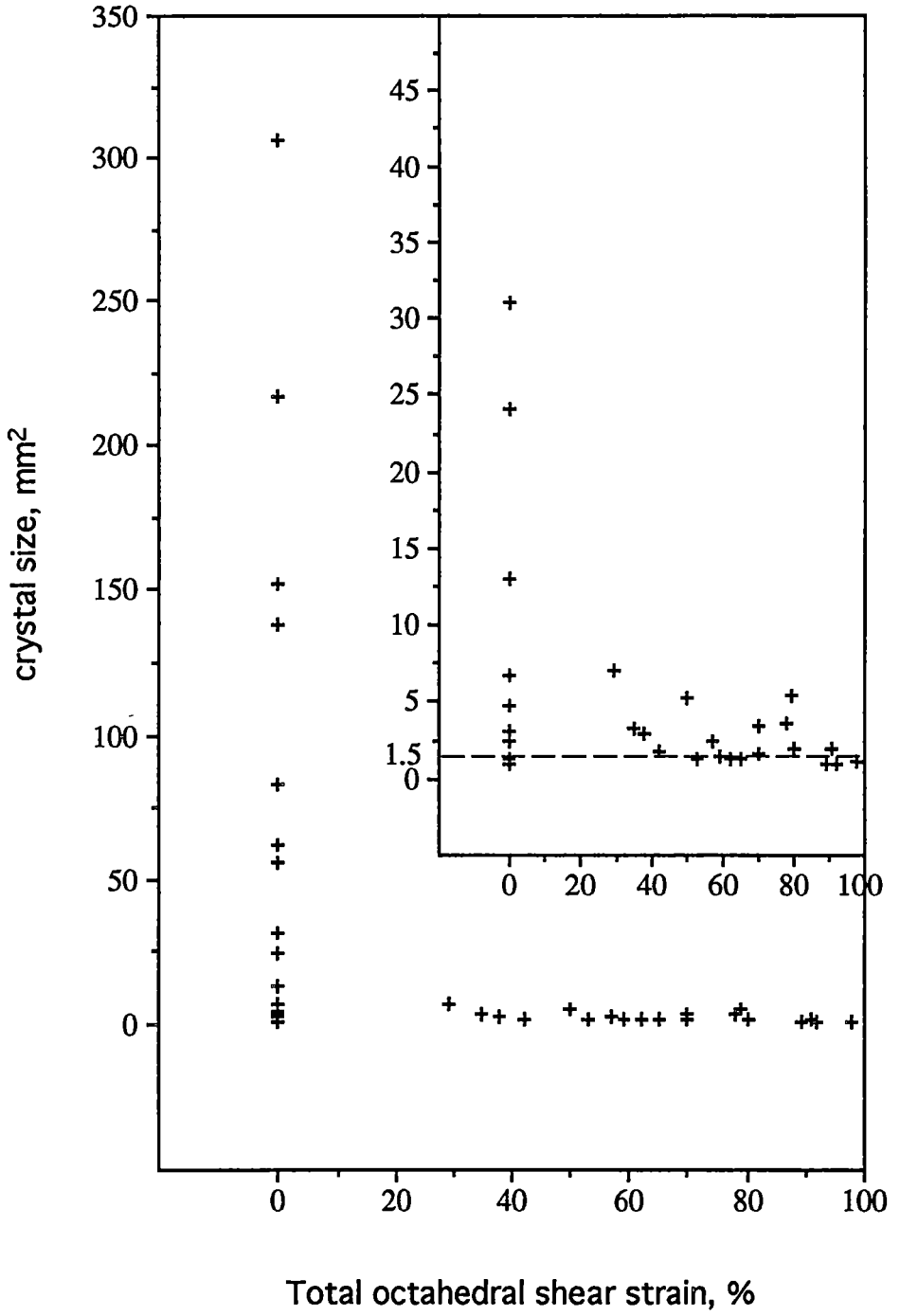

Figure 5.1 Crystal size in shear as a function of total octahedral shear strain. The dashed line indicates the mean crystal size of laboratory prepared ice samples beyond 59% octahedral shear strain.

As expected from Section 4.2, for the compression tests on the Wisconsin and Holocene ice along the axis of the core, if "softness" results from impurities alone, the Wisconsin ice should deform more rapidly than the Holocene ice at all stages of the deformation. If fabric, and different rates of its development, are the determining factor, the minimum strain rate for the Holocene ice should be greater than that of the Wisconsin ice. Alternatively, for simple shear tests on the Wisconsin and Holocene ice along the basal plane of the core, if "softness" results from impurities alone, the effects will be seen as for the compression tests. If fabric, and different rates of its development, are the determining factor, by contrast, the minimum strain rate for the Wisconsin ice should be greater than that for the Holocene ice.

5.3.1 Effect of impurities on tertiary flow

Across all the ice samples the dust concentrations are different by two orders of magnitude and the highest dust concentrations in the Wisconsin ice (in the AGZ77 core) are a factor of 651 greater that the lowest dust concentration in the Transition ice (in the BHC1 core (see Chapter 2)). From Figure 5.2, the tertiary strain rates for the ice containing higher dust concentration are not greater than those for the ice containing lower dust concentration. Therefore, the dust concentration seems not to affect the deformation.

Similarly, even though the soluble (Na, Ca, Mg, Cl, SO_4 and NO_3 ions) impurity concentrations in some Wisconsin samples are an order of magnitude higher than those in some Holocene samples (see Chapter 2), Figure 5.3 indicates that there is no relation between the tertiary strain rate and the soluble impurity concentrations.

The result that the soluble or insoluble impurity concentrations seem not to affect the flow of the ice seems compatible with the results found the compression in Chapter 4.

5.3.2 Effect of initial crystal orientation fabric on minimum strain rate

It was seen in Section 5.2.1, that the minimum strain rate was dependent on the initial crystal orientation fabric. The minimum strain rates found for the shear tests are much

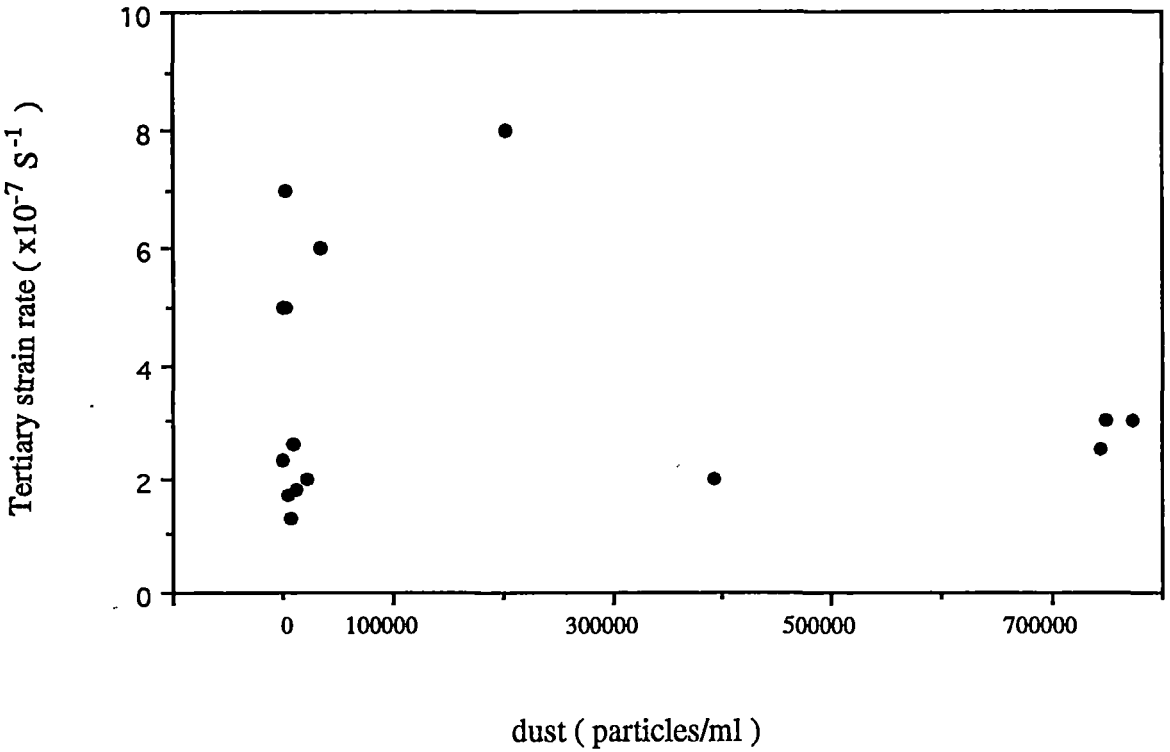

Figure 5.2 Tertiary strain rates in simple shear as a function of dust concentrations

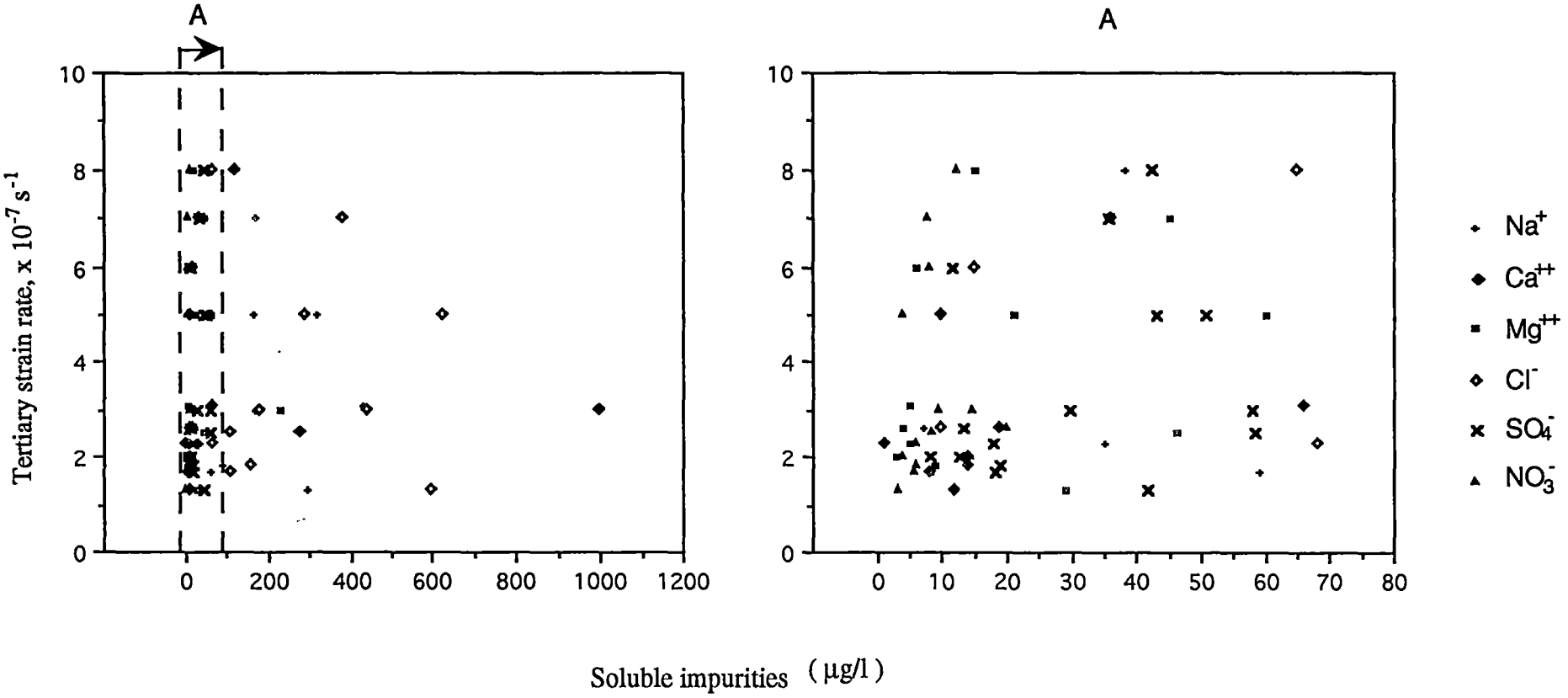

Figure 5.3 Tertiary strain rates in shear as a function of soluble impurities. The right figure is an enlargement of the section between the two dashed lines shown in the left figure.

higher for the samples exhibiting a single maximum fabric than for the samples showing a circle girdle fabric. This is independent of the climatic period from which the ice samples originated. For the BHC1 core the Holocene samples exhibit higher minimum strain rates than Wisconsin samples. This phenomenon can only be explained by the crystal orientation fabric. The single maximum fabric is an easy glide fabric for shear and this pattern facilitates enhanced flow more readily than other (hard glide) fabrics (e.g. circle girdle for shear). The flow for the ice with an easy glide fabric exhibits a high minimum strain rate - sometimes as high as the tertiary strain rate, and the flow for the ice with a hard glide fabric a low minimum strain rate.

The simple shear tests further strengthen the results from the compression tests that the minimum strain rate is mainly dominated by the crystal orientation fabric.

5.4 STEADY STATE FLOW OF ICE IN SHEAR DEFORMATION

Like the compression tests in Chapter 4, the shear tests in this Chapter also confirm the existence of steady state ice flow, as established by previous experiments (Russell-Head, 1985; Gao, unpublished). Further, the study of steady state ice flow is now extended to the anisotropic ice of the Wisconsin and Holocene periods obtained from the ice cores in the Northern Hemisphere and Antarctica.

At an octahedral shear strain of ~1 to 30% a steady state tertiary strain rate was established. The strain required to establish the steady state ice flow is more for the ice with an incompatible fabric than for the ice with a compatible fabric. This steady state strain rate is maintained for at least a further 239% strain.

With the development of this steady state strain rate a steady state crystal orientation fabric - a two maxima fabric for laboratory prepared ice, and central tendency for field ice are also developed. It is clear that for an incompatible fabric in shear, such as a circle girdle or multiple maximum off the vertical fabric, more strain is required to develop a steady state crystal orientation fabric.

Also along with the attainment of this steady state creep rate, a steady state (or equilibrium) crystal size is established. The actual value of this equilibrium size seems independent of stress configuration. The strain required for establishment of this equilibrium crystal size seems dependent on the initial crystal size and crystal orientation fabric.

Similar to the compression tests, it is also shown that this steady state ice flow in the shear configuration is independent of the sample initial conditions, i.e. no matter whether the sample has random or small circle girdle fabrics or already single maximum fabric patterns, no matter whether it has large crystals or small crystals and no matter whether high impurity concentrations or low impurity concentrations. The results also show the independence of the steady state flow in shear on the sample origin or history, i.e. no matter whether the test sample is laboratory prepared or from an ice core drilled from a natural ice mass, and no matter whether it is Holocene in origin or Wisconsin , and no matter whether from the Northern Hemisphere or Antarctica.

5.5 SUMMARY

One set of simple shear tests has been performed on ice samples taken from the Wisconsin and Holocene ice from the AGZ77, BHC1 and DYE3 cores. The tests were carried out at 0.2 MPa octahedral shear stress and -5 °C - the same test conditions as described for the compression tests of Chapter 4. The results indicated by the shear tests described here would also seem to strengthen the findings of Chapter 4.

With increasing strain in the shear tests, the deformation of both the Wisconsin ice and the Holocene ice tends to reach a steady state tertiary flow and the ice initially displaying single maximum fabrics reach it at smaller strains. No evidence has been found to indicate that the Wisconsin ice deforms more rapidly than the Holocene ice or that the flow of the ice is affected by the soluble (dust) or insoluble impurity concentrations. The single maximum fabric is an easy glide crystal orientation fabric for shear. This pattern facilitates enhanced flow by a factor of 14.4 over the minimum flow rate for a hard glide

fabric (such as a circle girdle fabric in shear). Therefore, it seems that the measured enhanced flow in the Wisconsin ice (with a strong single maximum fabric and high impurity concentrations) in the AGZ77 core and in the DYE3 core is primarily due to the crystal vertical orientations at these test conditions.

6. CONCLUSIONS AND PROPOSALS FOR FURTHER WORK

6.1 CONCLUSIONS

Ice deformation experiments in two different stress configurations, uniaxial compression along the axis of the ice core and simple shear approximately parallel to the ice basal plane, have been used to examine the flow rates of samples selected from three ice sheets. The ice sheets are the Law Dome Ice Cap, a small (200 km diameter) coastal ice cap adjacent to the main East Antarctic Ice Sheet, Agassiz Ice Cap in Ellesmere Island Canada, and the Greenland Ice Cap. The samples were chosen from cores drilled through the ice sheets and they were selected from depths such that different climatic periods were represented. These climatic periods were the pre-Wisconsin (the transition from the last interglacial to the Wisconsin), the Wisconsin (the last glacial period), the Wisconsin to Holocene transition and the Holocene (the present interglacial period).

Each of the deformation tests was carried out at an octahedral shear stress of 0.2 MPa and a temperature of -5.0 °C.

With the progression of strain, the deformation of the samples tended to reach a constant steady state (tertiary) flow rate. The path to steady state flow is dependent upon the relationship between stress configuration and crystal orientation fabric pattern. Ice with a c-axis fabric pattern compatible with the applied stress configuration (small circle girdle pattern for compression and single maximum pattern for shear) reached steady state flow directly, without passing through a minimum creep stage.

Examination of the tertiary strain rate and impurity concentrations failed to find any significant difference between the flow rates of Wisconsin and Holocene ice, despite significant variations in the impurity concentrations.

The experimental results show that crystal size and the presence of impurities (in the concentrations found in the different ice samples) seems not to affect the ice flow rates at the temperature and stress tested. The ice flow rates are found to be determined mainly by

crystal orientation fabric pattern. It is concluded therefore, that the more rapid flow measured in some field projects for the Wisconsin ice is primarily due to enhanced crystal orientation strength.

6.2 STEADY STATE ICE FLOW

Steady state ice flow has been established by previous laboratory experiments in both compression and simple shear configurations. The uniaxial compression tests and simple shear tests described in this report extend the steady state ice flow to the anisotropic Wisconsin and Holocene ice from the ice cores from Greenland, Agassiz and Antarctica.

Along with attainment of steady state (tertiary) strain rate, a preferred crystal orientation fabric is developed. The preferred crystal orientation fabric is a steady state fabric and its pattern is a small circle girdle pattern for the compression configuration and a central tendency pattern for the simple shear configuration.

A steady state (or equilibrium) crystal size seems also to be developed with the establishment of a steady state strain rate. The actual equilibrium crystal size in the tests described in this thesis appears independent of ice initial conditions (i.e. crystal size, crystal orientation fabric and impurity concentrations).

6.3 PROPOSALS FOR FURTHER EXPERIMENTAL PROGRAMS

In the experimental project described in this thesis, ice mechanical experiments have been performed separately in uniaxial compression and in simple shear configurations on the selected ice core samples. These two stress configurations are commonly considered as special extreme cases in natural ice masses, while the ice on ice sheets is mainly governed by more complex stress systems. Tests in more complicated stress configurations (e.g. combined compression and shear) are required to further the study of the flow of natural ice masses.

In order to avoid the long times required to carry out laboratory deformation tests, a stress of 0.2 MPa and a temperature of -5.0 °C were chosen for this project. Tests at low

temperatures and stresses are required to fully understand the flow of the cold polar ice masses.

It has been found from this experimental project that crystal orientation fabric pattern provides the dominant determinant of ice flow rates. The tested samples have included ice with c-axis fabric patterns including single maximum, circle girdle, multi-maximum and random patterns. There is still a need for further tests on other ice with different fabric patterns, such as is exhibited by the Vostok core from Antarctica. Vostok ice is deformed *in situ* in tension along the flow direction. As a result, the c-axes are clustered about a vertical plane transverse to the flow direction (Alley, 1988; Lipenkov and others, 1989). Deformation tests on samples from the Vostok core are in progress. Compression tests on ice with a single maximum c-axis fabric pattern (such as AGZ77 core), aligned correctly in test rigs, and shear tests on ice with a multi-maxima fabric pattern are also required.

For ice with an incompatible c-axis fabric - applied stress configuration relation, it is clear that large strains are required to establish steady state ice flow and associated steady state crystal orientation fabric and steady state (equilibrium) crystal size. By performing multiple repeat compression tests to large total strain (>100%) and simple shear tests, also to large total strain (>300%) on ice core samples and laboratory prepared samples with various crystal sizes, a better quantitative description of fabric might be developed. Also, a better understanding of the equilibrium crystal size will be determined.

One problem associated with running simple shear tests using present techniques concerns sample geometry. The simple shear becomes closer to extension due to distortion of the sample at large strains. This distortion of the sample may be compensated by cutting the initial sample to a parallelepiped angled away from the shear direction (Li, unpublished).

The effect of impurities on the ice flow should be further investigated, especially at the warm temperatures typical of the basal layers of the ice sheets. For this purpose, tests on ice core samples with a range of dust or sulphate values are required, and on laboratory prepared ice doped with various amounts of dust, sulphate and other soluble impurities.

REFERENCES

Alley, R.B., Perepezko, J.H. and Bentley, C.R. 1986a Grain growth in polar ice: I. Theory. *Journal of Glaciology* **32** (112) : 415-424.

Alley, R.B., Perepezko, J.H. and Bentley, C.R. 1986b Grain growth in polar ice: II. Application. *Journal of Glaciology* **32** (112) : 425-433.

Alley, R.B. 1988 Fabric in polar ice sheets: development and prediction. *Science* **240** (4851) : 493-495.

Azuma, N. and Higashi, A. 1984 Mechanical properties of Dye 3 Greenland deep ice cores. *Annals of Glaciology* **5** : 1-8.

Azuma, N. and Higashi, A. 1985 Formation processes of ice fabric pattern in ice sheets. *Annals of Glaciology* **6**: 130-135.

Bouchez, J.L. and Duval, P. 1982 The fabric of polycrystalline ice deformed in simple shear: experiments in torsion, natural deformation and geometrical interpretation. *Textures and Microstructures* **5** : 171-190.

Budd, W.F. 1968 The longitudinal velocity of large ice masses. *IAHS* Publication **79** : 58-77.

Budd, W.F. 1969 The dynamics of ice masses. *ANARE Scientific Reports*. A(IV) (108): 216pp.

Budd, W.F. 1972 The development of crystal orientation fabrics in moving ice. *Zeitschrift fur Gletscherkunde und Glazialgeologie* **8** (1-2) : 65-105.

Budd, W.F., and Matsuda, M. 1974 Nijiku-kuripu asshuka ni okeru takesshohyo no sentaku-hoisei ni tsuite [On preferred orientation of polycrystalline ice by biaxial creep]. *Teion-kagaku: Low Temperature Science* Series A (32) : 261-265.

Budd, W.F. and Jacka, T.H. 1989 A review of ice rheology for ice sheet modelling. *Cold Regions Science and Technology* **16** : 107-144.

Butkovich, T.R. and Landauer, J.K. 1958 The flow law for ice. *IAHS* Publication **47** : 318-327.

Dahl-Jensen, D. 1985 Determination of the flow properties at Dye 3, south Greenland, by bore-hole-tilting measurements and perturbation modeling. *Journal of Glaciology* **31** (108) : 92-98.

Dahl-Jensen, D. and Gundestrup, N.S. 1987 Constitutive properties of ice at Dye 3, Greenland. IUGG General Assembly of Vancouver, Aug.1987, *IASH* Publication **170**:31-43.

Dansgaard, W., Clausen, H.B., Gundestrup, N.S., Hammer, C.U., Johnsen, S.J. Kristinsdottir, P.M. and Reeh, N. 1982 A new Greenland deep ice core. *Science* **218** (4579),: 1273-1277.

Dansgaard, W., Clausen, H.B., Gundestrup, N.S., Johnsen, S.J. and Rygner, C. 1985 Dating and climatic interpretation of two deep Greenland ice cores. In: *Greenland Ice Core: Geophysics, Geochemistry, and the Environment* (ed. by C.C. Langway, Jr., H. Oeschger and W. Dansgaard), 77-84. Geophysical Monograph No. 33, American Geophysical Union, Washington, D.C., USA.

Duval, P. and Le Gac, H. 1980 Does the permanent creep-rate of polycrystalline ice increase with crystal size? *Journal of Glaciology* **25** (90) : 151-157.

Duval, P. and Lorius, C. 1980 Crystal size and climatic record down to the last ice age from Antarctic ice. *Earth and Planetary Science Letters* **48** (1) : 59-64.

Duval, P. 1981 Creep and fabrics of polycrystalline ice under shear and compression. *Journal of Glaciology* **27** (95) : 129-140.

Duval, P., and Le Gac, H. 1982 Mechanical behaviour of Antarctic ice. *Annals of Glaciology* **3**: 92-95.

Etheridge, D.M. 1989 Dynamics of the Law Dome ice cap, Antarctica, as found from bore-hole measurements. *Annals of Glaciology* **12:** 46-50.

Etheridge, D.M. 1990 Scientific plan for deep ice drilling on Law Dome. *ANARE Research Notes* **76.**

Fisher, D. A. and Koerner, R. M. 1986 On the special rheological properties of ancient microparticle-laden northern hemisphere ice as derived from bore-hole and core measurements. *Journal of Glaciology* **32** (112) : 501-510.

Fisher, D. A. 1987 Enhanced flow of Wisconsin ice related to solid conductivity through strain history and recrystallization. IUGG General Assembly of Vancouver, Aug.1987, *IASH* Publication **170**:45-51.

Fisher, D. A. and Koerner, R. M. 1988 The effects of wind on $\delta^{18}O$ and accumulation give an inferred record of seasonal δ amplitude from the Agassiz Ice Cap, Ellesmere Island, Canada.. *Annals of Glaciology* **10** : 34-37.

Gao, X.Q. and Jacka, T.H. 1987 The approach to similar tertiary creep rates for Antarctic core ice and laboratory prepared ice. *Journal de Physique* Colloque C1, **48** (Supplement to No. 3) : 289-296.

Gao, X.Q. unpublished 1989 Laboratory studies of the development of anisotropic crystal structure and flow properties of ice sheets. *Ph.D.Thesis, Meteorology Department, The University of Melbourne.*

Gao, X.Q. and Jacka, T.H. and Budd, W.F. 1989 The development of ice crystal anisotropy in shear and comparisons of flow properties in shear and compresson. *Proceedings of the International Symposium on Antarctic Research.* China Ocean Press : 32-40.

Glen, J.W. 1955 The creep of polycrystalline ice. Proceedings of the Royal Society (London). Series A, **228** (1175) : 519-538.

Glen, J.W. 1958 The flow law of ice: A discussion of the assumptions made in glacier theory, their experimental foundations and consequences. *IAHS* Publication **47** : 171-183.

Gow, A.J. and Williamson, T. 1976 Rheological implications of the internal structure and crystal fabrics of the West Antarctic ice sheet as revealed by deep core drilling at Byrd Station. *CRREL Report* **76-35.**

Gundestrup, N.S. and Hansen, B.L. 1984 Bore - hole survey at Dye 3, South Greenland. *Journal of Glaciology* **30** (106) : 282-288.

Hammer, C.U. 1980 Acidity of polar ice cores in relation to absolute dating, past volcanism, and radio echoes. *Journal of Glaciology* **25** (93) : 359-372.

Hammer, C.U., Clausen, H.B., Dansgaard, W., Neftel, A., Kristinsdottir, P. and Johnson, E. 1985 Continuous impurity analysis along the Dye 3 deep core. In: *Greenland Ice Core Geophysics, Geochemistry and the Environment* (ed. by C.C. Langway, H. Oeschger and W. Dansgaard), 90-94. Geophysical Monograph No.33, American Geophysical Union, Washington, D.C., USA.

Han, J.K. and Young, N.W. 1988 Ice structure, bubble properties and stratigraphy in the BHC1 ice core from Law Dome, Antarctica. Studies on Glaciology, No. 5, A collection of Antarctic scientific exploration. 153-163.

Herron, M.M. 1982 Impurity sources of F^-, Cl^-, NO_3^- and SO_4^- in Greenland and Antarctic precitation. *Journal of Geophys. Res.* **87** (C4) : 3052-3064.

Herron, S.L. and Langway, C.C. 1982 A comparison of ice fabrics and textures at Camp Century, Greenland and Byrd Station, Antarctica. *Annals of Glaciology* **3** : 118-124.

Herron, M.M. and Langway, C.C. 1985 Chloride, nitrate, and sulfate in the Dye 3 and Camp Century, Greenland ice cores. In: *Greenland Ice Core Geophysics, Geochemistry and the Environment* (ed. by C.C. Langway, H. Oeschger and W. Dansgaard), 77-84. Geophysical Monograph No.33, American Geophysical Union, Washington, D.C., USA. :

Herron, S.L., Langway, C.C. and Brugger, K.A. 1985 Ultrasonic velocities and crystalline anisotropy in the ice core from Dye 3 Greenland. In: *Greenland Ice Core Geophysics, Geochemistry and the Environment* (ed. by C.C. Langway, H. Oeschger and W. Dansgaard), 23-31. Geophysical Monograph No.33, American Geophysical Union, Washington, D.C., USA. :

Higashi, A. and Shoji, H. 1979 Mechanical tests of Antarctic deep core ice under hydrostatic pressure : instrumentation and preliminary results. *Oyo-butsuri* **48** (1) : 41-47.

Hooke, R. LeB. 1973 Structure and flow in the margin of the Barnes Ice Cap, Baffin Island, N.W.T., Canada. *Journal of Glaciology* **12** (66) : 423-438.

Hooke, R. LeB. 1981 Flow law for polycrystalline ice in glaciers: comparison of theoretical predictions, laboratory data and field measurements. *Reviews of Geophysics and Space Physics* **19** (4) : 664-672.

Hooke, R. LeB. and Hudleston, P.J. 1980 Ice fabrics in a vertical flow plane. Barnes Ice Cap, Canada. *Journal of Glaciology* **25** (92) : 195-214.

Hooke, R. LeB. and Hudleston, P.J. 1981 Ice fabrics from a borehole at the top of the south dome, Barnes Ice Cap, Baffin Island. *Geological Society of America Bulletin* **92** : 274-281.

Hooke, R. LeB., Gao, X.Q., Jacka, T.H. and Souchez, R.A., 1988 Rheological contrast between Pleistocene and Holocene ice in Barnes Ice Cap, Baffin Island, N.W.T., Canada: a new interpretation. *Journal of Glaciology* **34** (118) : 364-365.

Huang, M., Ohtomo, M., Wakahama, G. 1982 Repeated recrystallization of polycrystalline ice. *Low Temperature Science* **A41**: 13-23.

Huang, M., Wang, W., Li, J., Li, G. and Xie, Z. 1988 Repeated compression-annealing experiments for the ice from Antarctica. Studies on Glaciology, No. 5, A collection of Antarctic scientific exploration. 153-163.

Jacka, T.H. 1984a The time and strain required for development of minimum strain rates in ice. *Cold Regions Science and Technology* **8** (3) : 261-268.

Jacka, T.H. 1984b Laboratory studies on relationships between ice crystal size and flow rate. *Cold Regions Science and Technology* **10** (1) : 31-42.

Jacka, T.H. and Lile, R.C. 1984 Sample preparation techniques and compression apparatus for ice flow studies. *Cold Regions Science and Technology* **8** (3) : 235-240.

Jacka, T.H. and Maccagnan, M. 1984 Ice crystallographic and strain rate changes with strain in compression and extension. *Cold Regions Science and Technology* **8** (3) : 269-286.

Jacka, T.H. and Budd, W.F. 1989 Isotropic and anisotropic flow relations for ice dynamics. *Annals of Glaciology* **12** : 81-84.

Jacka, T.H. and Gao, X.Q. 1989 Structure characteristics of snow firn at the surface part on Law Dome Ice Cap, Antarctica. *Proceedings of the International Symposium on Antarctic Research.* China Ocean Press : 41-52.

Jacka, T.H. 1994 Investigations of discrpancies between laboratory studies of the flow of ice: density, sample shape and size, and grain-size. *Annals of Glaciology* **19**: 146-154.

Jacka, T.H. and Li, J. 1994 The steady state crystal size of deforming ice. *Annals of Glaciology* **20** :

Jones, S.J. 1982 The confined compressive strength of polycrystalline ice. *Journal of Glaciology* **28** (98) : 171-177.

Jones, S.J. and Chew, H.A.M. 1981 On the grain-size dependence of secondary creep. *Journal of Glaciology* **27** (97) : 517-518.

Jones, S.J. and Chew, H.A.M. 1983 Effect of sample and grain size on the compressive strength of ice. *Annals of Glaciology* **4** : 129-132.

Kamb, W.B. 1972 Experimental recrystallization of ice under stress. In: (Heard, H.C., Borg, I.Y. Carter, N.L. and Raleigh, C.B. eds.) *Flow and Fracture of Rocks* American Geophysical Union, Geophysical Monograph **16** : 211-241.

Kamb, W.B. and Shreve, R.L. 1963 Texture and fabric of ice at depth in a temperate glacier. *Transactions of the American Geophysical Union* **44** : 103. (Abstract).

Koerner, R. M. and Fisher, D. A. 1979 Discontinuous flow, ice texture, and dirt content in the basal layers of the Devon Island ice cap. *Journal of Glaciology* **23** (89) : 209-222.

Langway, C.C. Jr. 1958 Ice fabrics and the Universal Stage. *SIPRE Technical Report* **62**.

Langway, C.C. Jr., Oeschger, H. and Dansgaard, W. 1985 The Greenland Ice Sheet Program in perspective. In*: Greenland Ice Core: Geophysics, Geochemistry, and the Environment* (ed. by C.C. Langway, Jr., H. Oeschger and W. Dansgaard), 9-18. Geophysical Monograph No. 33, American Geophysical Union, Washington, D.C., USA.

Langway, C.C. jr, Shoji, H. and Azuma, N. 1988 Crystal size and orientation patterns in the Wisconsin - age ice from Dye 3, Greenland. *Annals of Glaciology* **10** : 109-115.

Legrand, M. and Delmas, R.J. 1986 Relative contributions of tropospheric and stratospheric sources to nitrate in Antarctic snow. *Tellus* **38B (3-4):** 236-249.

Legrand, M. and Delmas, R.J. 1988 Soluble impurities in four Antarctic ice cores over the last 30000 years. *Annals of Glaciology* **10 :** 116-120.

Li Jun. unpublished 1994 Interrelation between flow properties and crystal structure of snow and ice. *Ph.D.Thesis, Meteorology Department, The University of Melbourne.*

Lile, R.C. 1978 The effect of anisotropy on the creep of polycrystalline ice. *Journal of Glaciology* **21** (85) : 475-483.

Lile, R.C. 1984 The flow law for isotropic and anisotropic ice at low strain rates. *ANARE Report* **132.**

Lipenkov, V.Ya., Barkov, N.I.,Duval,P. and Pimienta, P., 1989 Crystalline texture of the 2083 m ice core at Vostok Station, Antarctica. *Journal of Glaciology* **35** (121) : 392-398.

Matsuda, M. and Wakahama, H. 1978 Crystallographic structure of polycrsytalline ice. *Journal of Glaciology* **21** (85) : 607-620.

Morgan, V.I. 1979 A system for accurate temperature control of small fluid baths. *Journal of Glaciology* **22** (87) : 389-391.

Morgan, V.I., Davis, E.R. and Wehrle, E. 1984 A Rigsby stage with remote computer compatible output. *Cold Regions Science and Technology* **10** (1) : 89-92.

Nye, J.F. 1953 The flow law of ice from measurements in glacier tunnels, laboratory experiments and the Jungfraufirn bore hole experiment. *Proceedings of the Royal Society* Series A **219** (1139) : 477-489.

Paterson, W.S.B. 1977 Secondary and tertiary creep of glacier ice as measured by borehole closure rates. *Reviews of Geophyics and Space Physics* **15** (1) : 47-55.

Paterson,W.S.B. 1991 Why ice - age ice is sometimes " soft ". *Cold Regions Science and Technology* **20:** 75-98.

Pickering, F.B. 1976 The basis of quantitative metallography. *Whetsone, Metals and Metallurgy Trust for the Institute of Metallurgical Technicians.*

Pimienta, P., Duval, P. and Lipenkov, V.Ya. 1988 Mechanical behaviour of ice along the 2040 m Vostok core, Antarctica. *Annals of Glaciology* **10 :** 137-140.

Rigsby, G.P. 1958 Effect of hydrostatic pressure on velocity of shear deformation of single ice crystals. *Journal of Glaciology* **3** (24) : 273-278.

Rigsby, G.P. 1960 Crystal orientation in glacier and experimentally deformed ice. *Journal of Glaciology* **3** (27) : 589-606.

Russell-Head, D.S. and Budd, W.F. 1979 Ice sheet flow properties derived from borehole shear measurements combined with ice core studies. *Journal of Glaciology* **24** (90) : 117-130.

Russell-Head, D.S. 1985 Shear deformation of ice to large strains. *ANARE Research Notes* **28** : 118-121.

Shoji, H and Langway, C.C. 1984 Flow behaviour of basal ice as related to modelling considerations. *Annals of Glaciology* **5** : 141-148.

Shoji, H and Langway, C.C. 1985a Comparison of mechanical tests on the Dye3, Greenland ice core and artificial laboratory ice. *Annals of Glaciology* **6** : 305.

Shoji, H. and Langway, C.C. 1985b Mechanical properties of fresh ice core from Dye3, Greenland. *Geophysical Monograph*, American Geophysical Union **33** : 39-48.

Shoji, H. and Langway, C.C. 1987 Flow velocity profiles and accumulation rates from mechanical tests on ice core samples. IUGG General Assembly of Vancouver, Aug.1987, *IASH* Publication **170**: 67-77.

Shoji, H. and Langway, C.C. 1988 Flow-law parameters of the Dye 3, Greenland deep ice core. *Annals of Glaciology* **10 :** 146-150.

Steinemann, S. 1954 Flow and recrystallization of ice. *IAHS* Publication **39** : 449-462.

Steinemann, S. 1958 Experimentalle Untersuchungen zur Plastizitat von Eis. *Beitrage zur Geologie der Schweiz, Geotechnische Serie, Hydrologie* (10) : 1-72.

Shumskiy, P.A. 1958 The mechanism of ice straining and its recrystallization, in Physics of the movement of the ice. *IASH* Publication **47** : 244-248.

Tanaka, H. 1972 On preferred orientation of glacier and experimentally deformed ice. *Journal of Geological Society of Japan* **78** (12) : 659-675.

Thompson, L.G. 1977 Variations in microparticle concentration, size distribution and elemental composition found in Camp Century, Greenland, and Byrd Station, Antarctica deep ice cores. IUGG General Assembly of Vancouver, Aug./Sept. 1975, *IASH* Publication **118**: 351-364.

Thompson, L.G. and Mosley-Thompson, E. 1981 Microparticle concentration variations linked with climatic change: evidence from polar ice cores. *Science* **212** (4496): 812-815.

Thwaites, R.J., Wilson, C.J.L. and McCray, A.P. 1984 Relationship between borehole closure and crystal fabrics in an Antarctic ice core from Cape Folger. *Journal of Glaciology* **30** (105) : 171-179.

Vialov, S.S. 1958 Regularities of ice deformation. *IASH* Publication **47 :** 383-391.

Wakahama, G. 1967 On the plastic deformation of single crystals of ice. In: (Oura, H. ed.) *Physics of Snow and Ice, volum 1* Institute of Low Temperature Science, Hokkaido University, Sapporo. 291-311.

Watanabe, O.and Oura, H. 1968 Experimental studies on orientation of polycrystalline ice by unconfined compression. *Low temperature Science* **A26** : 1-28.

Weertman, J. 1963 The Eshelby-Schoeck viscous dislocation damping mechanism applied to the steady-state creep of ice. In: (W.D. Kingery, ed.) *Ice and Snow* MIT Press, Cambridge, Massachusetts, U.S.A. 28-33.

Wilson, C.J.L. and Russell-Head, D.S. 1982 Steady-state preferred orientation of ice deformed in plane strain at -1 °C. *Journal of Glaciology* **28** (98) : 145-160.

Xie, Z.C. 1985 Ice formation and ice structure on Law Dome, Antarctica. *Annals of Glaciology* **6 :** 150-153.

APPENDIX I

Creep curves and crystal structure measurements for uniaxial compression tests

1st column - Results of first compression test.

2nd column - Results of second compression test.

3rd column - Results of third compression test.

1st row - Creep curve of octahedral shear strain rate versus octahedral shear strain on log-log scales.

2nd row - Diagram of crystal orientation fabric.

3rd row - Diagram of c-axis distribution histogram.

4th row - Thin section photograph on 1:1 scales.

N - Number of crystals oriented.

S - Mean crystal area.

ε - Total octahedral shear strain.

σ - Standard deviation of the c-axis crystal angles to the vertical .

μ - Mean of the c-axis crystal angles to the vertical.

AGZ77_225A

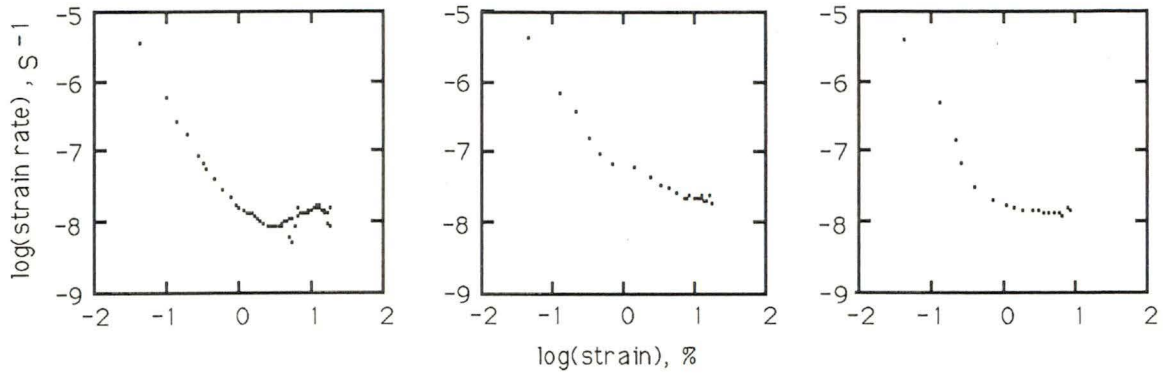

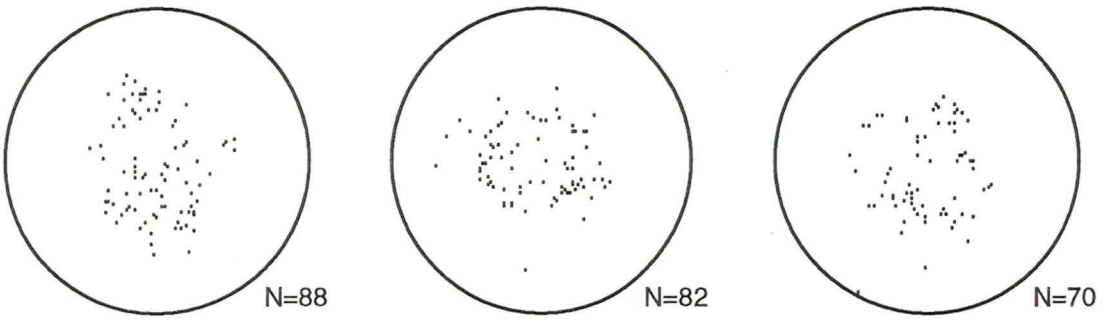

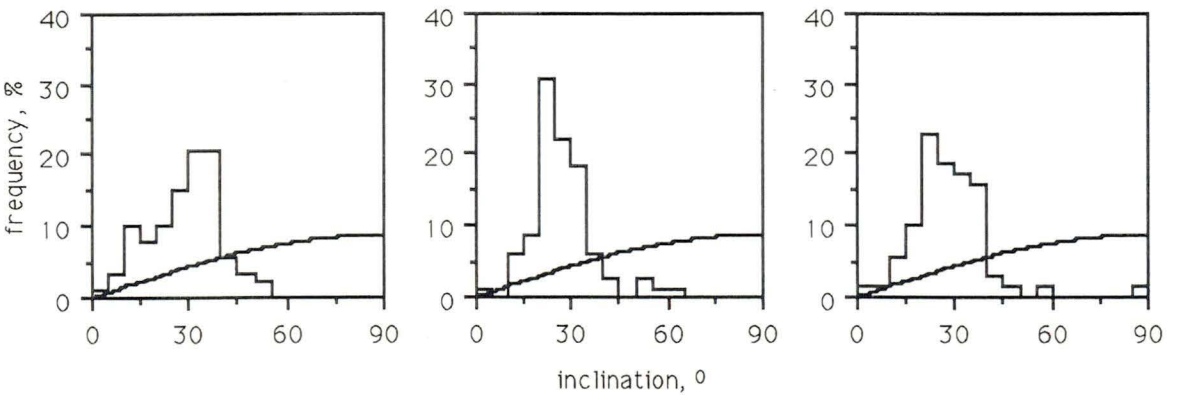

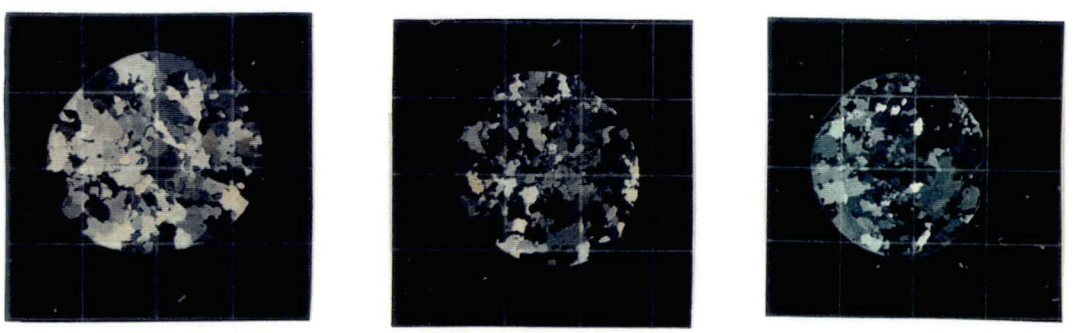

ε = 18.32 %
s = 2.53 mm²
σ = 11.08°
μ = 29.52°

ε = 35.84 %
s = 2.02 mm²
σ = 9.97°
μ = 27.59°

ε = 43.84 %
s = 2.15 mm²
σ = 11.82°
μ = 29.00°

AGZ77_225B

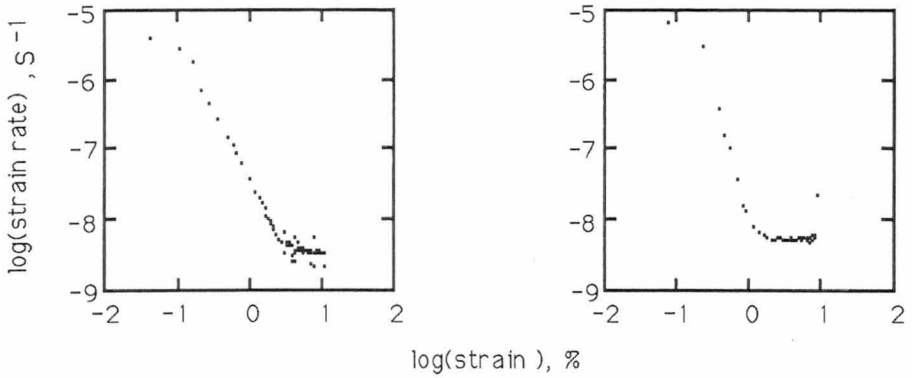

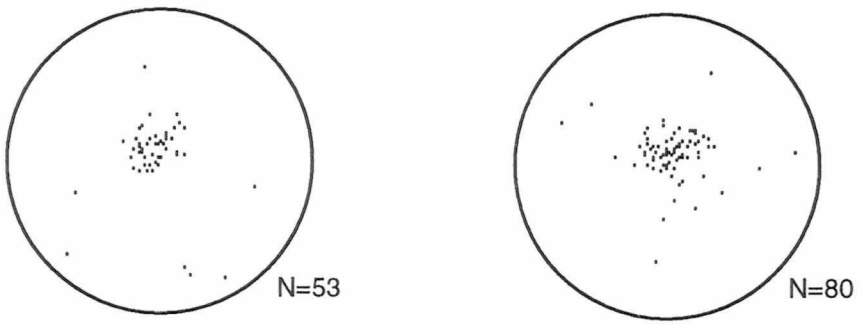

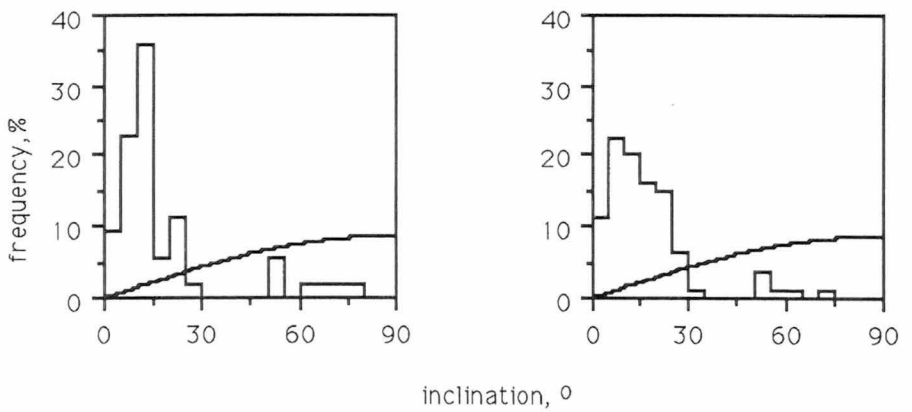

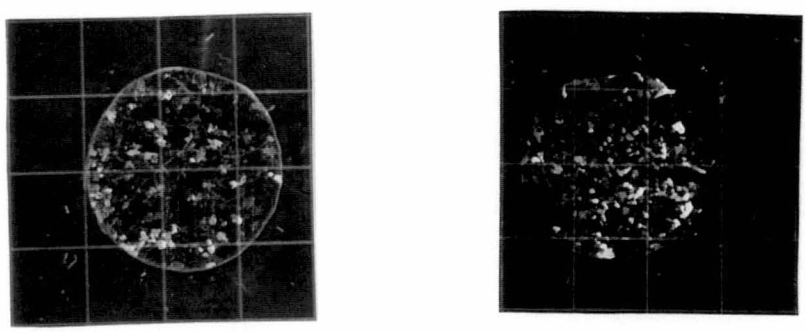

ε = 10.60 %
S = 0.91 mm^2
σ = 18.27 °
μ = 19.15 °

ε = 19.60 %
S = 0.78 mm^2
σ = 14.28 °
μ = 17.58 °

AGZ77_226

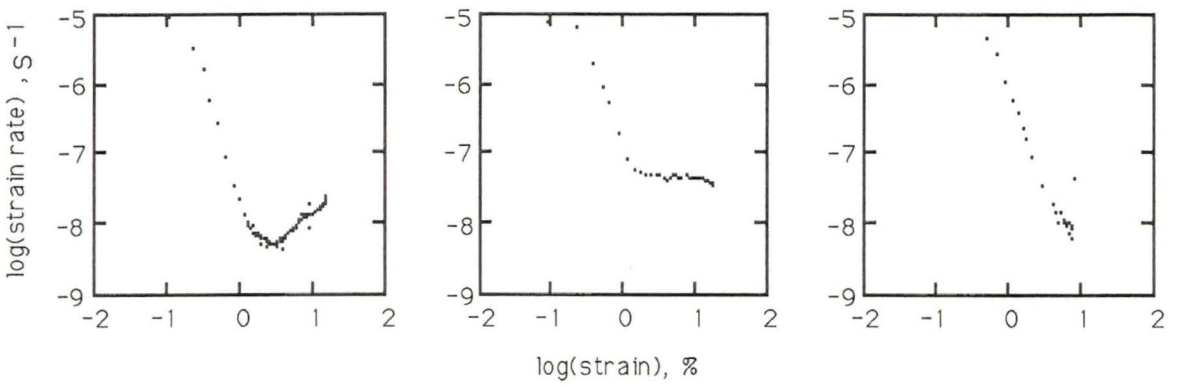

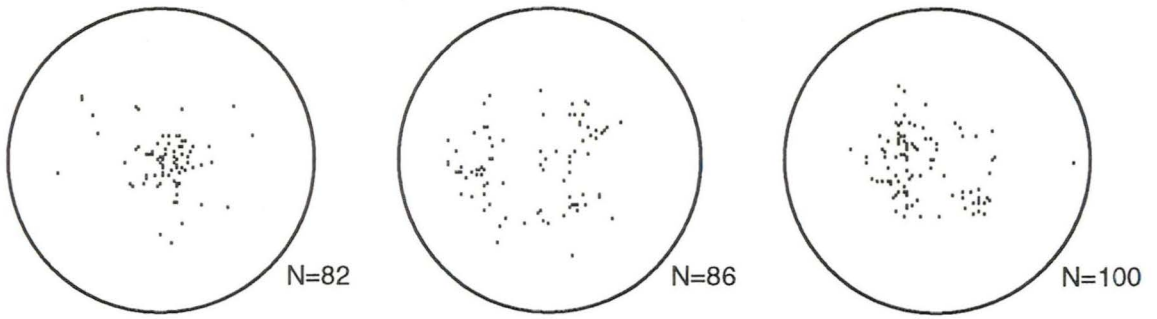

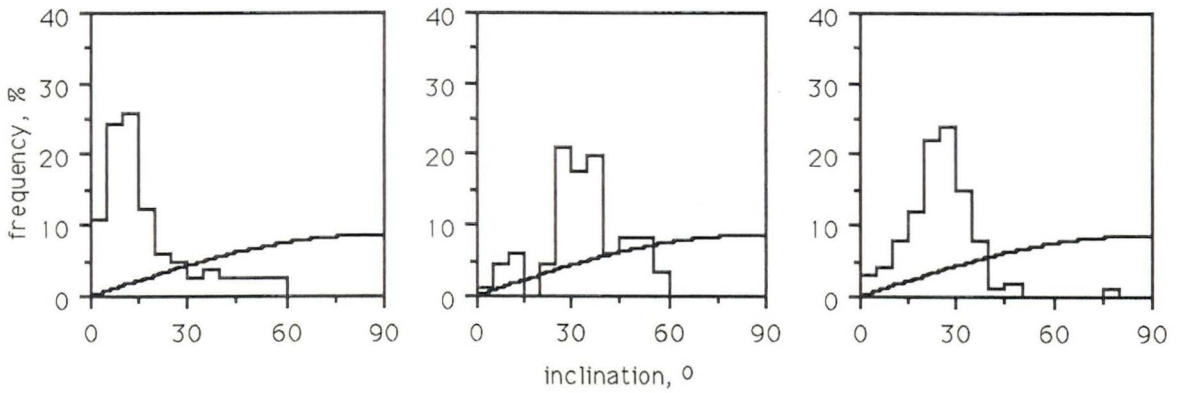

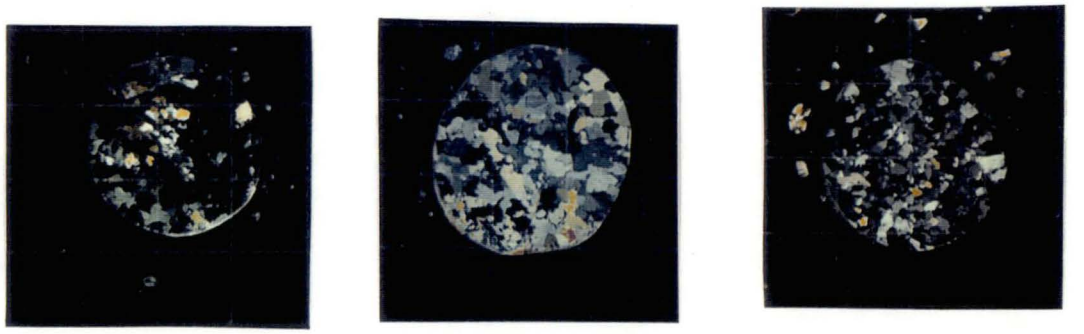

ε = 15.90 %	ε = 34.25 %	ε = 42.37 %
S = 0.92 mm^2	S = 1.95 mm^2	S = 0.66 mm^2
σ = 13.66°	σ = 12.70°	σ = 10.48°
μ = 17.68°	μ = 33.97°	μ = 25.63°

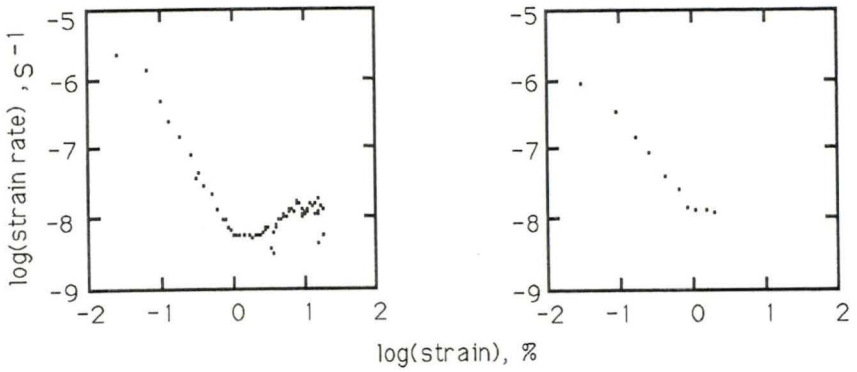

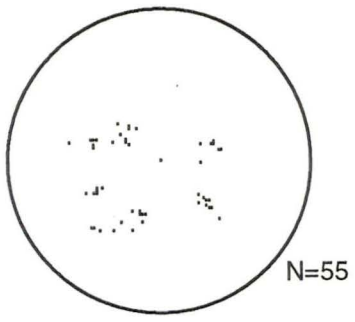

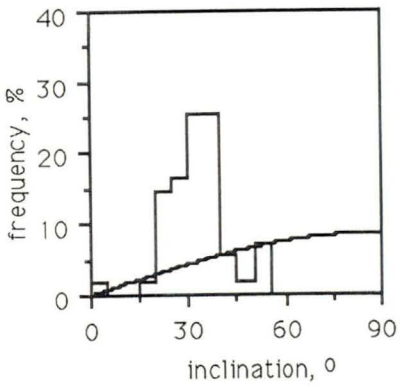

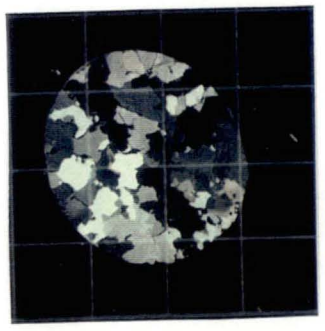

ε = 18.29 %

S = 2.15 mm^2

σ = 9.21 °

μ = 33.55 °

AGZ77_229

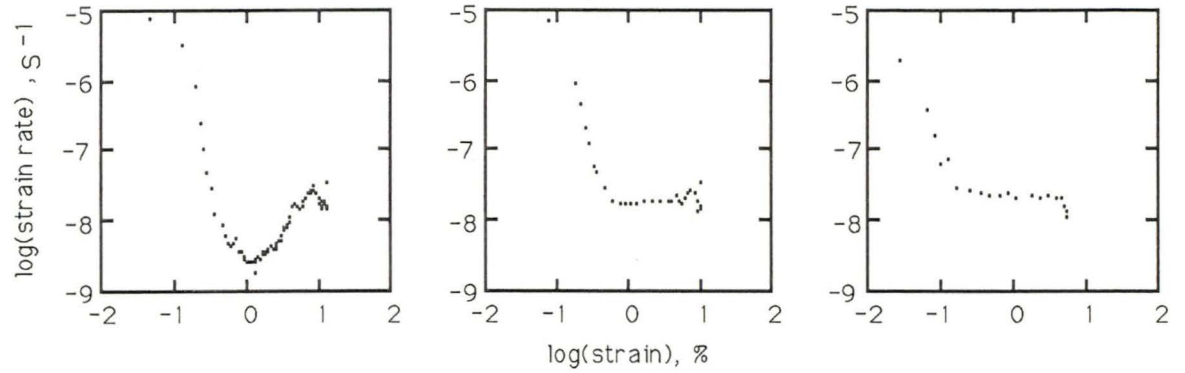

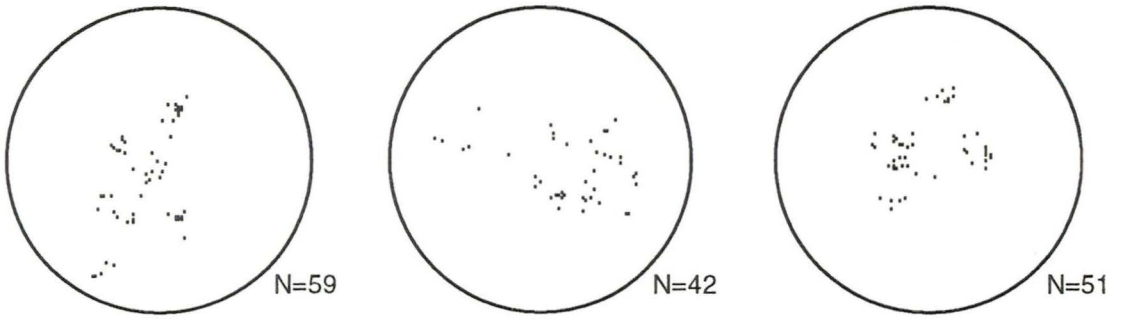

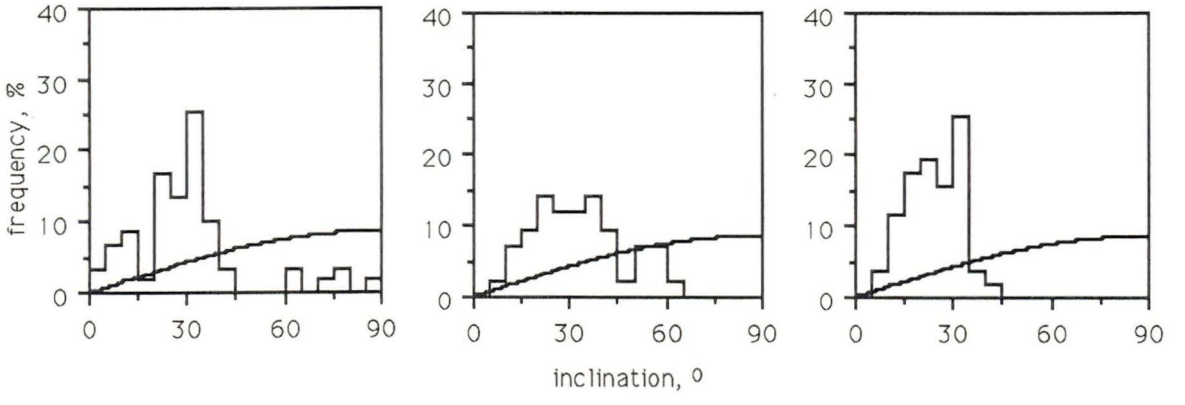

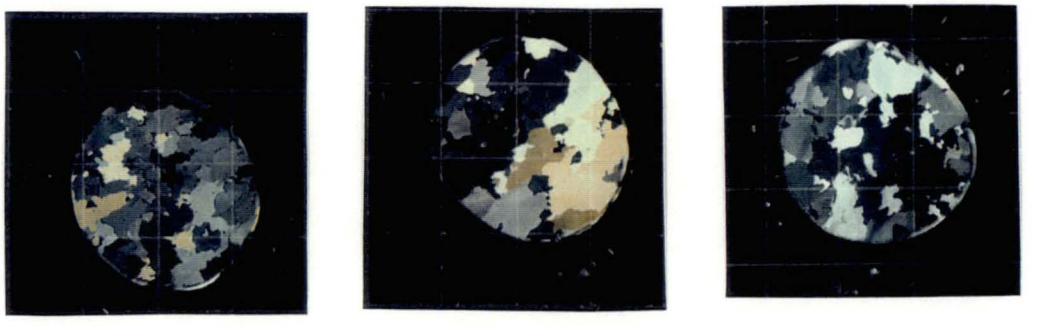

ε = 12.92 %	ε = 23.19 %	ε = 29.01 %
S = 5.85 mm^2	S = 9.04 mm^2	S = 5.96 mm^2
σ = 17.88°	σ = 14.13°	σ = 8.37°
μ = 30.71°	μ = 33.29°	μ = 24.80°

AGZ77_230

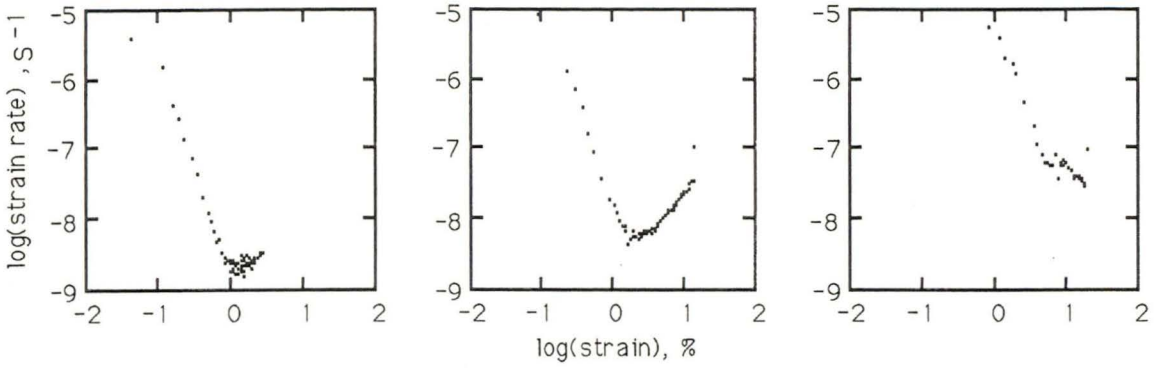

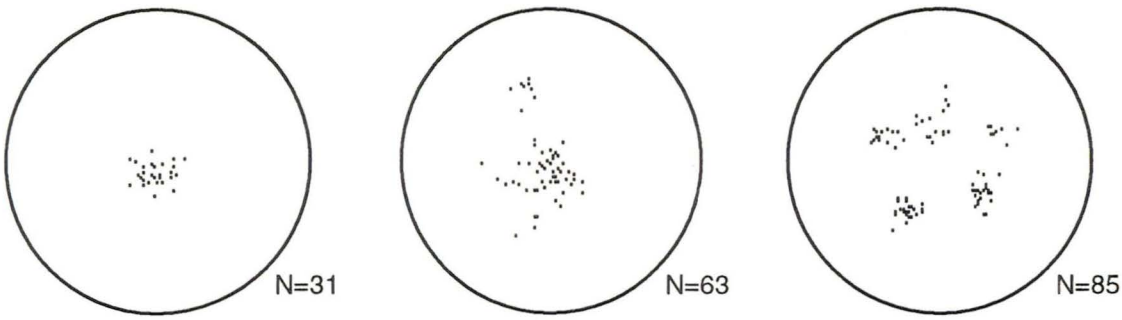

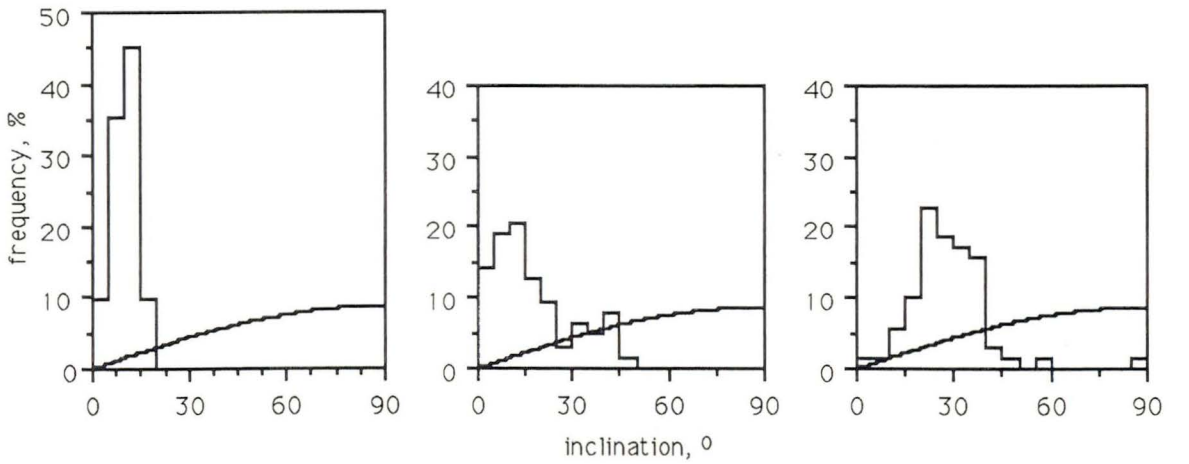

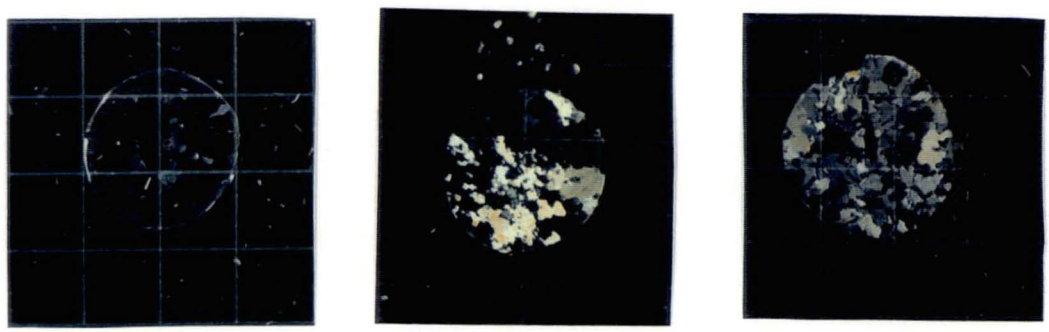

ε = 2.69 %	ε = 16.68 %	ε = 35.83 %
S = 2.15 mm^2	S = 1.91 mm^2	S = 1.65 mm^2
σ = 4.03°	σ = 13.09°	σ = 7.22°
μ = 10.61°	μ = 18.00°	μ = 29.82°

BHC1_73B

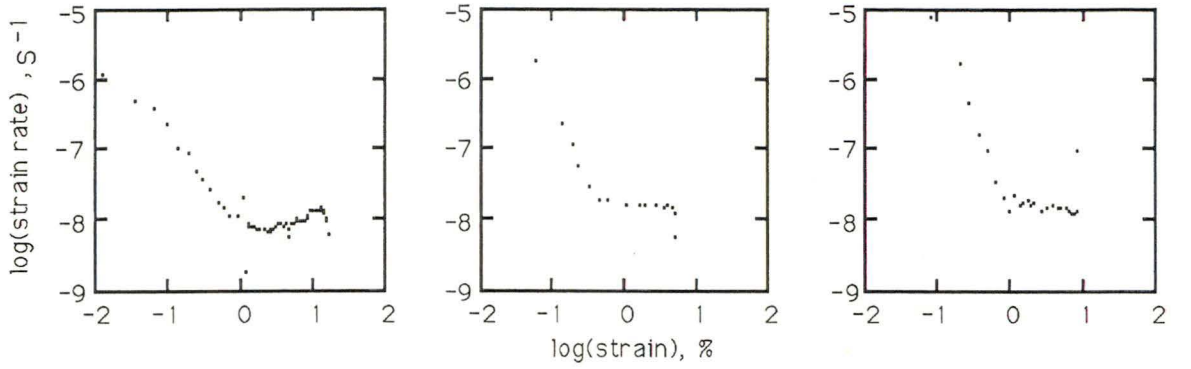

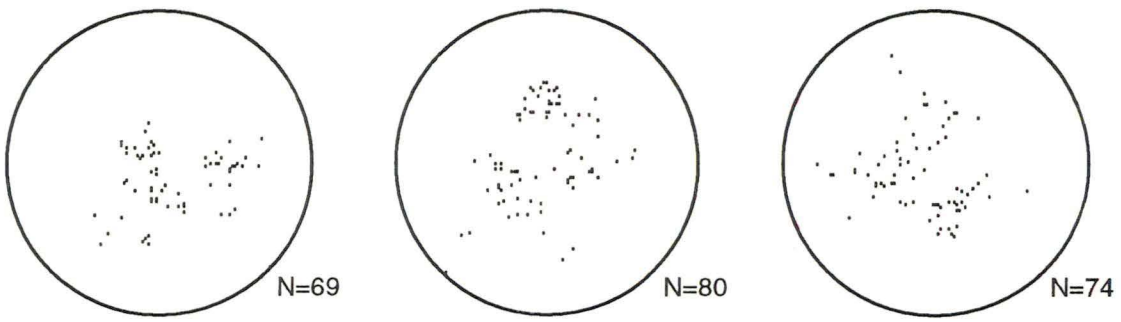

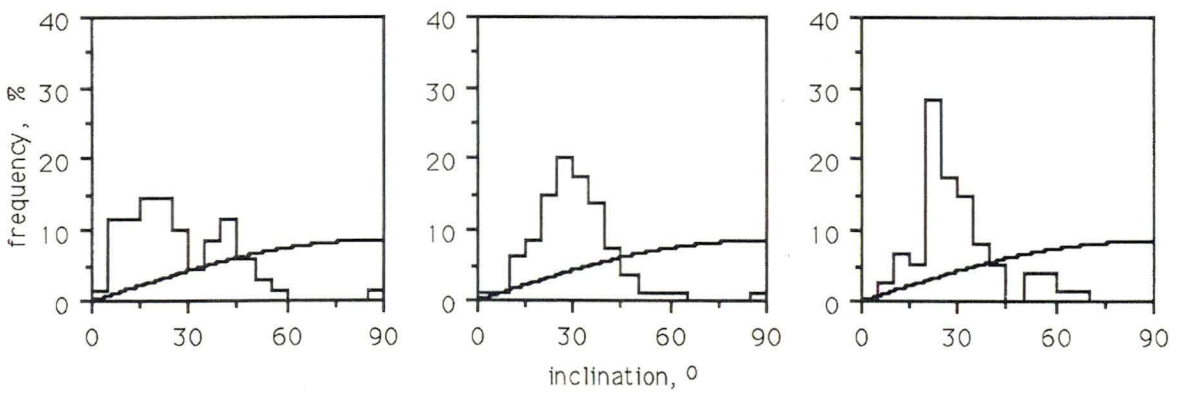

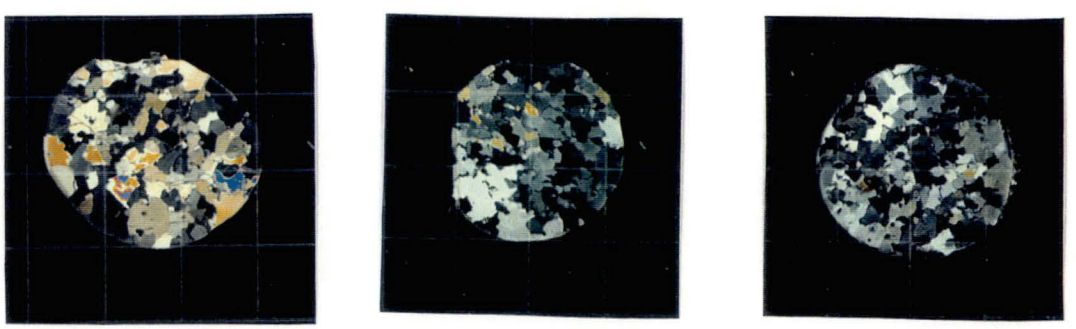

ε = 16.20 %	ε = 20.20 %	ε = 29.00 %
S = 4.08 mm²	S = 2.06 mm²	S = 2.15 mm²
σ = 15.79 °	σ = 12.50 °	σ = 12.56 °
μ = 27.81 °	μ = 30.94 °	μ = 30.11 °

BHC1_79C

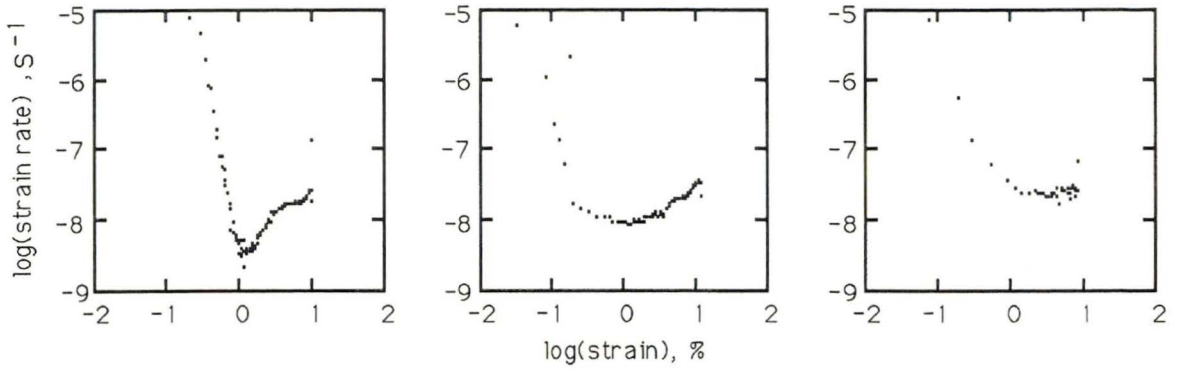

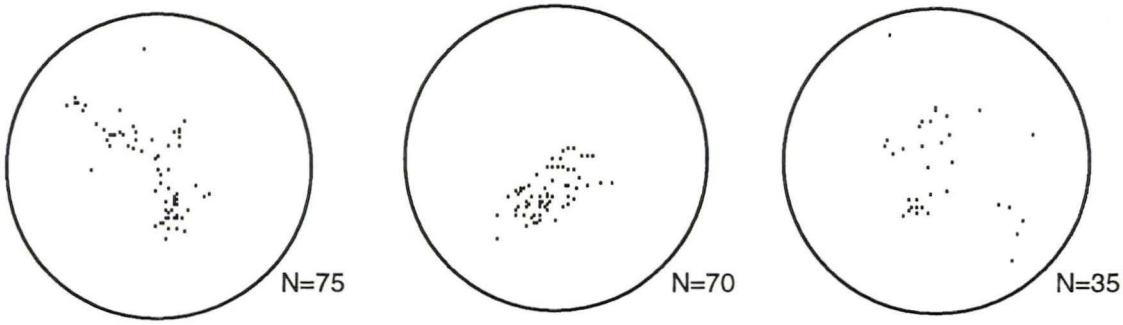

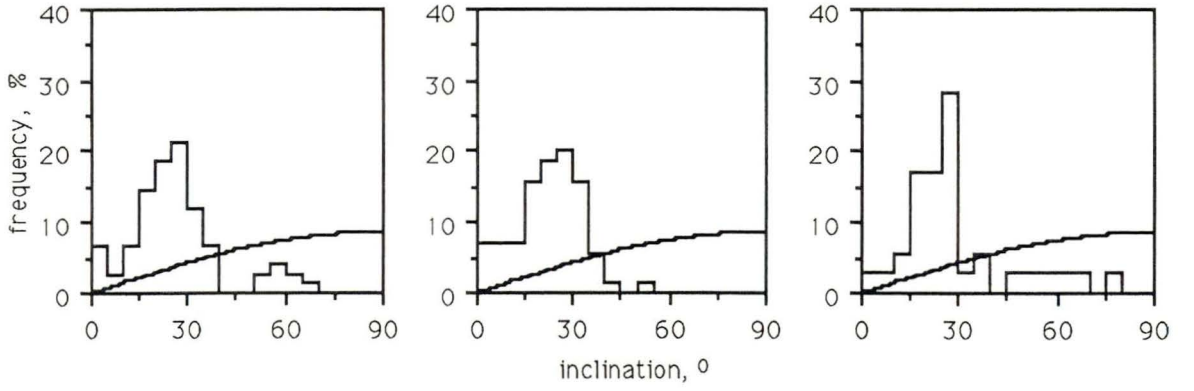

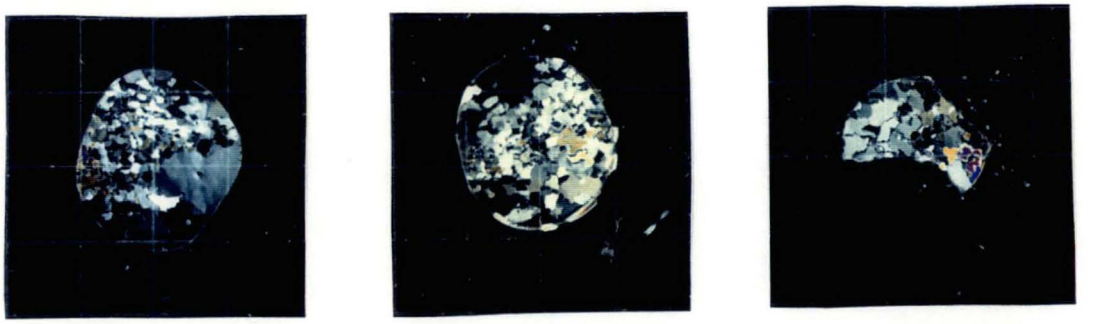

ε = 9.98 %	ε = 21.65 %	ε = 30.32 %
s = 2.27 mm^2	s = 1.70 mm^2	s = 1.22 mm^2
σ = 14.07°	σ = 10.54°	σ = 16.75°
μ = 26.97°	μ = 23.11°	μ = 29.80°

BHC1_84B

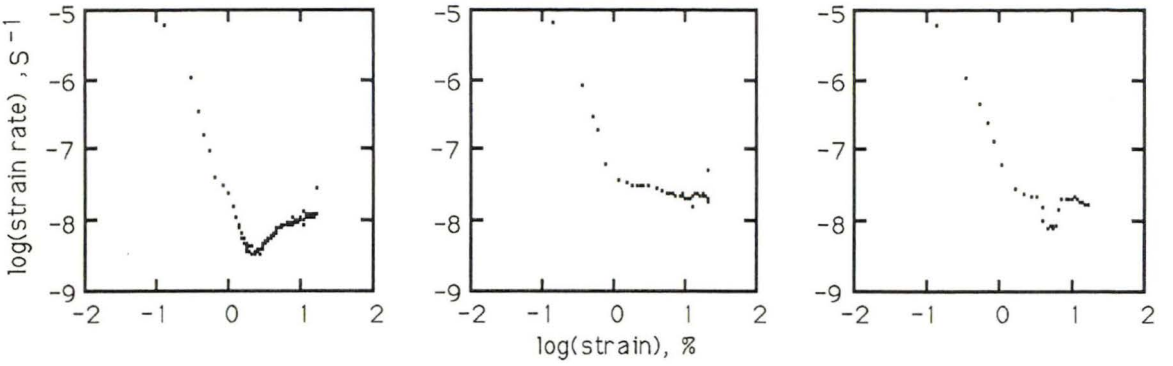

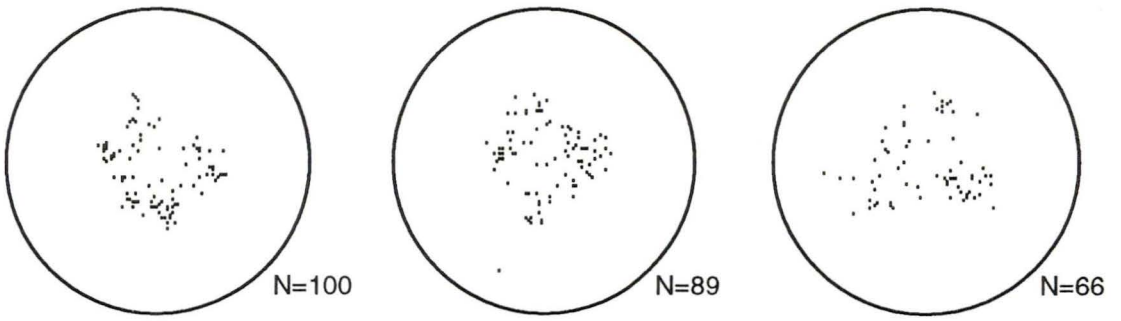

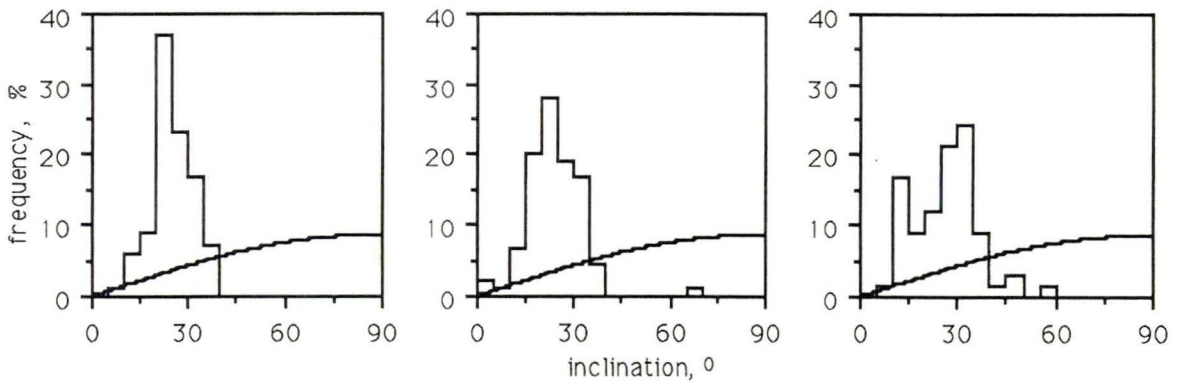

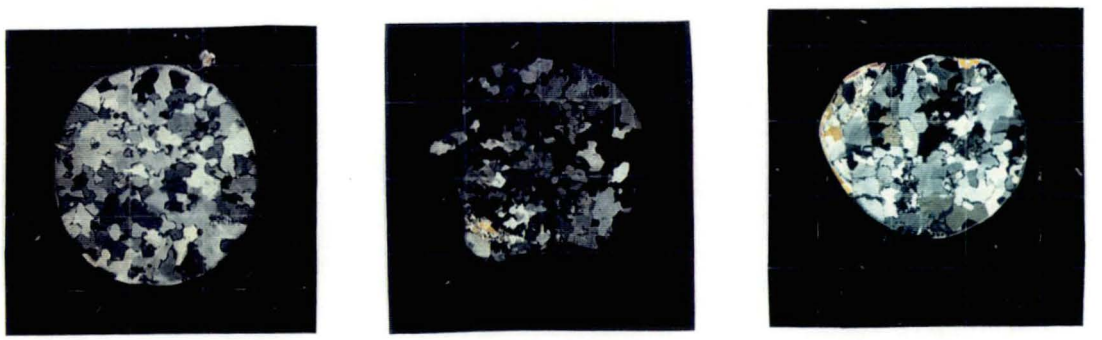

ε = 16.36 %	ε = 38.73 %	ε = 54.73 %
S = 2.60 mm^2	S = 2.22 mm^2	S = 2.19 mm^2
σ = 6.47°	σ = 8.53°	σ = 9.82°
μ = 25.89°	μ = 24.54°	μ = 27.11°

BHC1_108D

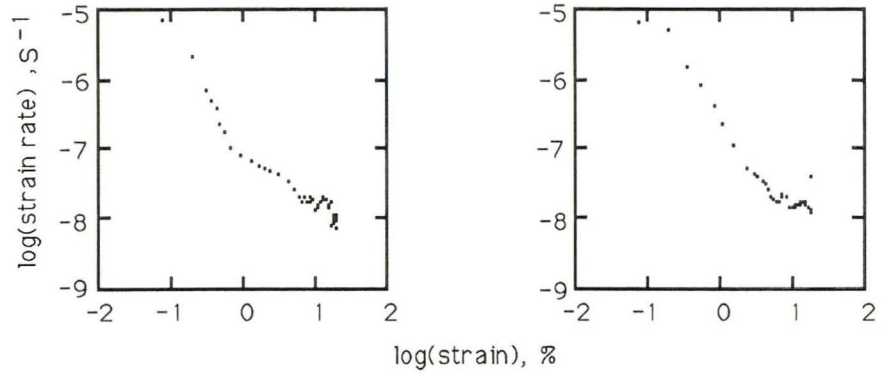

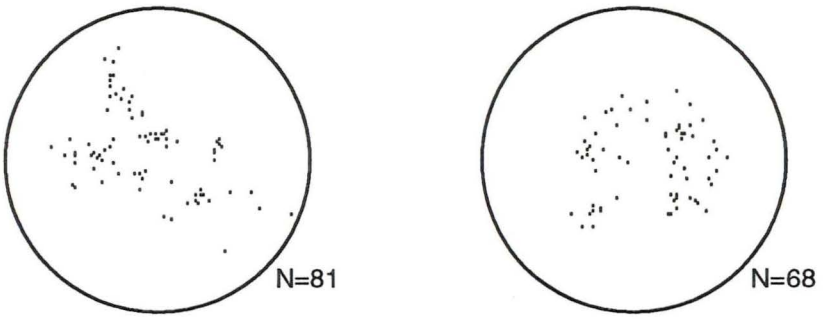

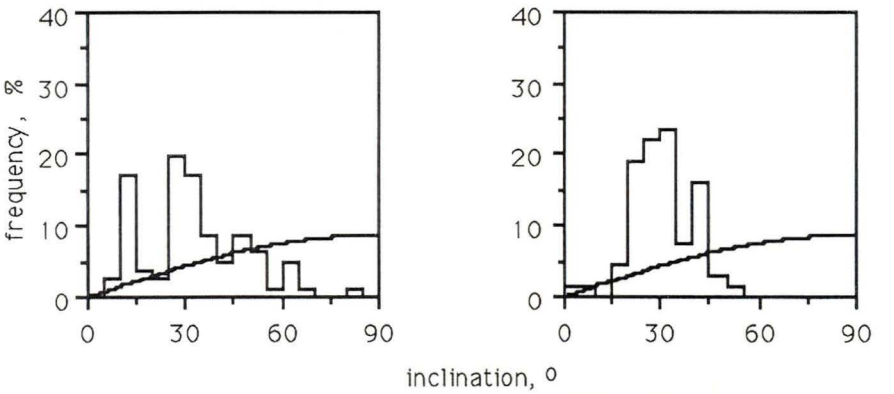

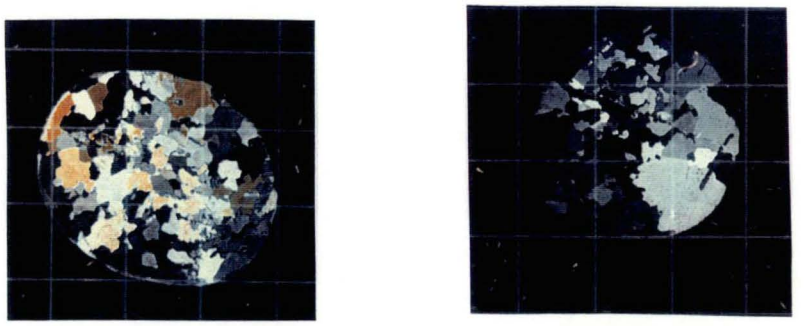

ε = 20.48 %
S = 3.12 mm²
σ = 15.78°
μ = 33.62°

ε = 39.48 %
S = 3.06 mm²
σ = 9.41°
μ = 31.40°

BHC1_116D

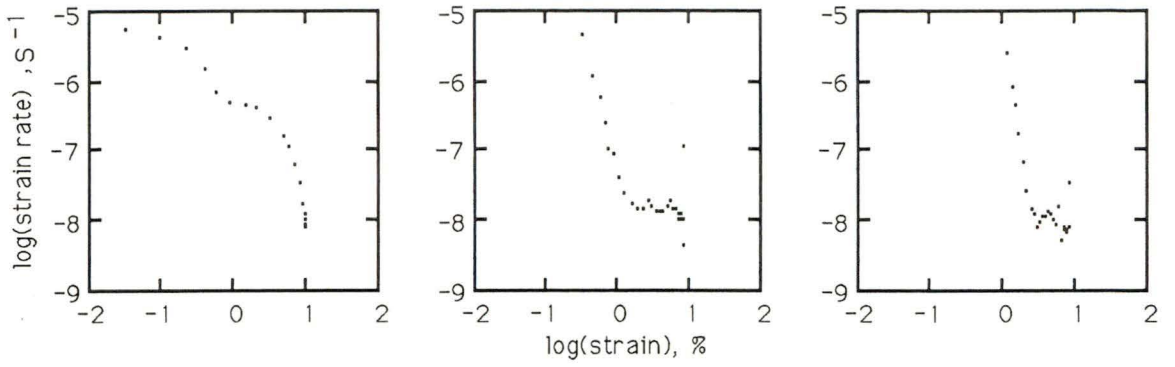

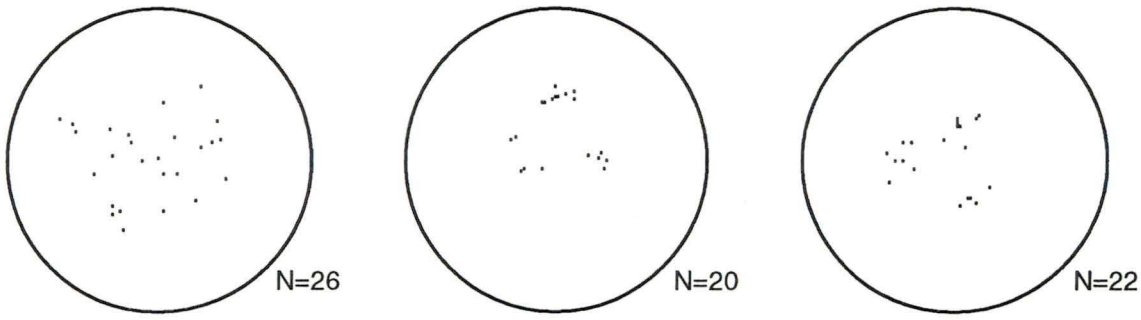

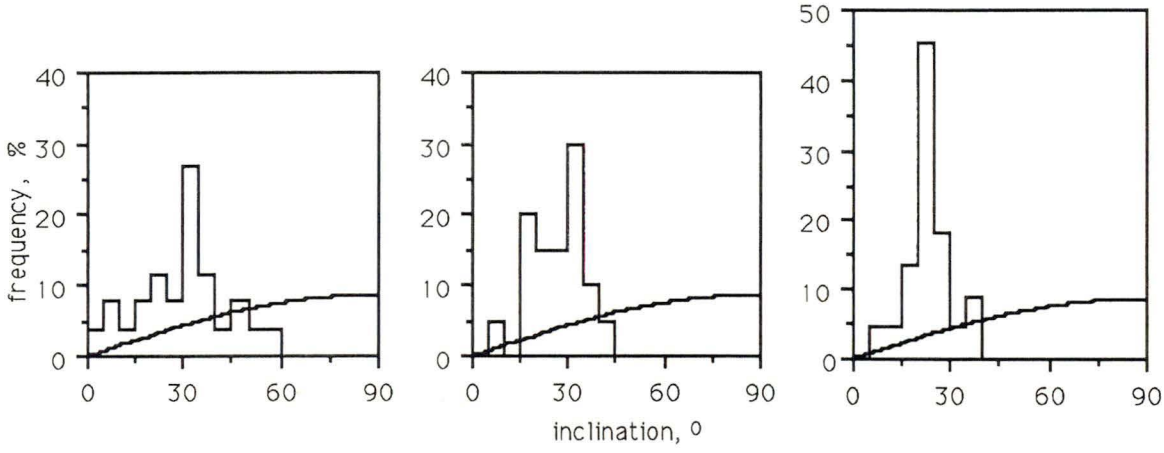

ε = 10.18 %	ε = 18.69 %	ε = 27.18 %
S = 4.75 mm^2	S = 9.88 mm^2	S = 21.25 mm^2
σ = 14.13°	σ = 8.50°	σ = 6.37°
μ = 30.15°	μ = 27.80°	μ = 23.73°

BHC1_121B

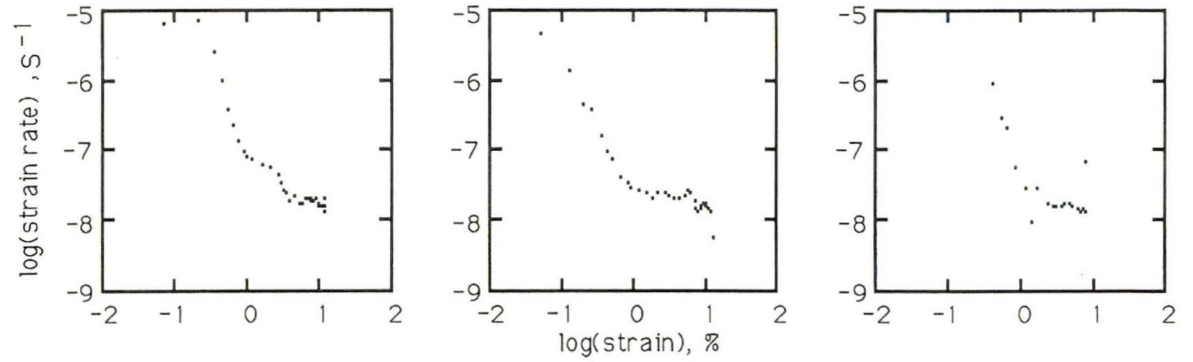

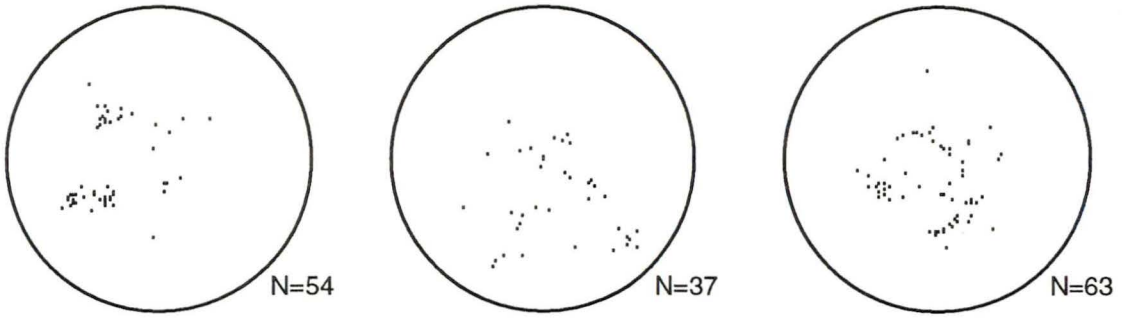

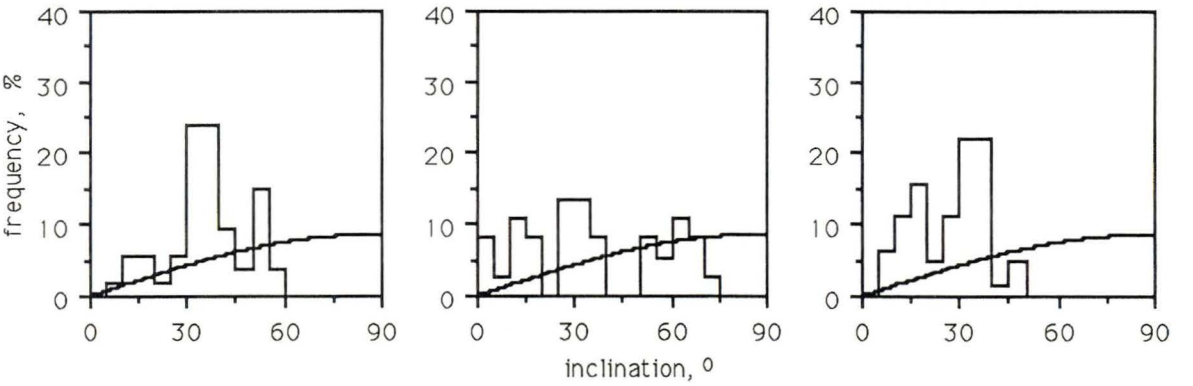

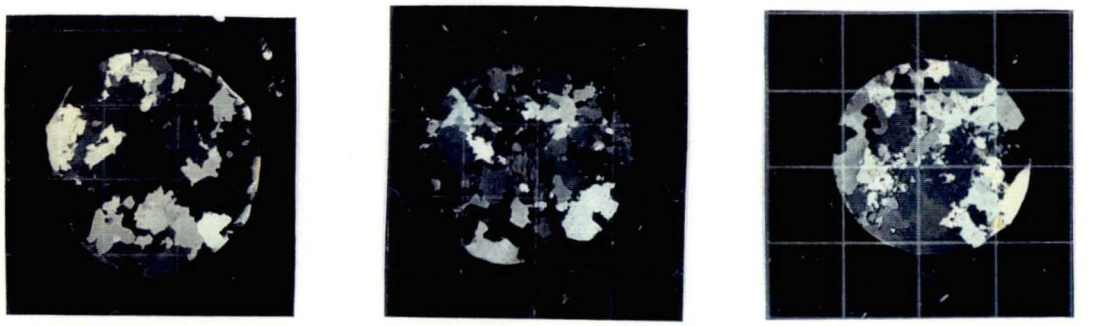

ε = 12.14 %	ε = 25.12 %	ε = 32.88 %
S = 6.24 mm^2	S = 3.18 mm^2	S = 2.87 mm^2
σ = 12.09°	σ = 21.75°	σ = 11.13°
μ = 36.76°	μ = 36.14°	μ = 28.03°

BHC1_134D

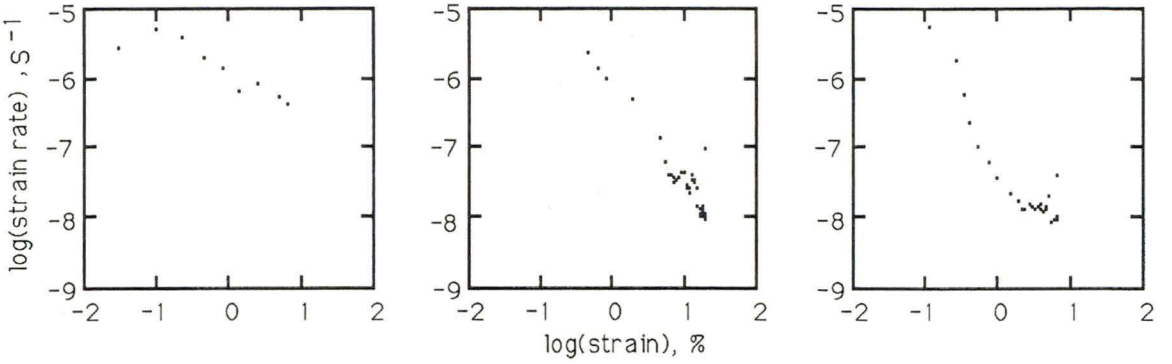

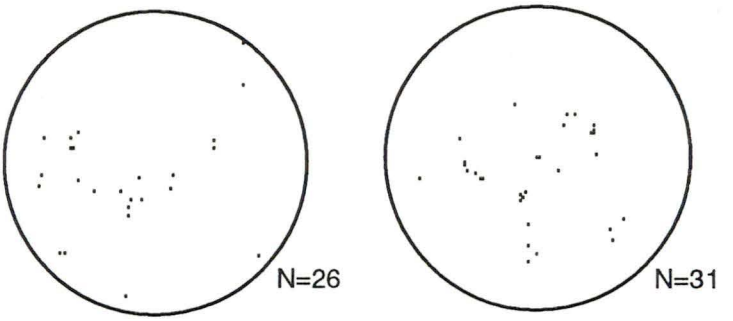

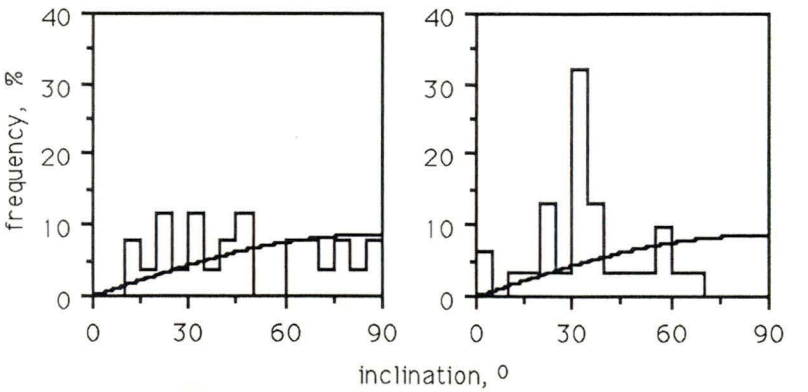

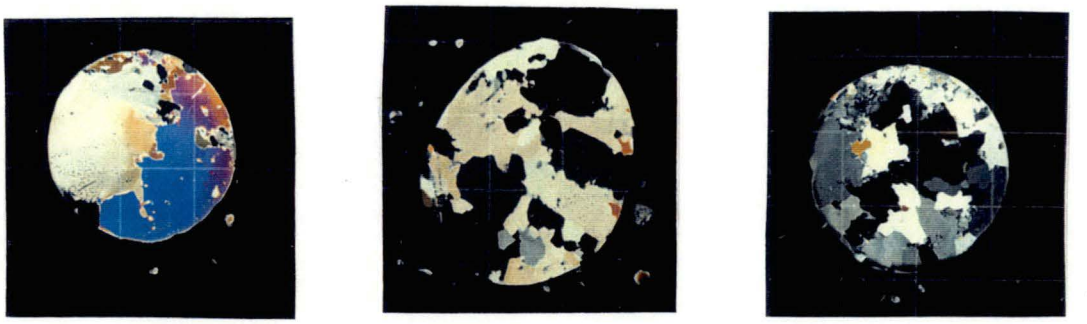

ε = 6.66 %	ε = 26.13 %	ε = 32.91 %
S = 11.17 mm^2	S = 10.83 mm^2	S = 5.04 mm^2
σ = -	σ = 24.24°	σ = 16.10°
μ = -	μ = 48.31°	μ = 34.77°

BHC1_138C

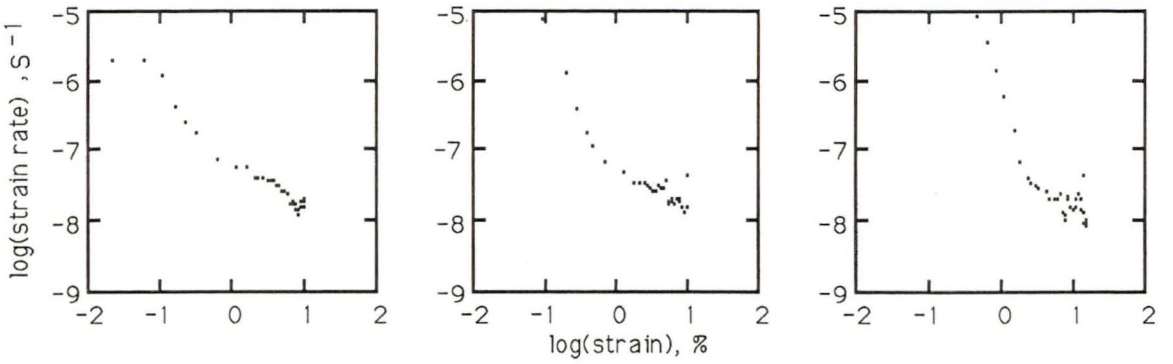

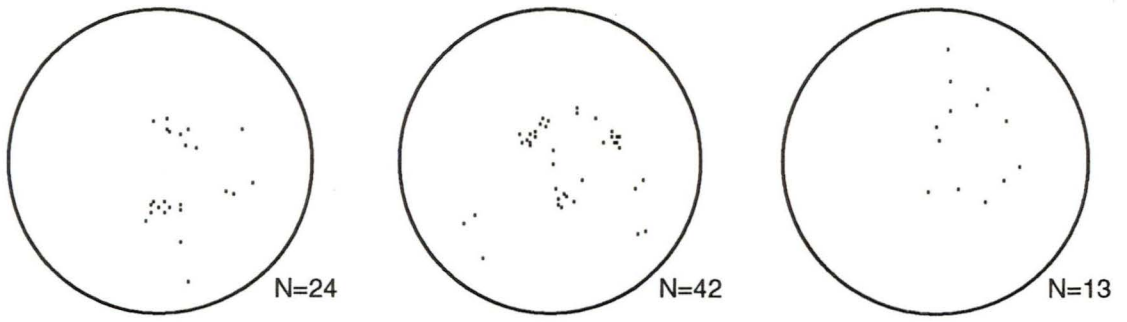

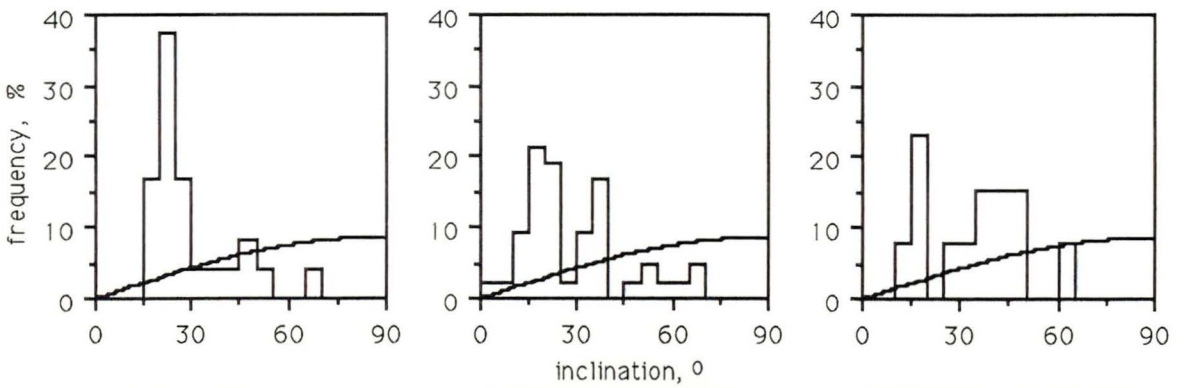

ε = 10.27 %	ε = 20.12 %	ε = 35.98 %
s = 11.60 mm^2	s = 6.21 mm^2	s = 8.68 mm^2
σ = 13.56°	σ = 16.18°	σ = 15.22°
μ = 29.88°	μ = 29.90°	μ = 34.38°

DYE3-T338

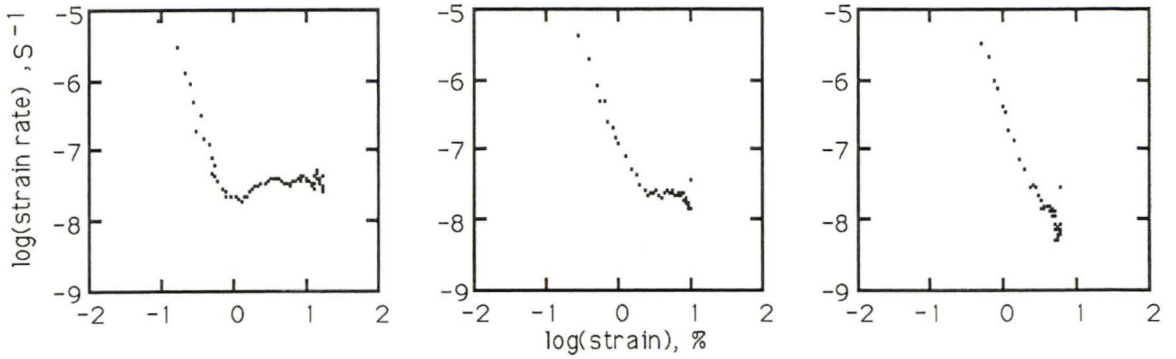

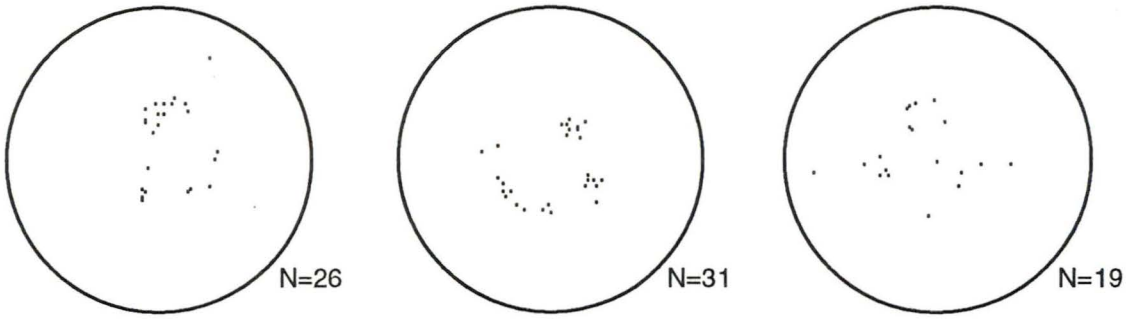

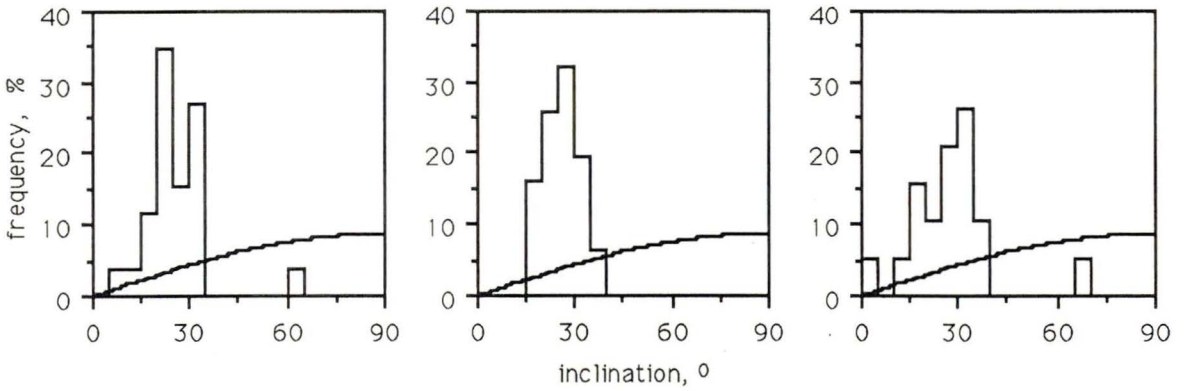

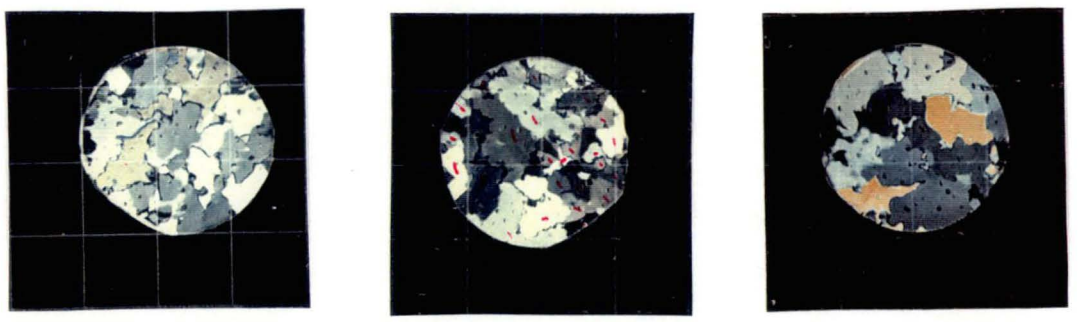

ε = 16.90 %	ε = 26.59 %	ε = 32.74 %
s = 13.23 mm^2	s = 10.42 mm^2	s = 19.22 mm^2
σ = 9.86°	σ = 5.42°	σ = 13.34°
μ = 26.46°	μ = 26.71°	μ = 28.58°

DYE3-T1556

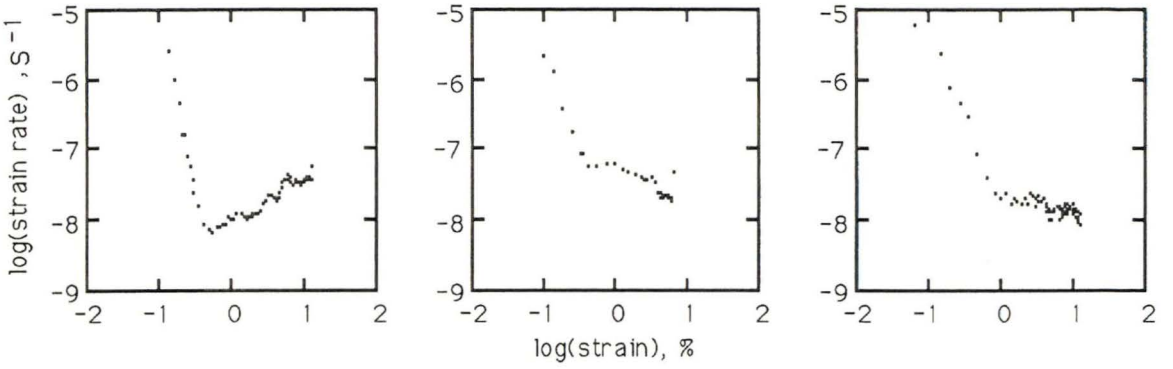

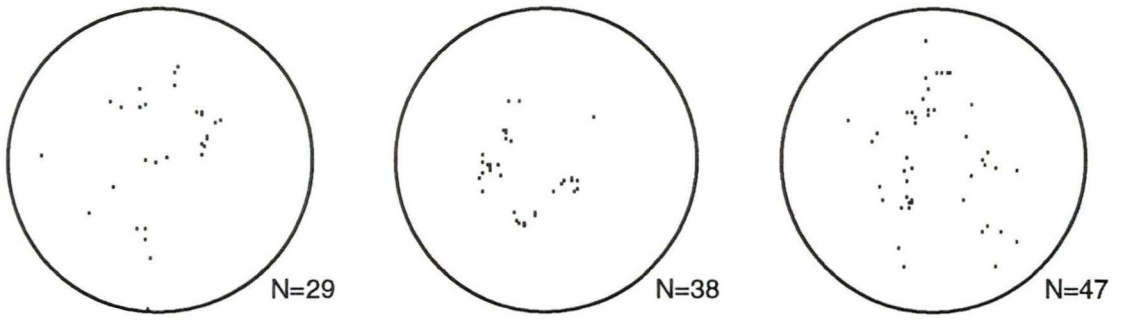

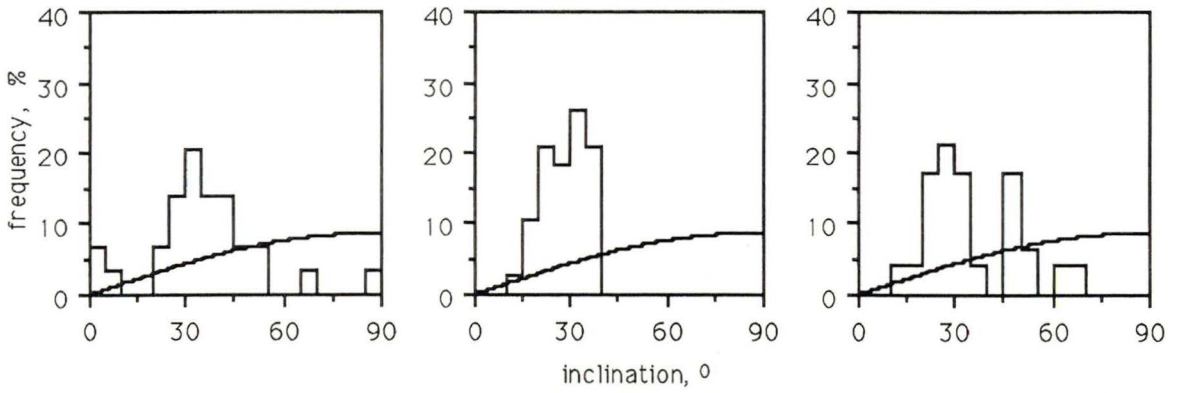

ε = 13.14 %	ε = 19.48 %	ε = 32.22 %
s = 13.09 mm^2	s = 11.54 mm^2	s = 11.53 mm^2
σ = 17.39°	σ = 7.27°	σ = 14.32°
μ = 36.17°	μ = 29.05°	μ = 35.60°

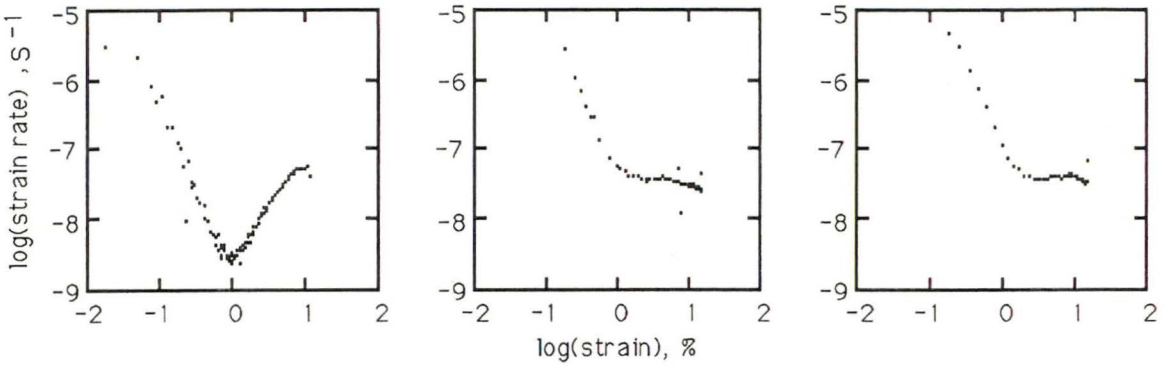

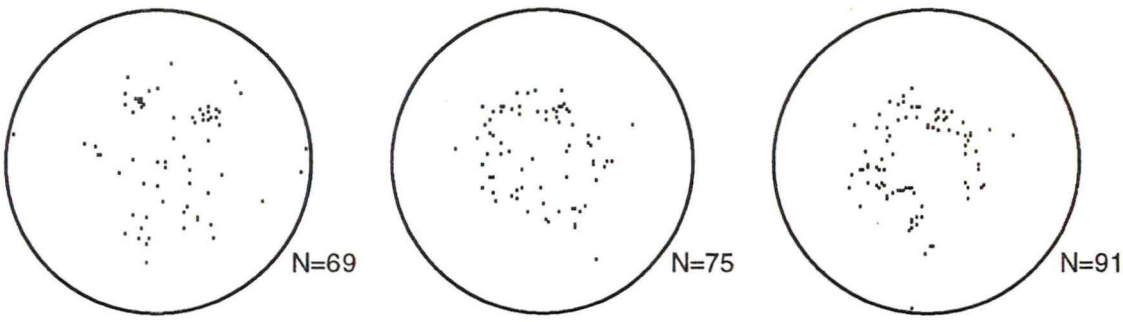

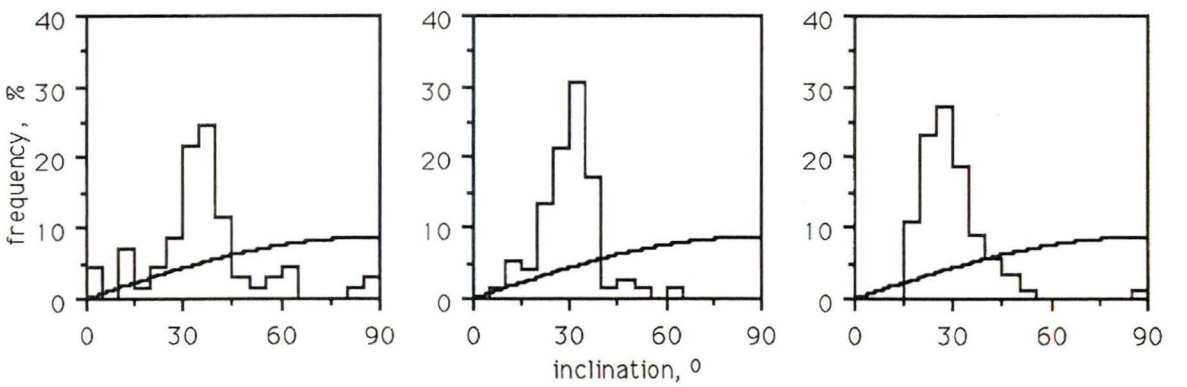

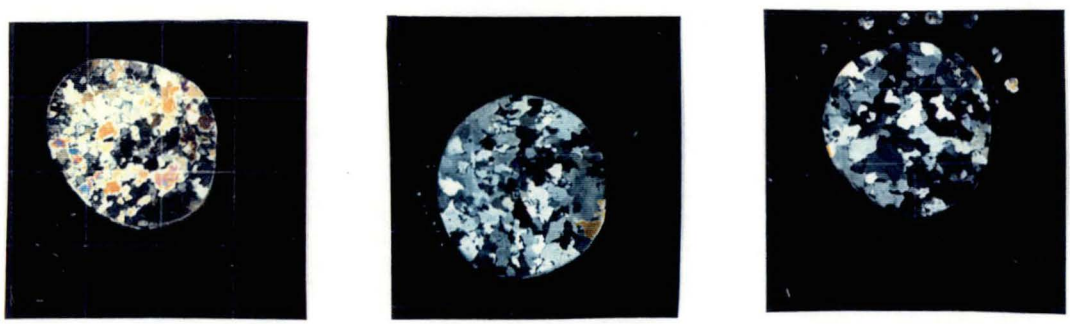

ε = 11.67 %	ε = 27.42 %	ε = 42.52 %
s = 2.93 mm^2	s = 3.55 mm^2	s = 1.61 mm^2
σ = 16.38°	σ = 8.94°	σ = 9.74°
μ = 36.46°	μ = 30.79°	μ = 30.16°

DYE3-T1922

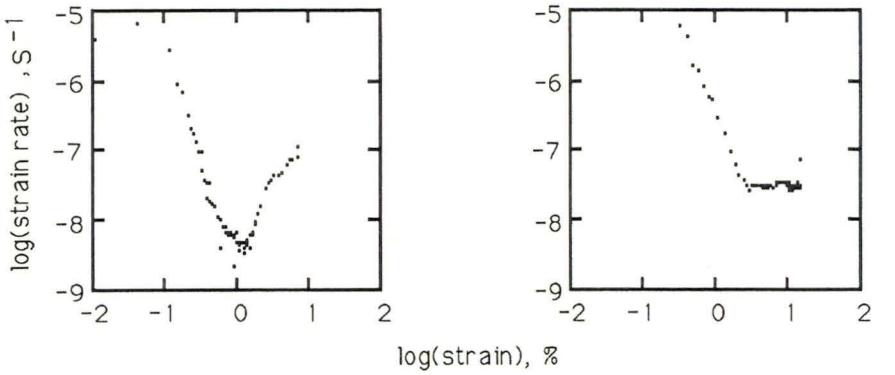

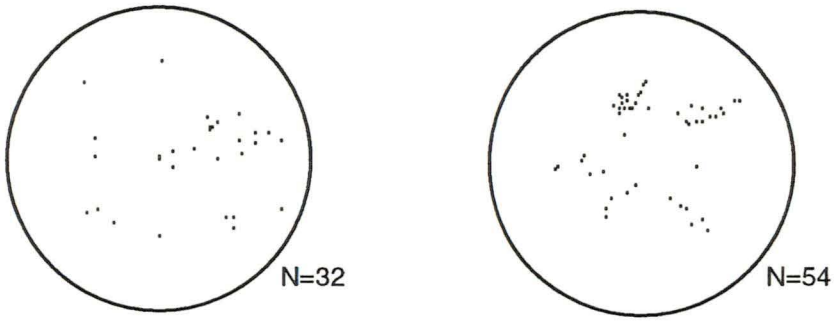

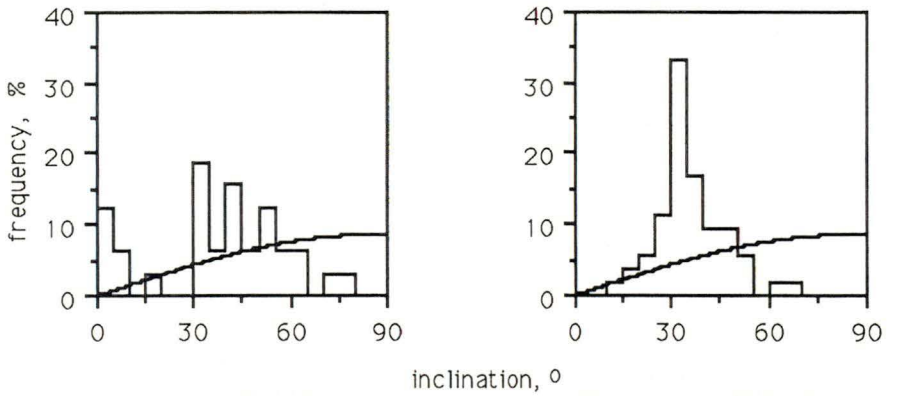

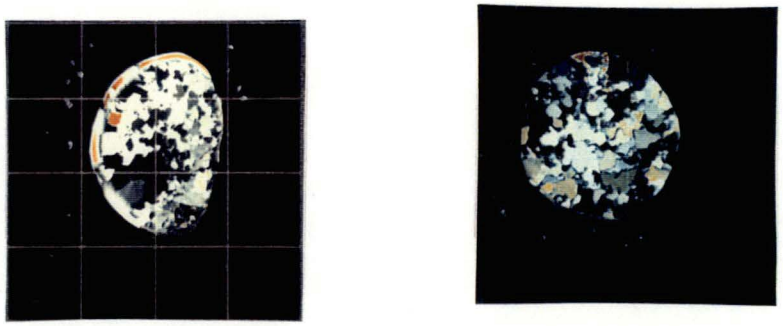

ε = 7.32 %
s = 1.53 mm²
σ = 20.75°
μ = 38.31°

ε = 22.62 %
s = 3.01 mm²
σ = 10.40°
μ = 36.74°

LAB1

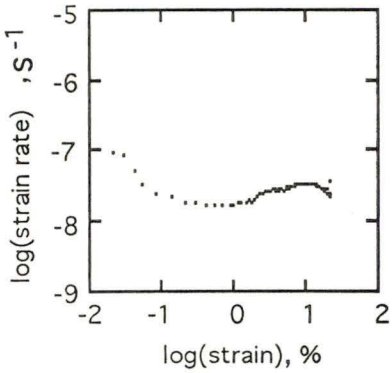

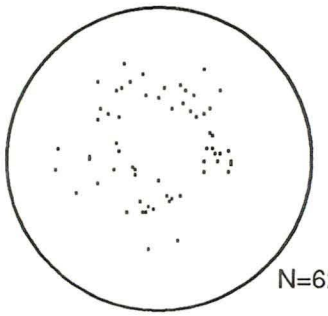

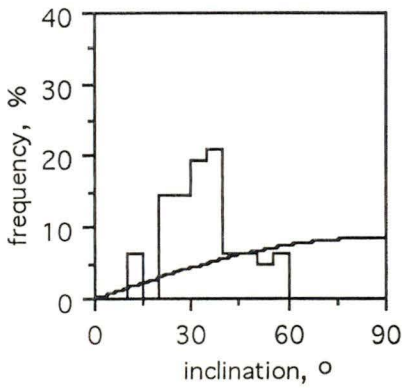

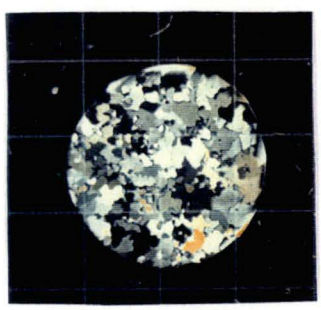

ε = 22.45 %

s = 1.66 mm²

σ = 11.06°

μ = 34.92°

LAB2

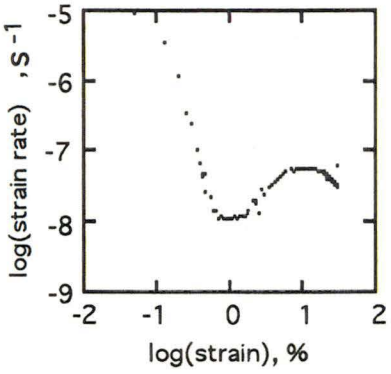

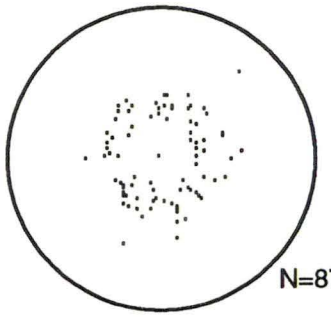

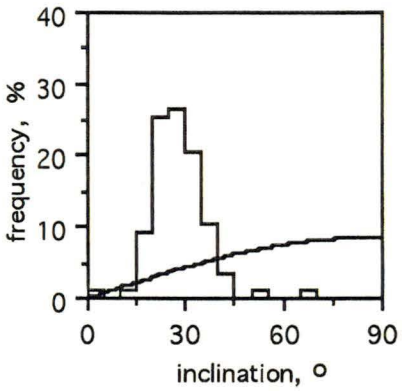

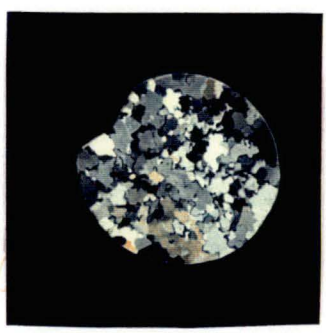

ε = 31.06 %

s = 2.09 mm²

σ = 8.37°

μ = 28.54°

LAB3

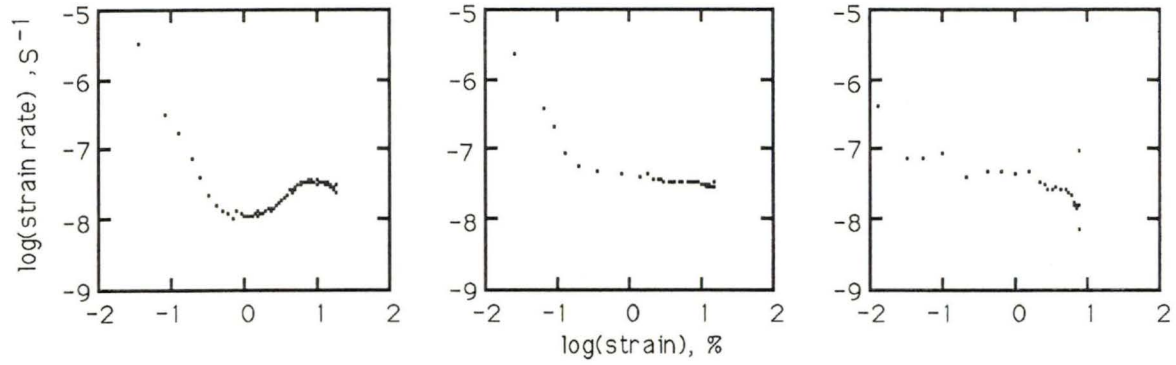

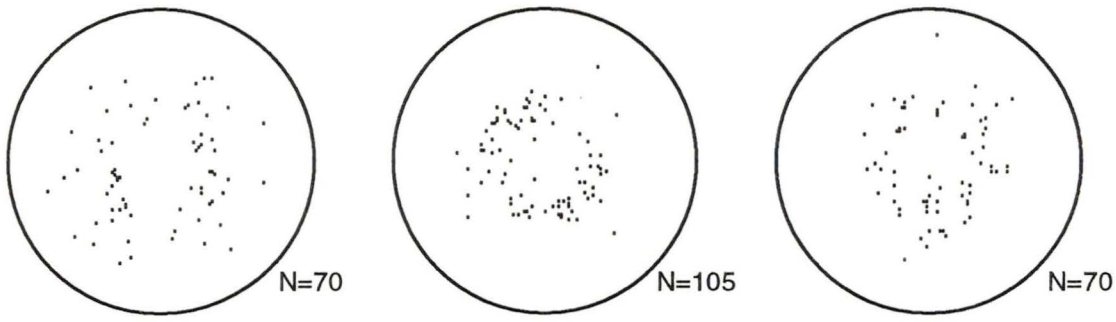

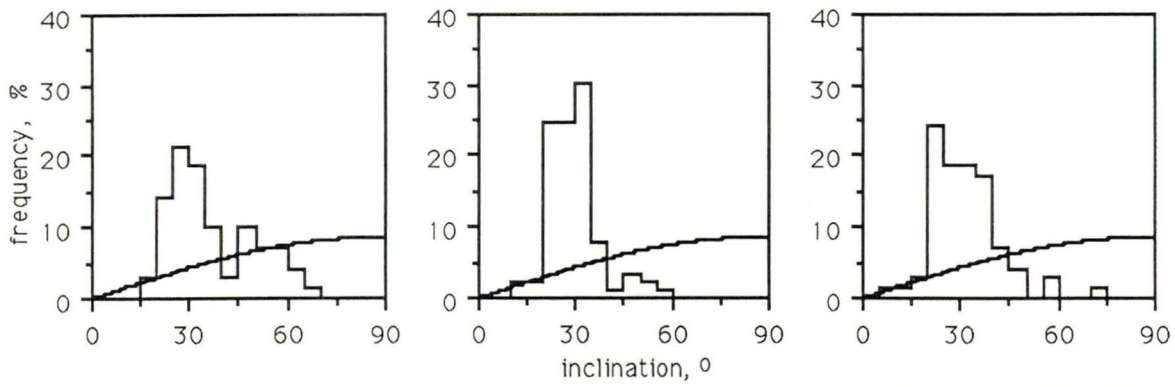

ε = 18.07 %	ε = 33.79 %	ε = 41.54 %
s = 2.11 mm^2	s = 2.51 mm^2	s = 2.79 mm^2
σ = 12.60°	σ = 7.96°	σ = 10.31°
μ = 31.26°	μ = 30.53°	μ = 31.89°

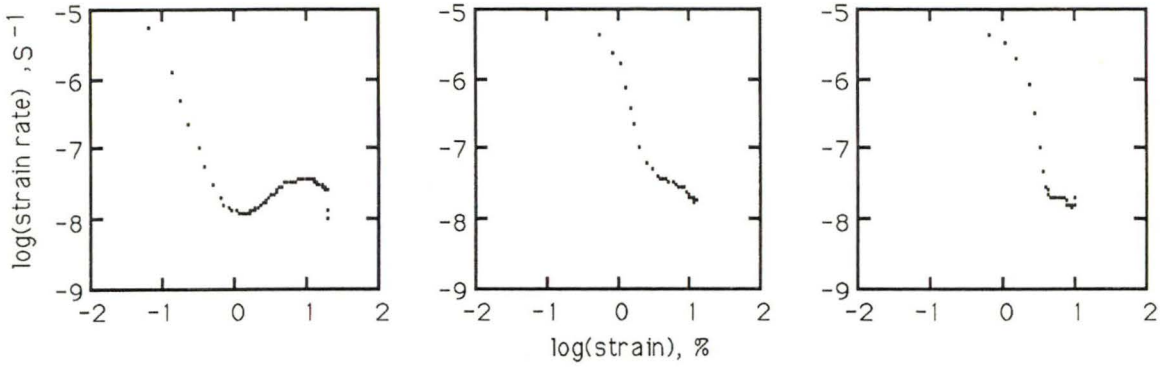

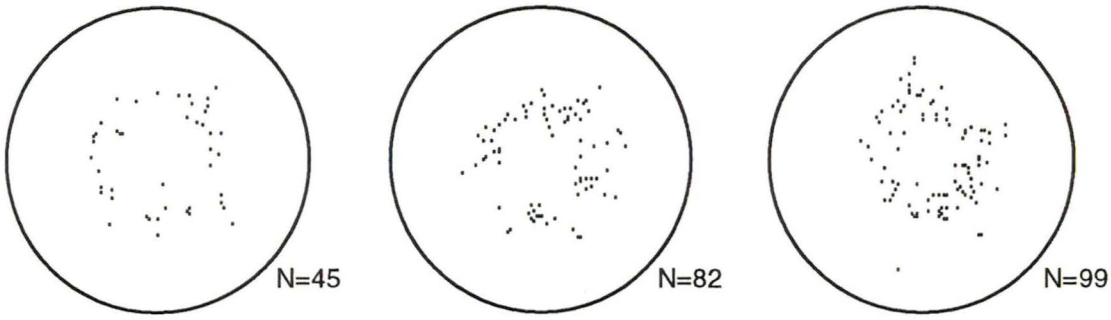

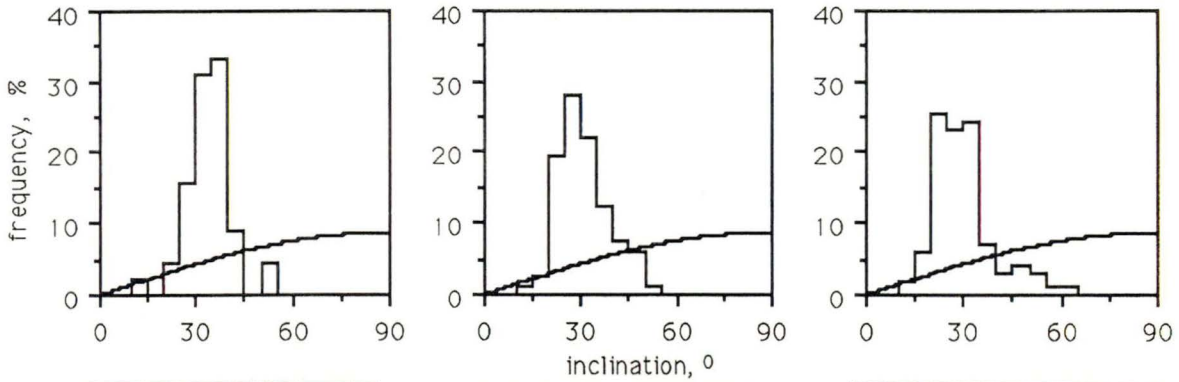

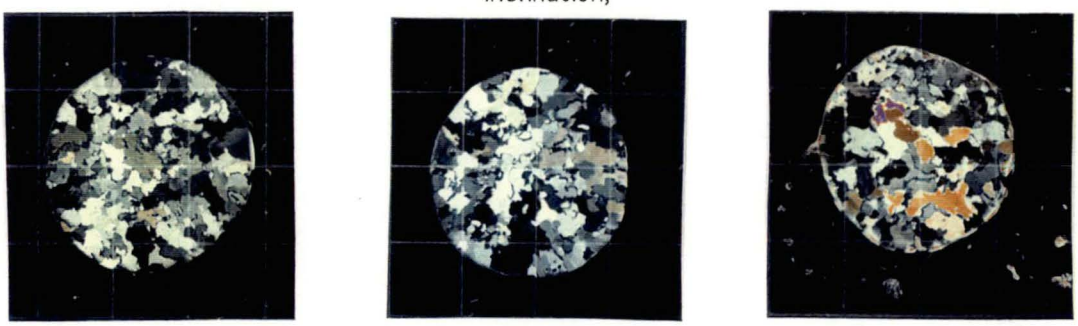

ε = 20.29 %	ε = 32.88 %	ε = 42.85 %
S = 2.11 mm^2	S = 2.75 mm^2	S = 2.71 mm^2
σ = 7.12°	σ = 7.65°	σ = 9.10°
μ = 34.67°	μ = 31.61°	μ = 30.65°

LAB5

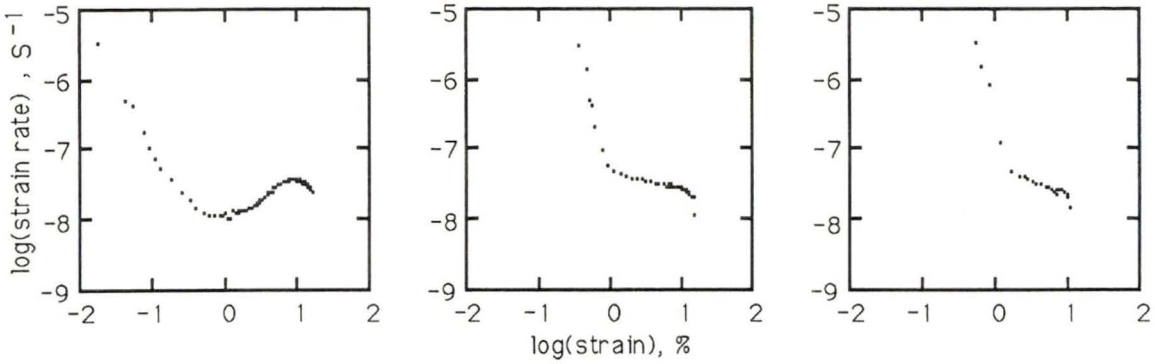

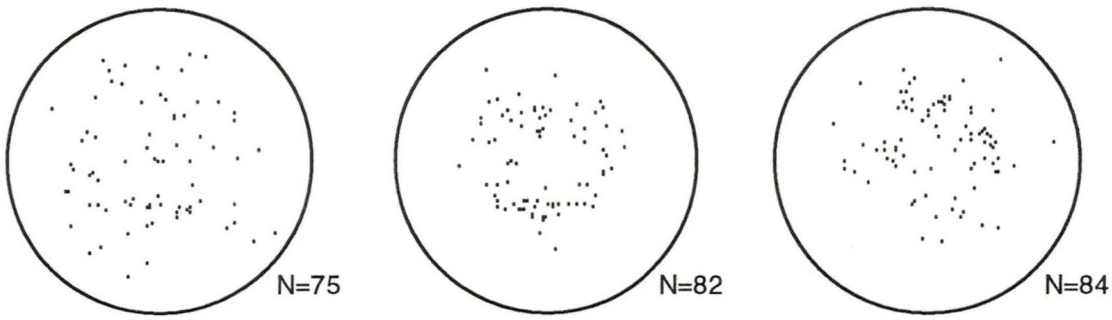

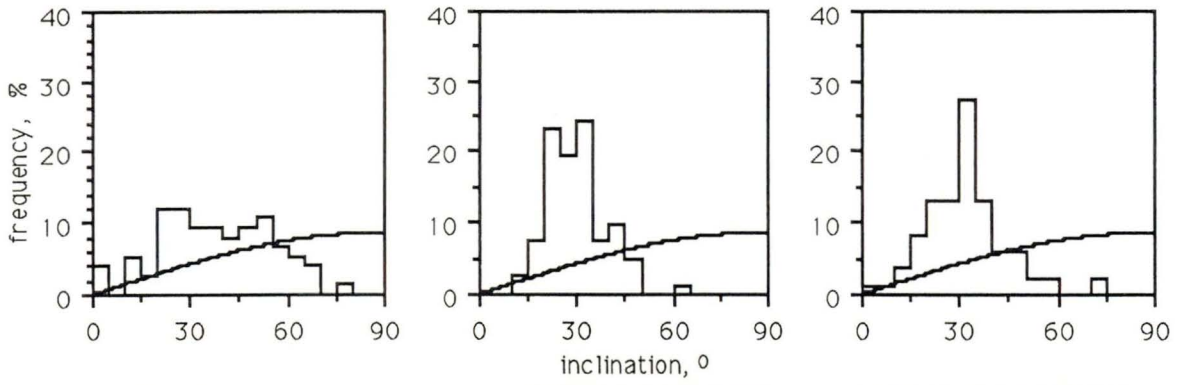

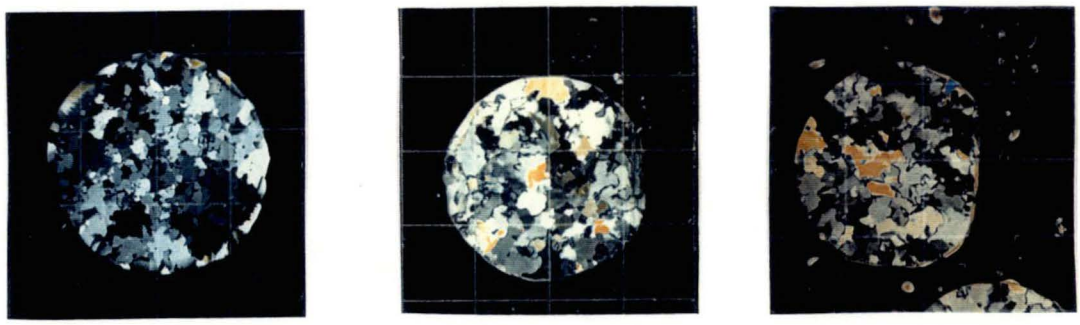

ε = 16.64 %	ε = 32.66 %	ε = 43.22 %
S = 1.59 mm^2	S = 2.73 mm^2	S = 2.61 mm^2
σ = 17.00°	σ = 8.74°	σ = 12.02°
μ = 38.85°	μ = 30.90°	μ = 32.74°

LAB6

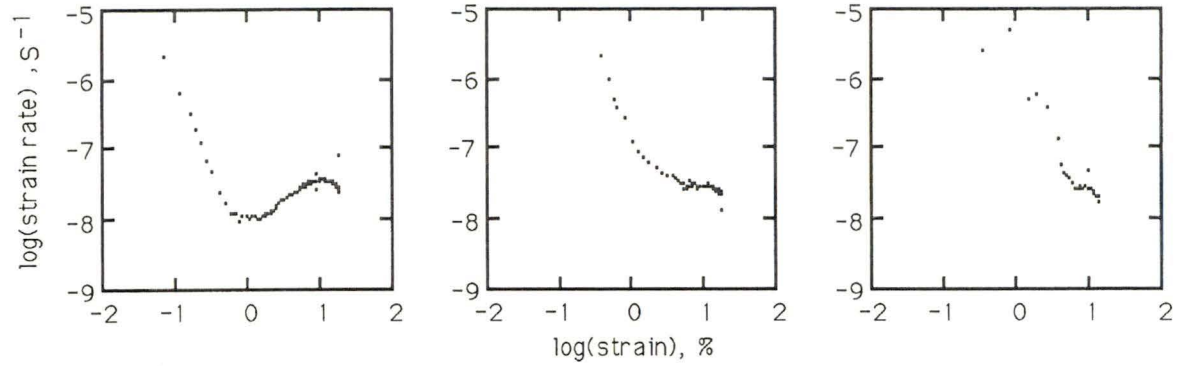

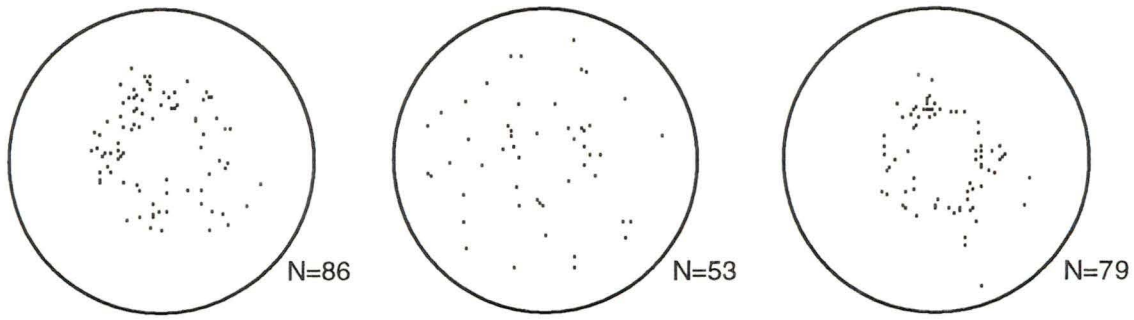

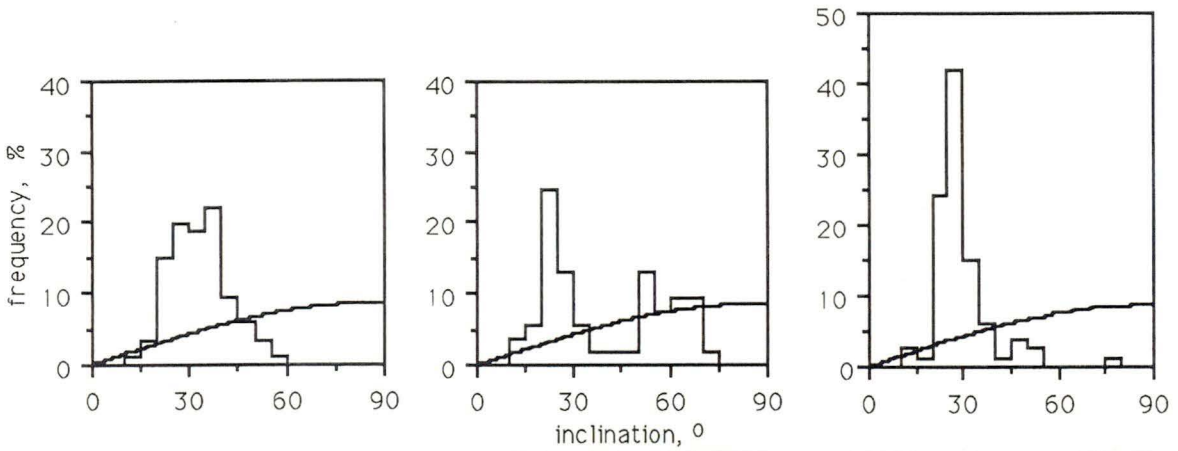

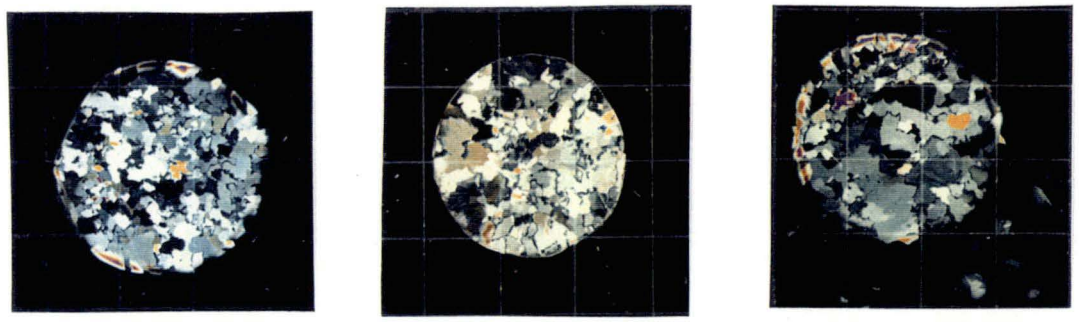

ε = 15.94 %	ε = 34.07 %	ε = 48.55 %
S = 1.40 mm^2	S = 1.78 mm^2	S = 2.51 mm^2
σ = 9.03°	σ = 18.50°	σ = 8.97°
μ = 33.56°	μ = 40.43°	μ = 30.10°

APPENDIX I I

Creep curves and crystal structure measurements

for simple shear tests

1st row - Creep curves of octahedral shear strain rate versus time and octahedral shear strain on log-log scales respectively.

2nd row - Diagrams of crystal orientation fabric with an arrow showing experimental shear direction before testing (left) and after testing (right).

3rd row - Diagrams of c-axis distribution histogram before testing (left) and after testing (right).

4th row - Thin section photographs on 1:1 scales before testing (left) and after testing (right).

N - Number of crystals oriented.

ε - Total octahedral shear strain.

S - Mean crystal area.

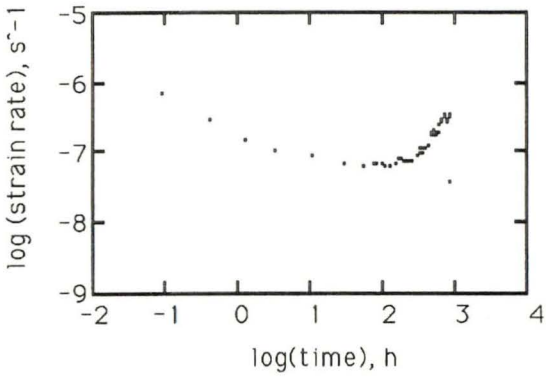

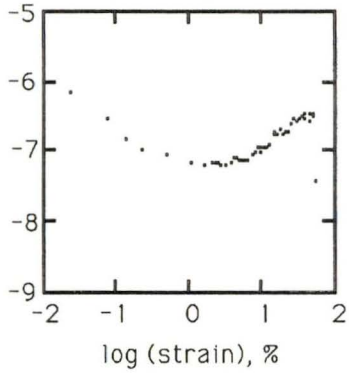

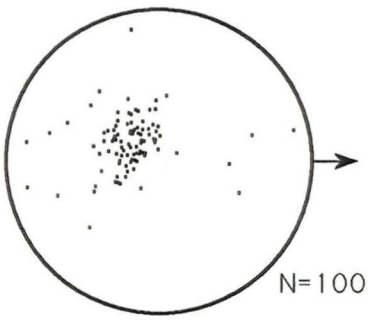

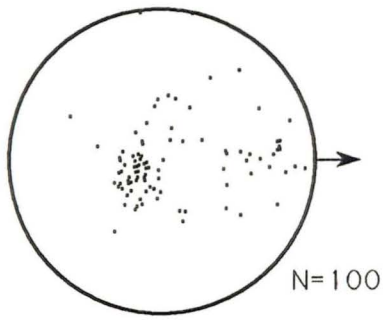

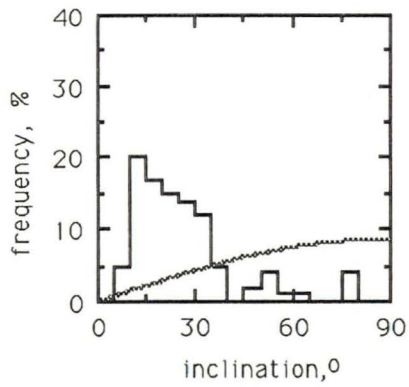

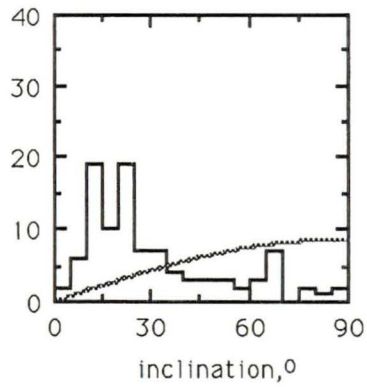

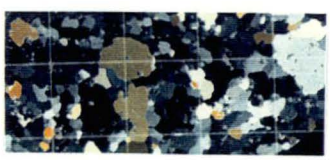

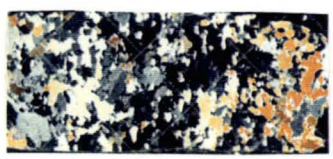

ε = 0%

S = 2.4 mm²

ε = 52.8 %

S = 1.3 mm²

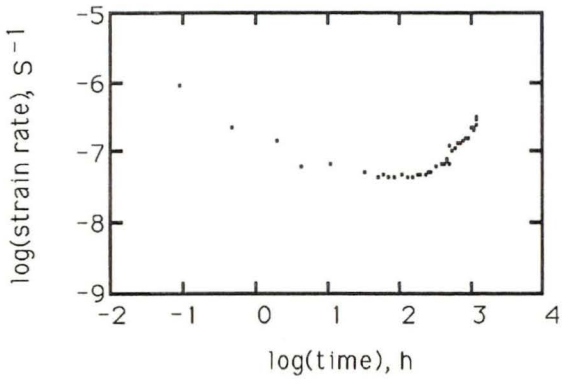

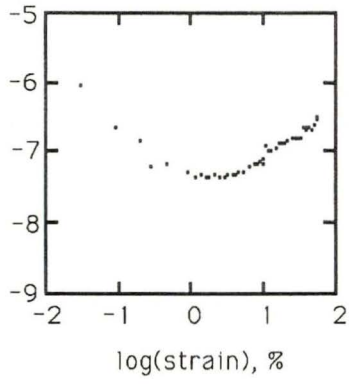

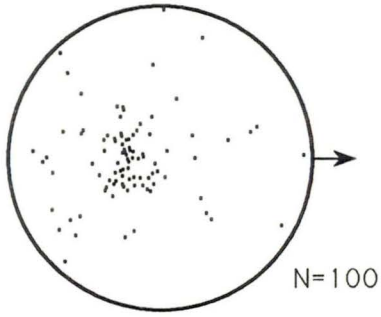

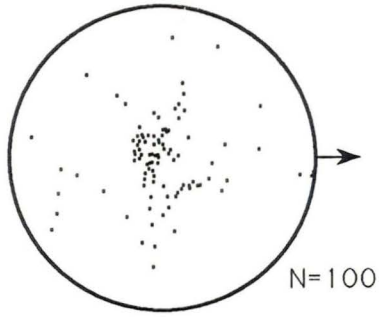

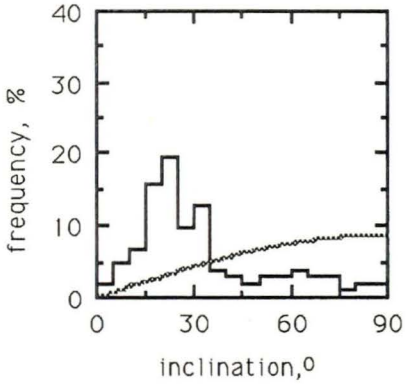

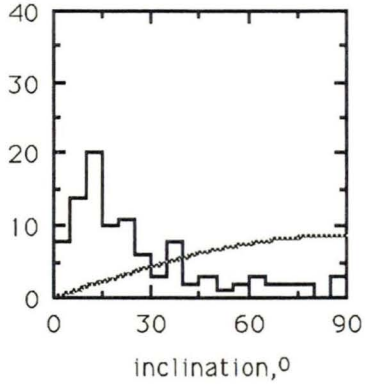

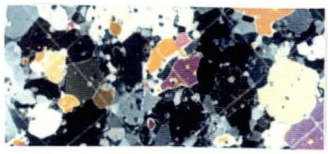

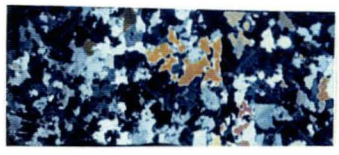

ε = 0 %

S = 4.7 mm²

ε = 57 %

S = 2.4 mm²

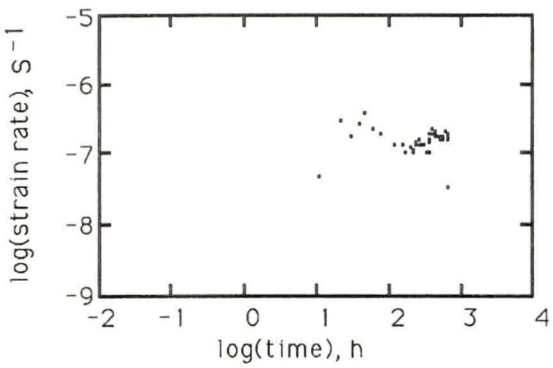

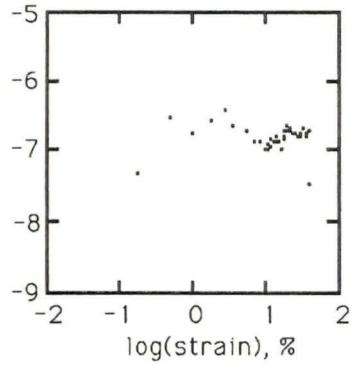

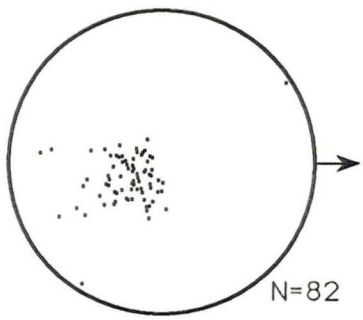

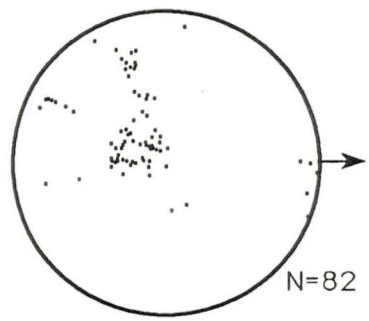

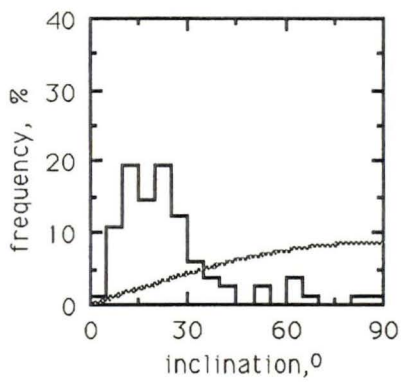

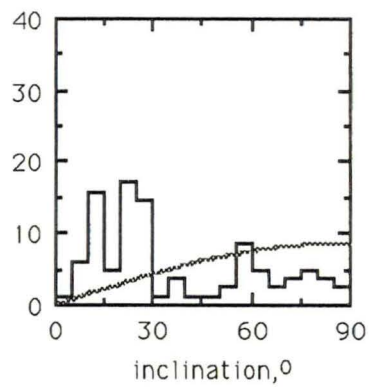

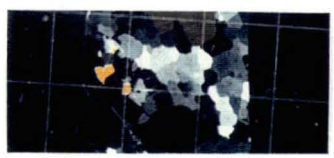

ε = 0%

S = 2.5mm²

ε = 38 %

S = 2.9 mm²

AGZ77_230

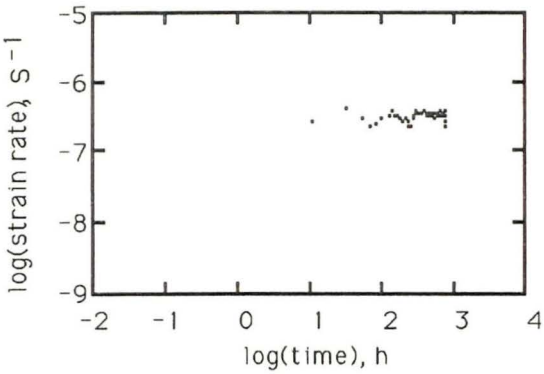

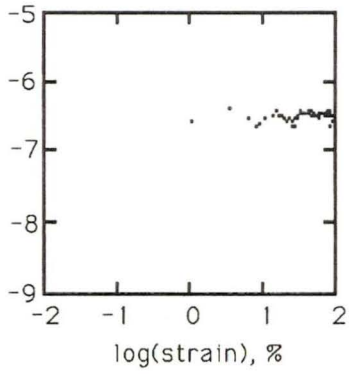

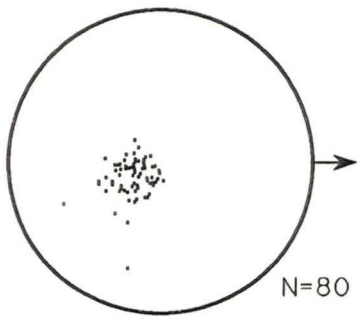

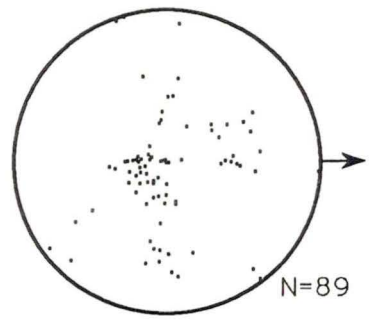

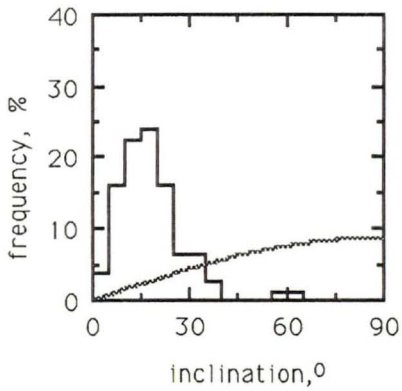

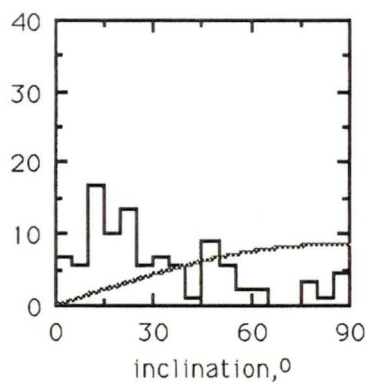

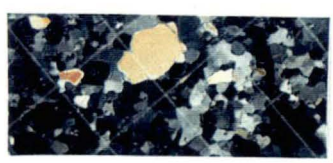

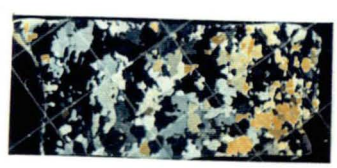

ε = 0%

S = 3.1 mm²

ε = 90.6 %

S = 3.1 mm²

BHC1_73B

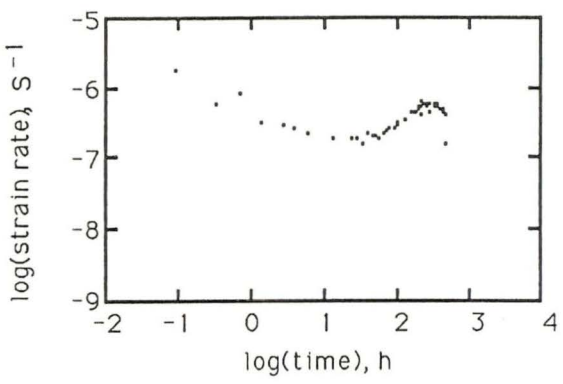

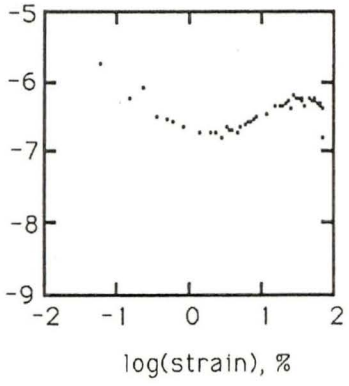

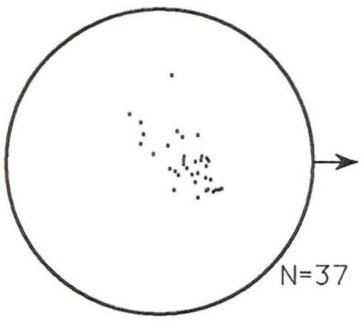

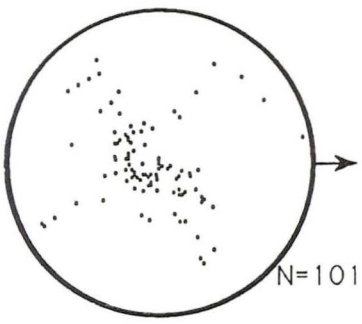

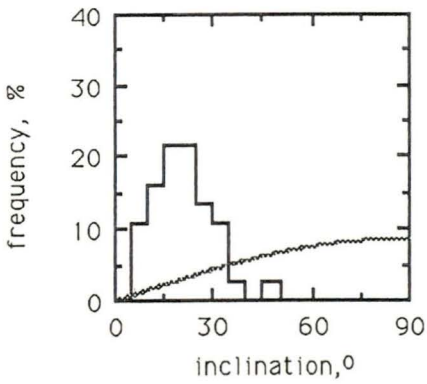

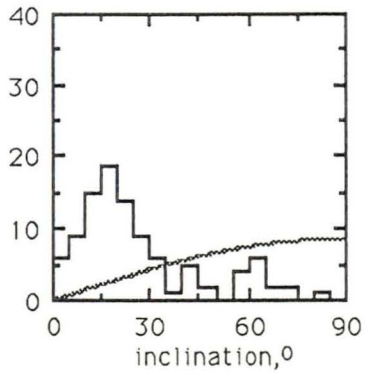

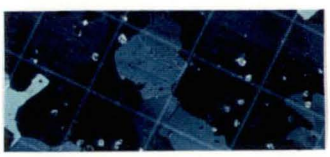

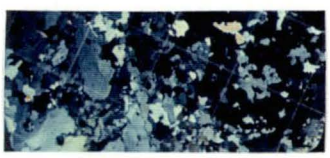

ε = 0 %

s > 31 mm²

ε = 70.4 %

s = 1.6 mm²

BHC1_79C

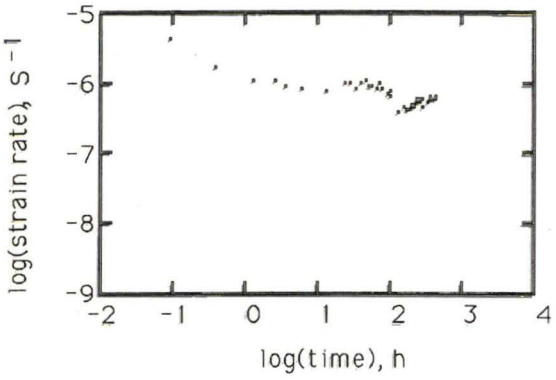

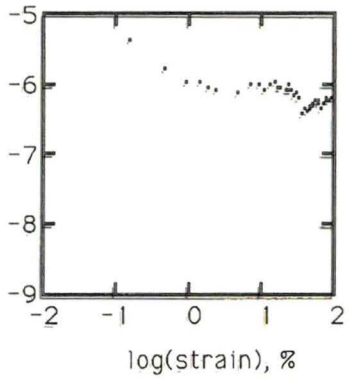

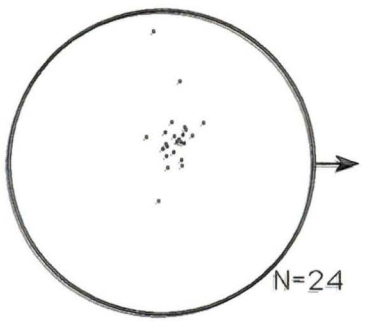

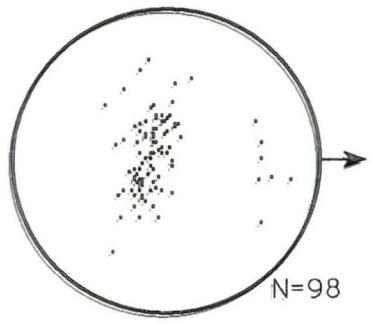

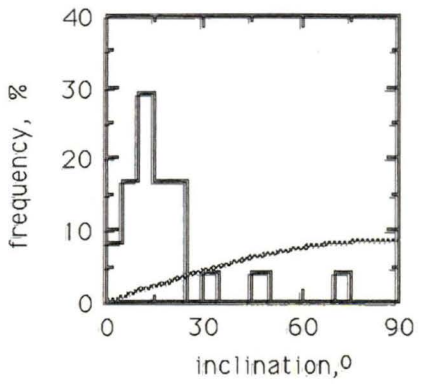

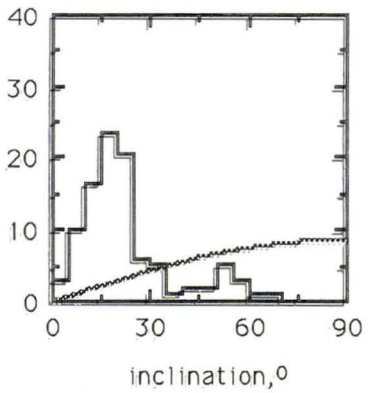

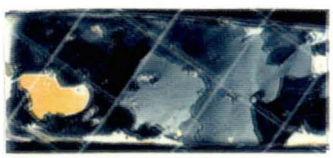

ε = 0 %

S > 24 mm^2

ε = 92.2 %

S = 1.0 mm^2

BHC1_84B

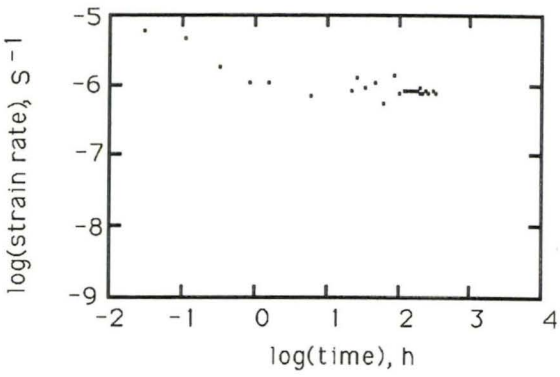

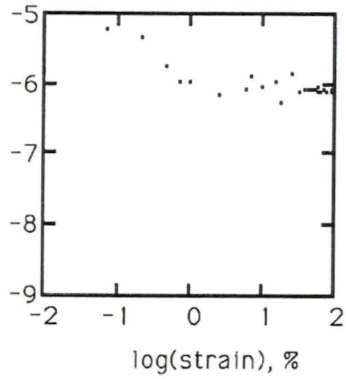

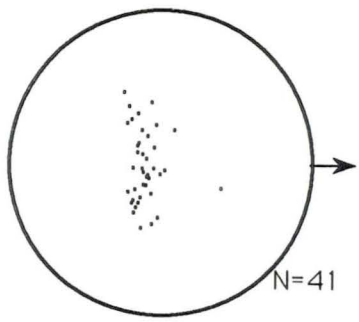

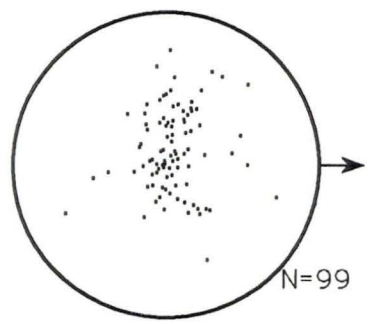

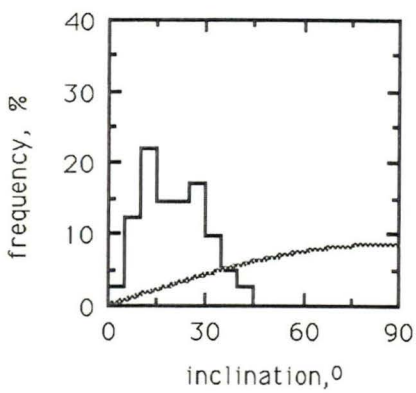

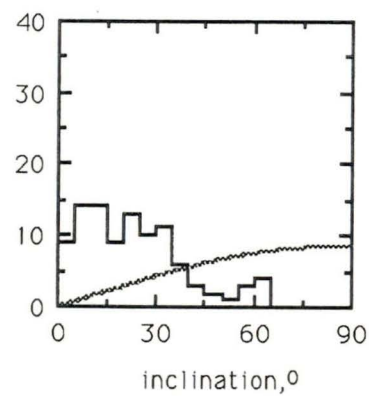

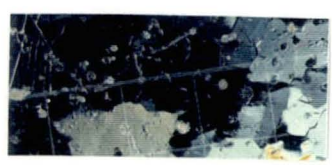

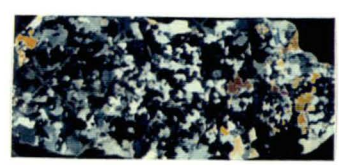

ε = 0 %

S > 62 mm²

ε = 98.1 %

S = 1.1 mm²

BHC1_108D

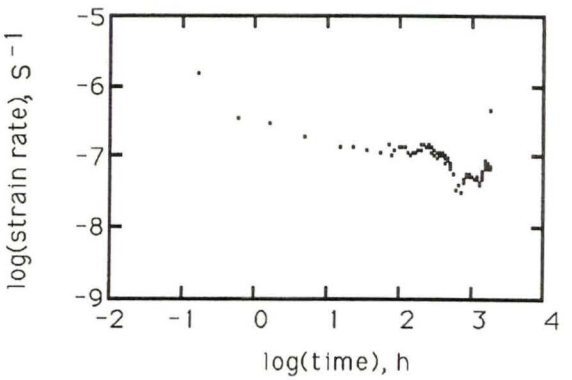

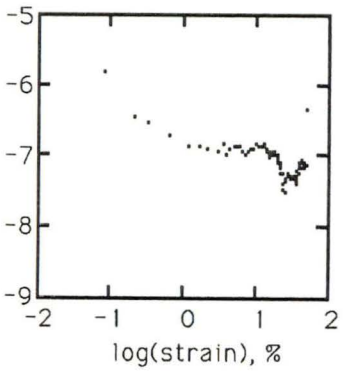

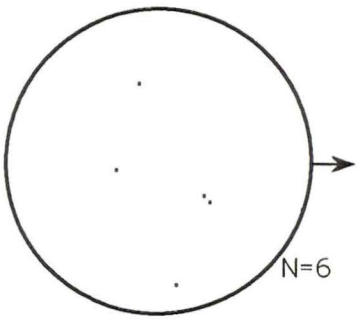

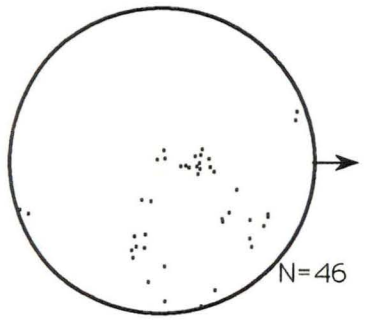

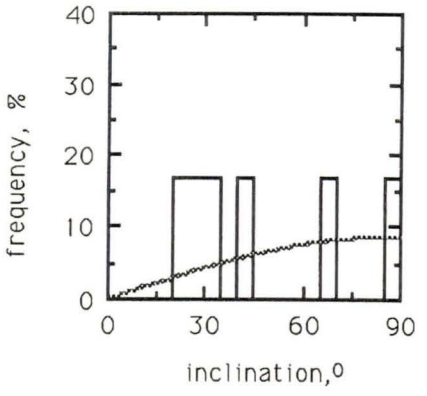

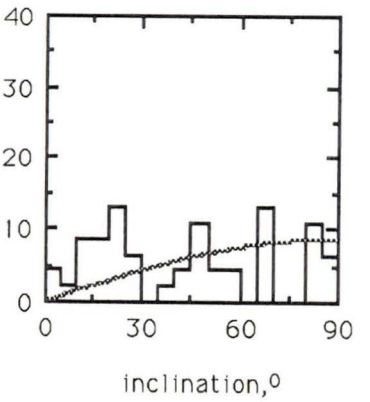

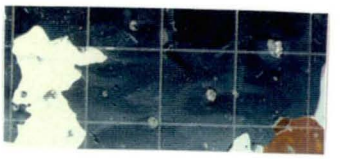

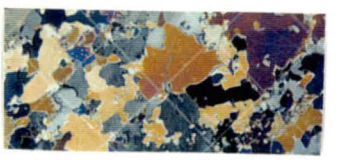

ε = 0 %

S > 217 mm²

ε = 49.5 %

S = 5.2 mm²

BHC1_116D

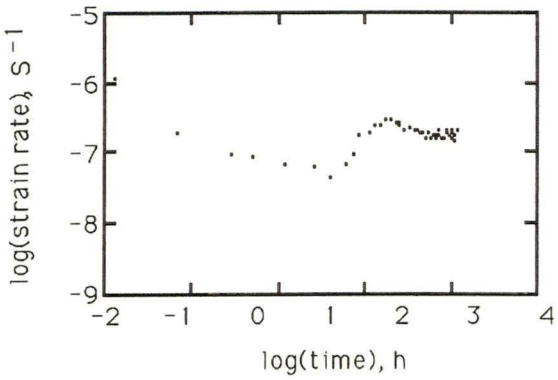

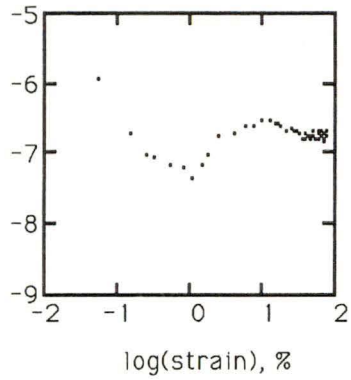

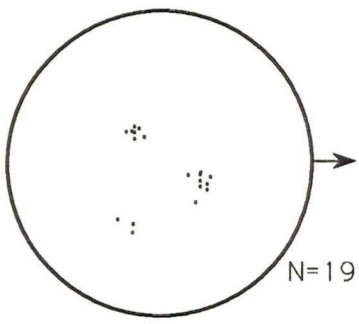

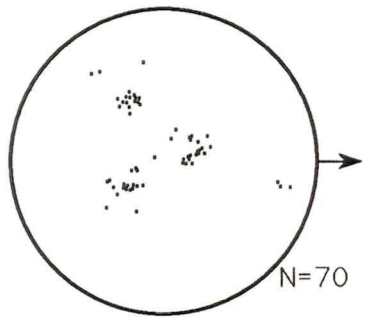

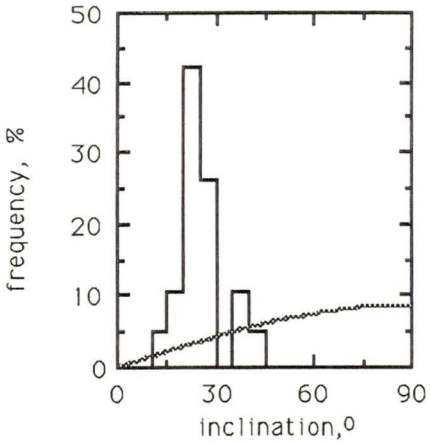

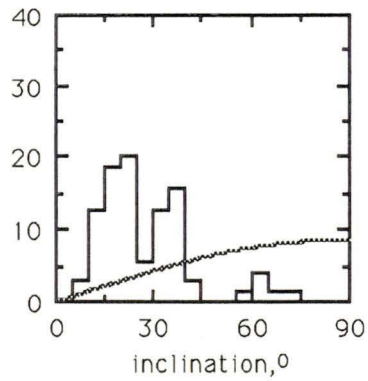

ε = 0 %

S > 138 mm²

ε = 78.7 %

S = 5.4 mm²

BHC1_121B

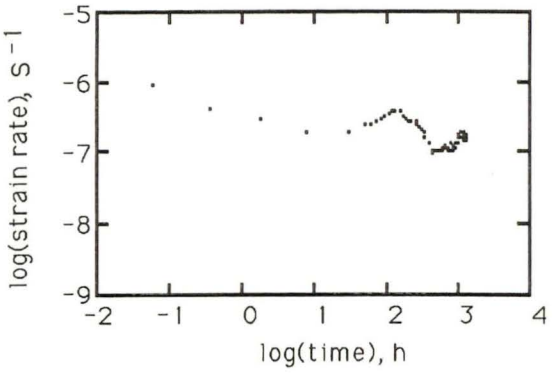

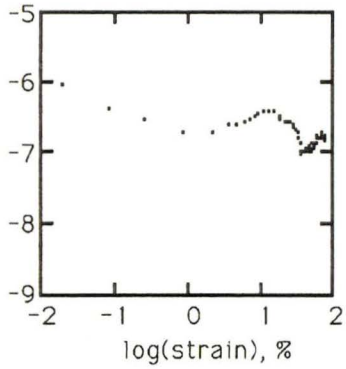

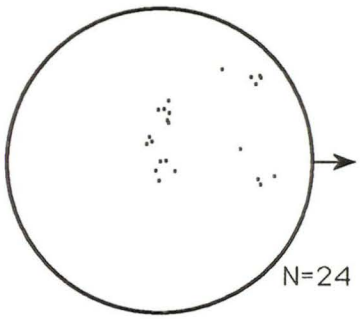

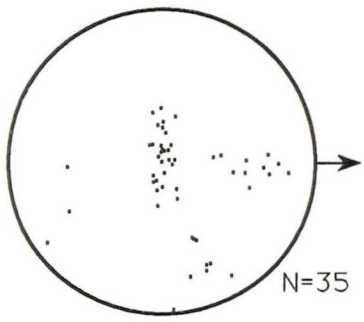

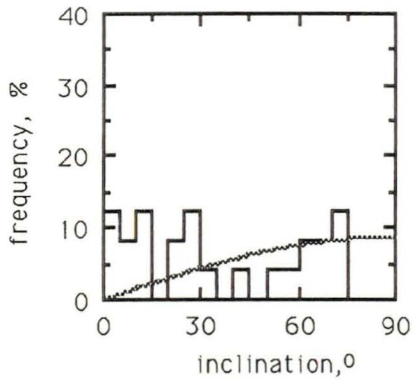

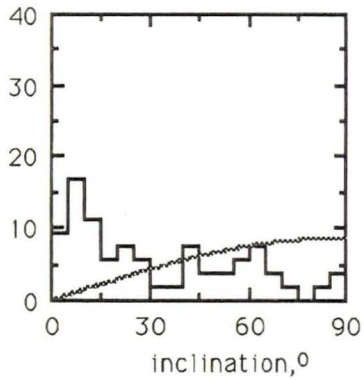

ε = 0 %

S > 83 mm²

ε = 77.7 %

S = 3.6 mm²

BHC1_134D

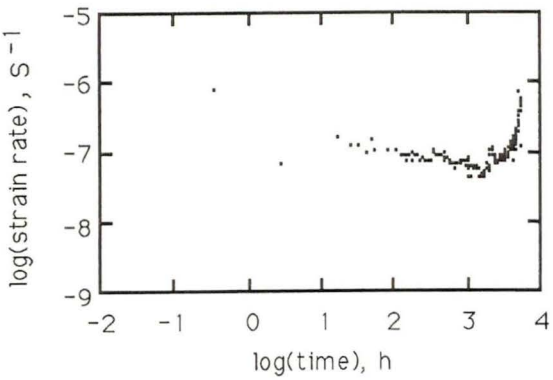

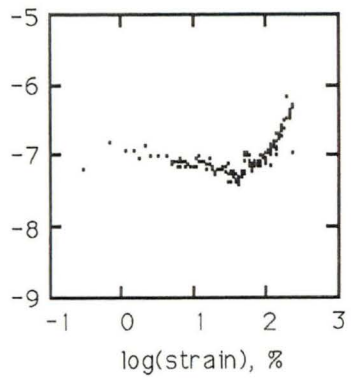

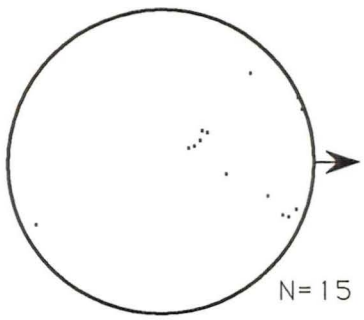

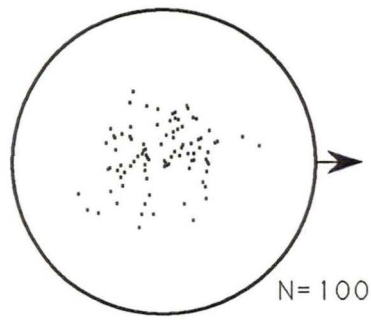

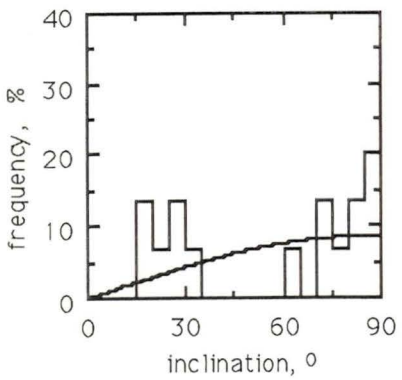

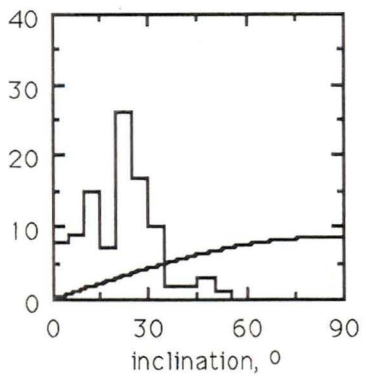

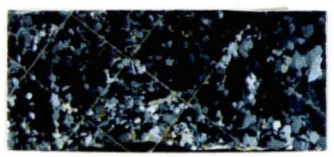

ε = 0 %

S > 152 mm²

ε = 239 %

S = 1.1 mm²

BHC1_138CT

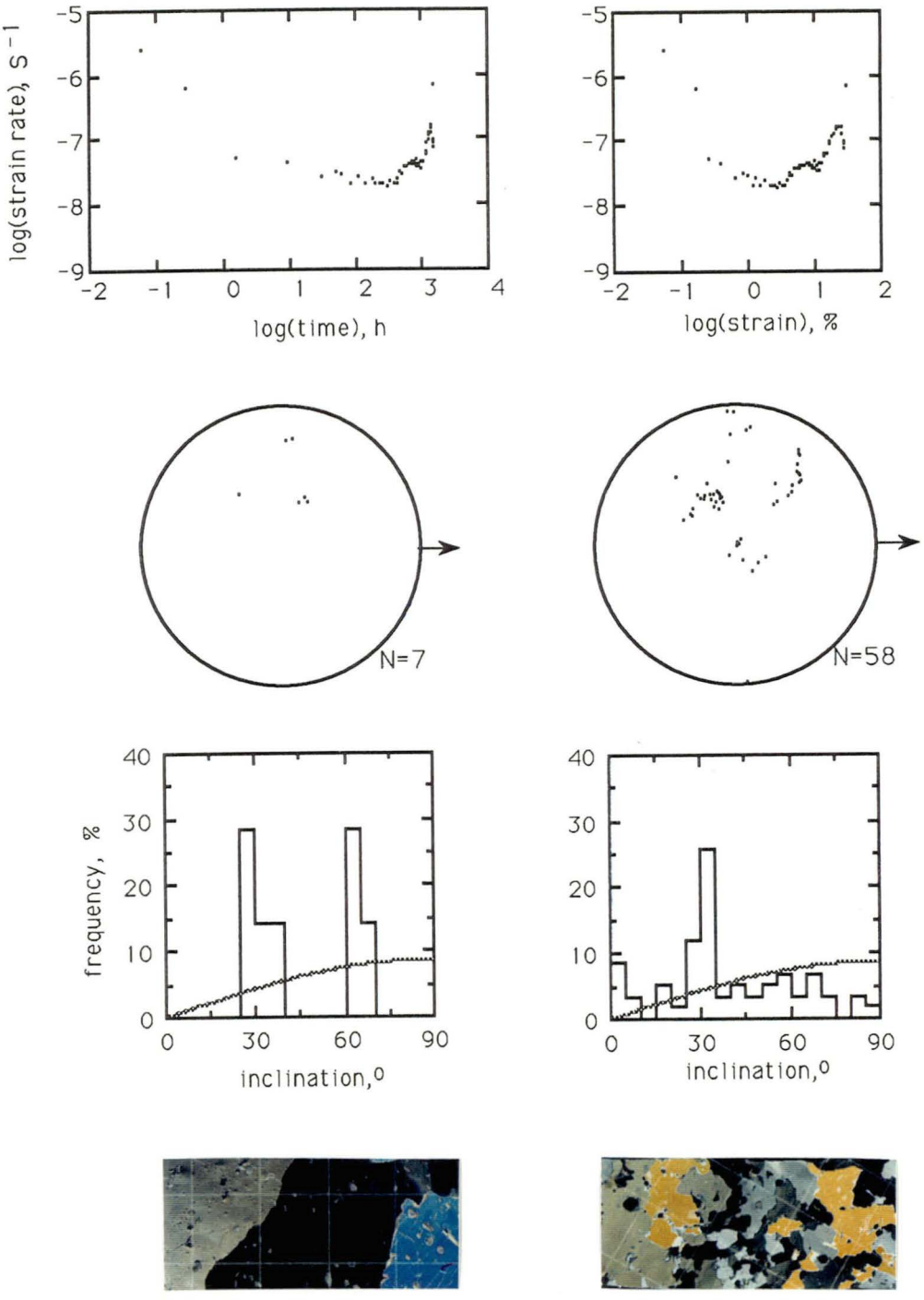

ε = 0 %

S > 306 mm²

ε = 29.1 %

S = 7.0 mm²

DYE3_T338

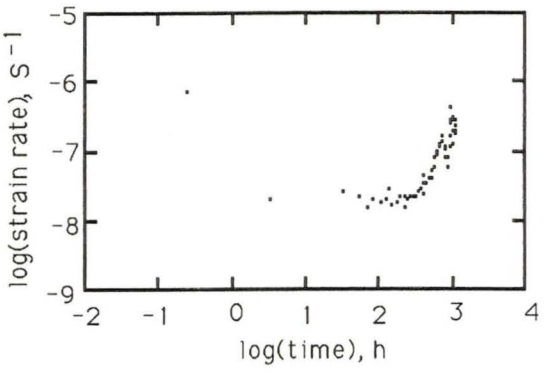

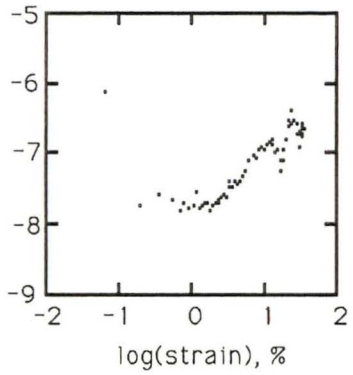

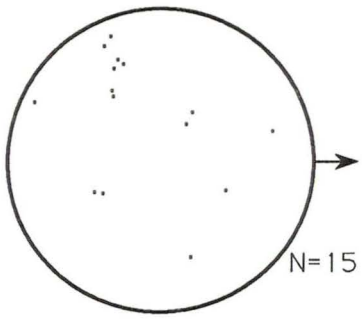

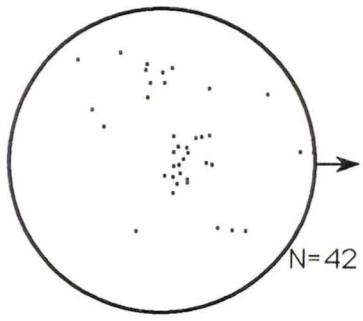

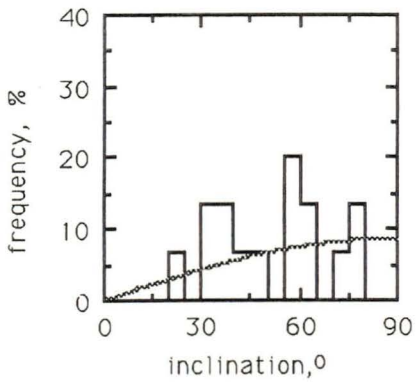

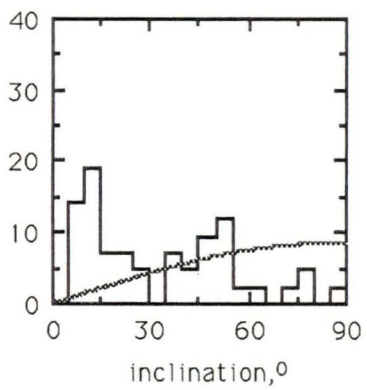

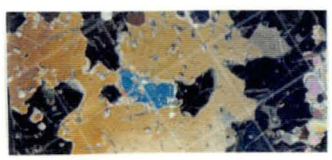

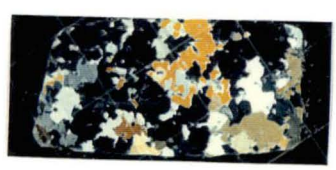

ε = 0 %

S = 56 mm²

ε = 34.5 %

S = 3.2 mm²

DYE3_T1556

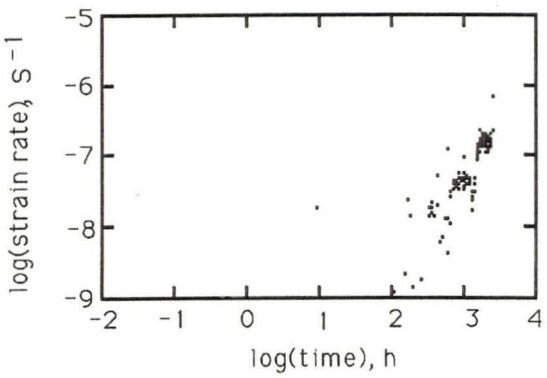

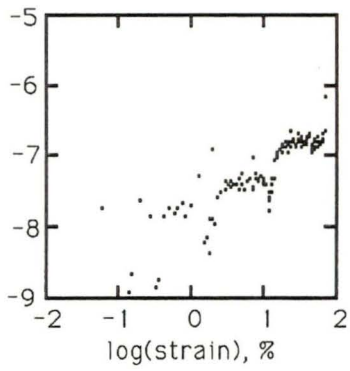

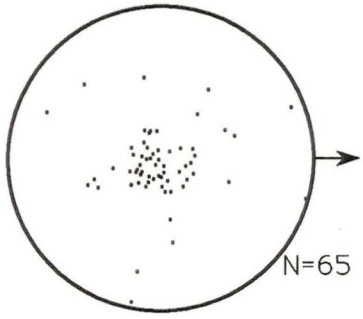

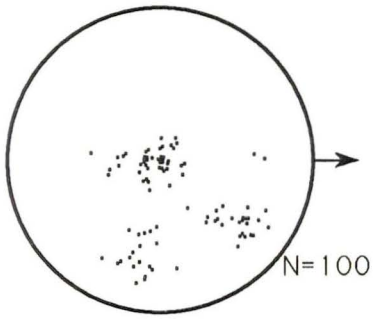

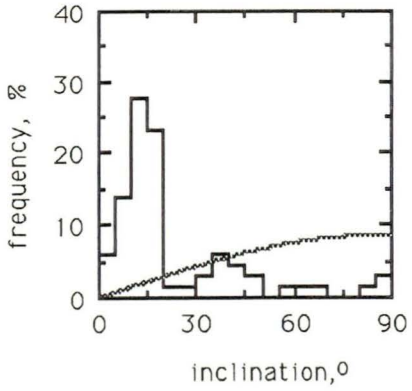

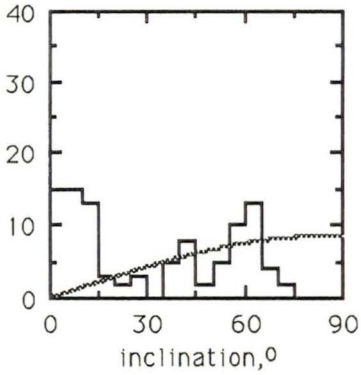

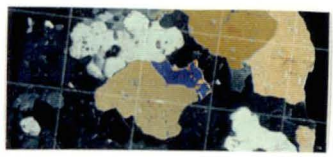

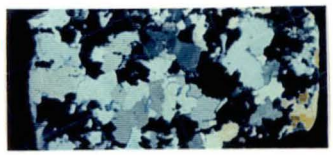

ε = 0 %

S = 12.9 mm²

ε = 69.8 %

S = 3.5 mm²

DYE3_T1763

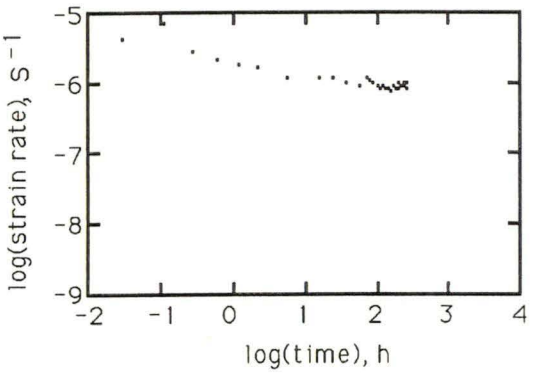

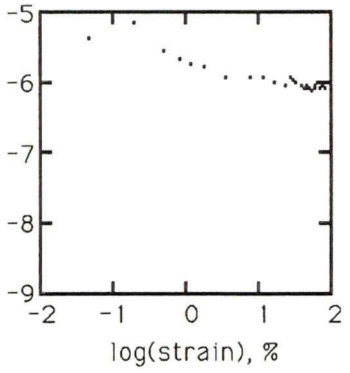

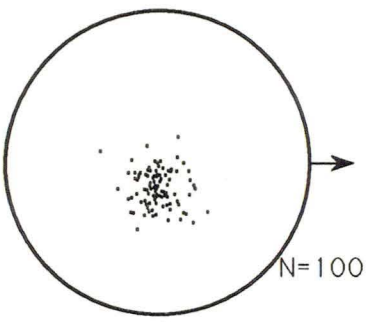

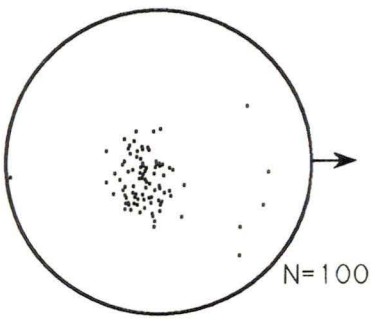

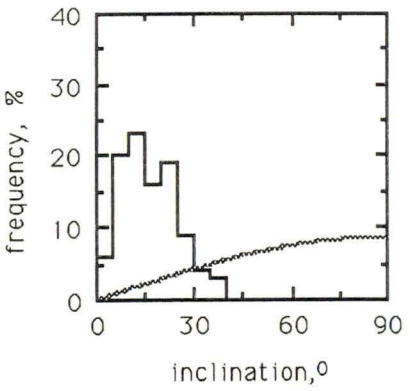

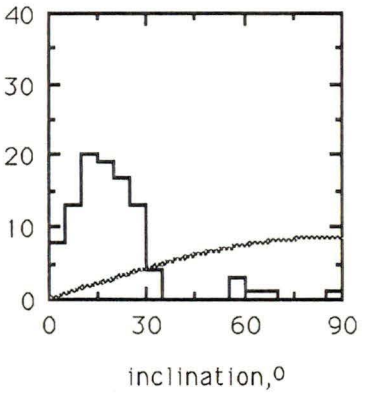

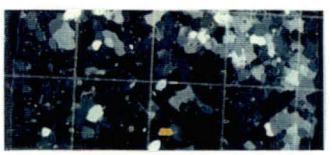

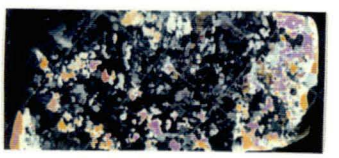

ε = 0%

S = 1.2 mm²

ε = 88.8 %

S = 0.9 mm²

DYE3_T1922

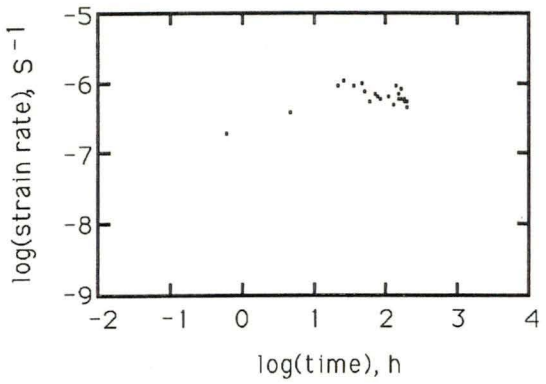

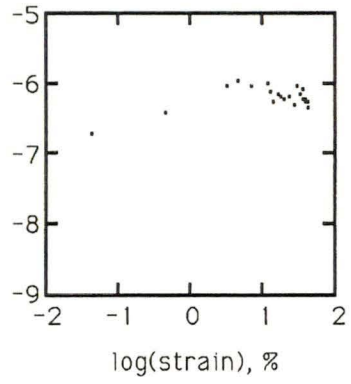

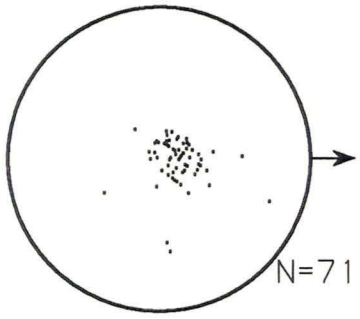

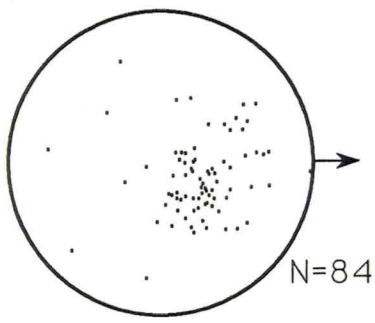

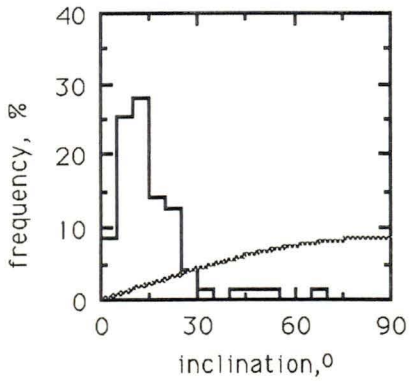

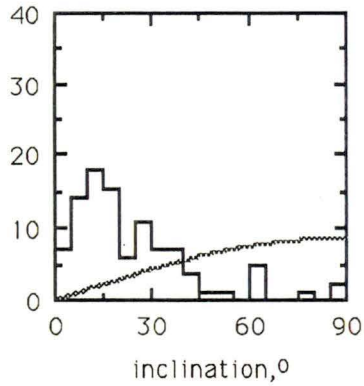

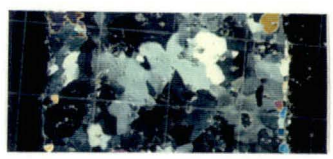

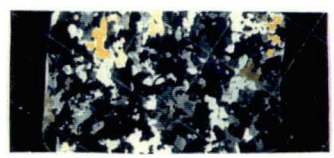

ε = 0%

S = 6.8 mm²

ε = 42.3 %

S = 1.7 mm²

LAB.1

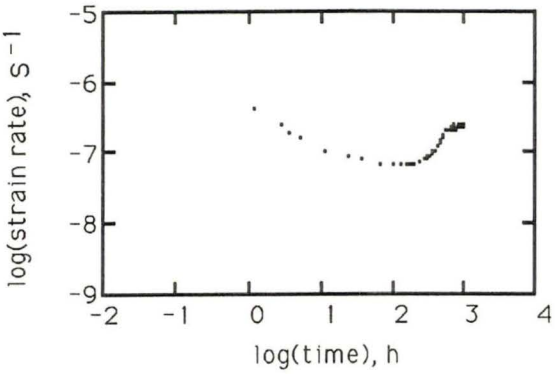

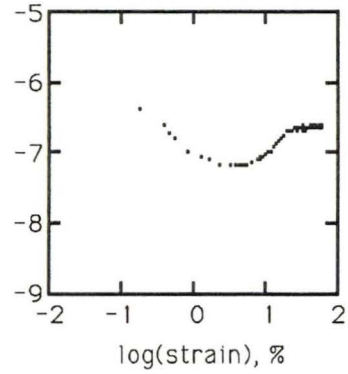

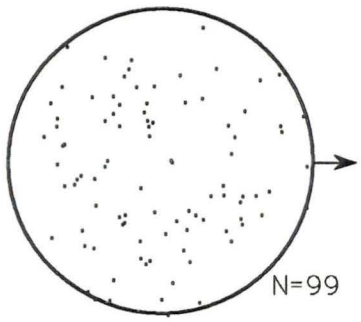

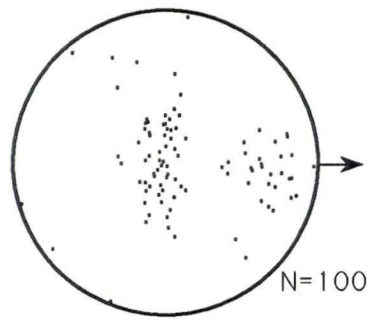

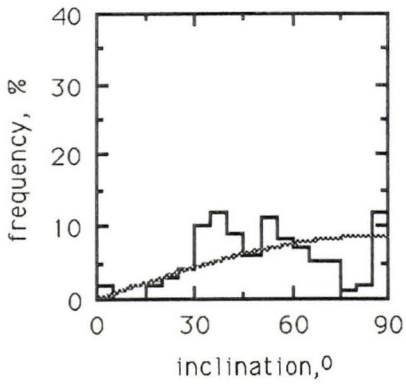

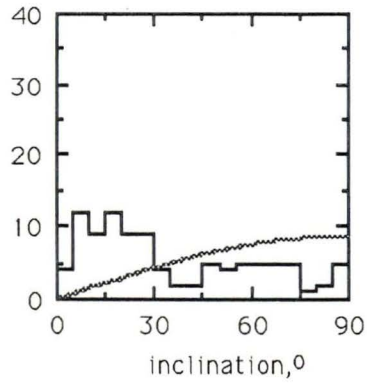

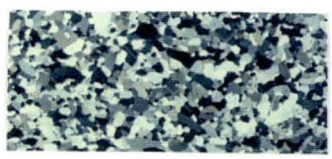

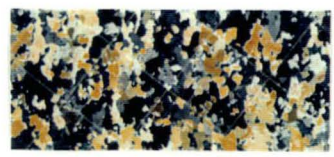

ε = 0%

S = 0.9 mm²

ε = 59.1 %

S = 1.5 mm²

LAB.2 LAB.3 LAB.4

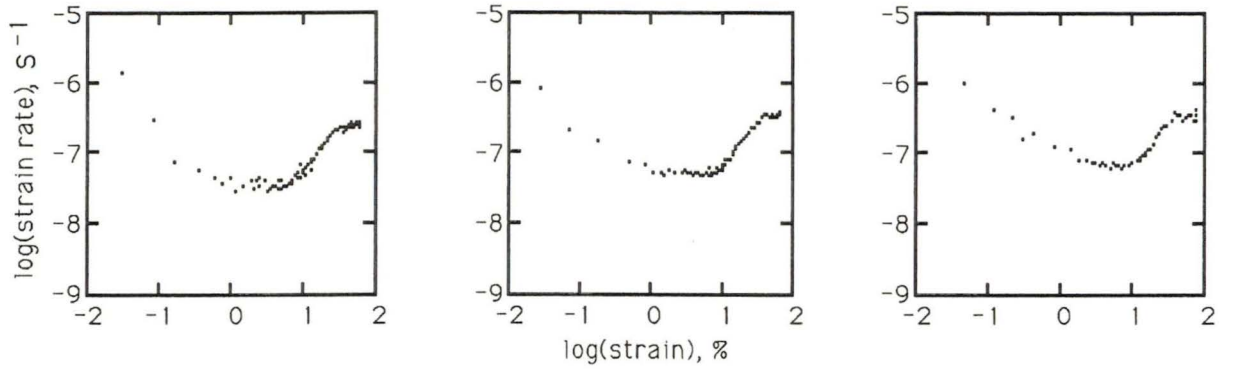

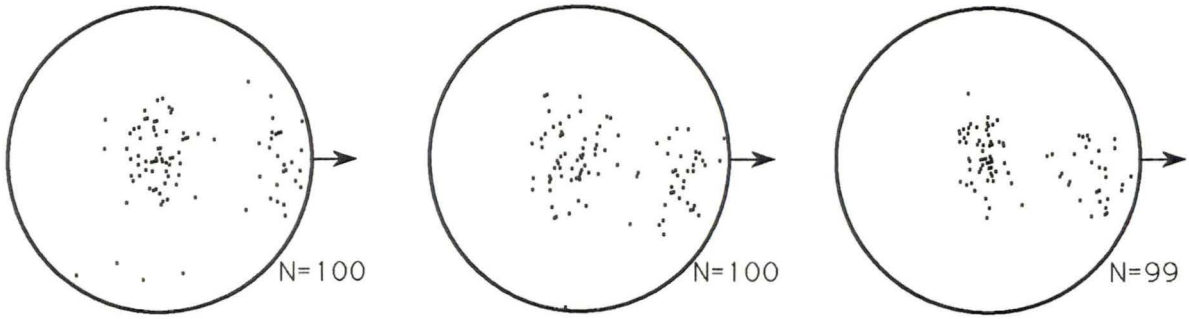

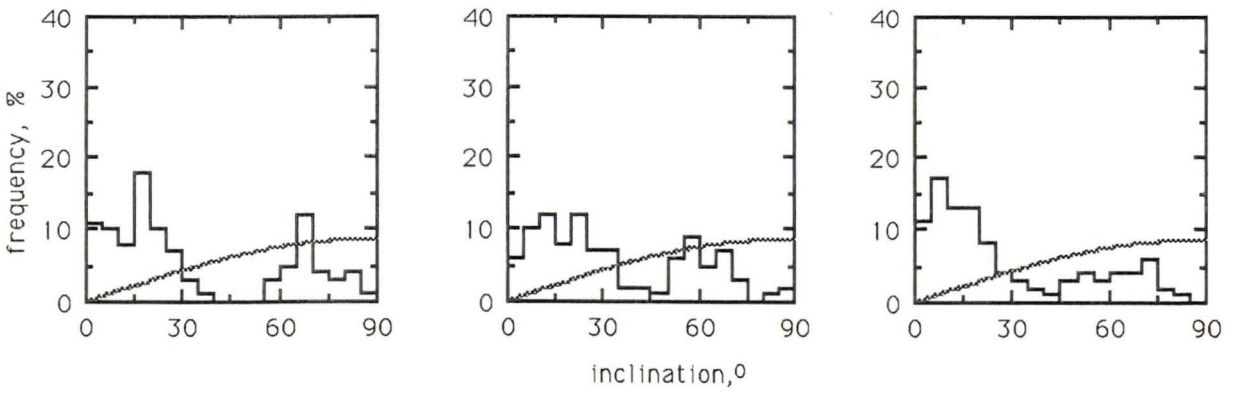

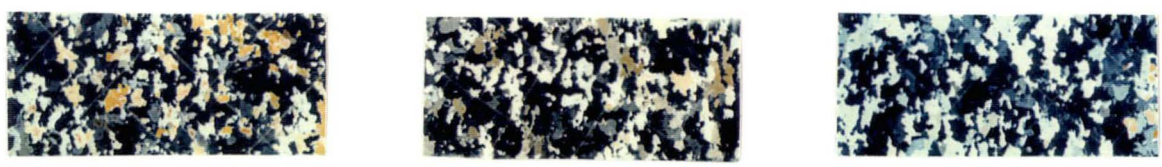

LAB.2	LAB.3	LAB.4
ε = 62.1 %	ε = 64.5 %	ε = 79.8 %
S = 1.3 mm²	S = 1.3 mm²	S = 1.9 mm²